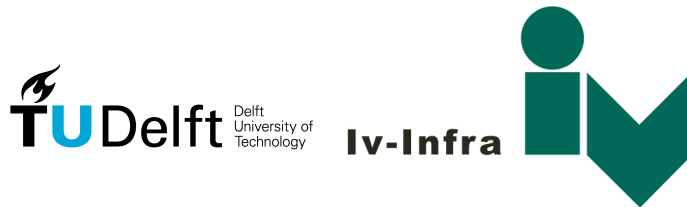


Background study and analytical model for railway bridge lateral dynamics

study of dynamics of railway bridges and applicability assessment of simplified dynamic analysing method.

Sijian Deng

A thesis presented for the degree of
Master of Science



Faculty of Civil Engineering and Geo-science Iv-Infra
Delft University of Technology Iv-Groep
The Netherlands
September 22, 2014

Contents

1 INTRODUCTION	5
1.1 Summary of topic	5
1.2 Motivation of the thesis	5
1.3 Objectives and research question	5
1.4 Main steps	5
1.5 Outline of the report	6
2 Basic concepts of railway bridge dynamics	7
2.1 Sources induce transverse dynamic reactions	7
2.2 Wheel-Rail Interface	7
2.2.1 Wheelset and track dimensions	7
2.2.2 Conicity and Equivalent Conicity of Wheels	7
2.2.3 Worn wheel profiles	8
2.2.4 Lateral Track Irregularities	8
2.3 Lateral movement of a wheelset on straight track	9
2.3.1 Theory according to Klingel	9
2.3.2 Hunting movement	10
2.4 Single and two-point contact between wheel and rail	10
2.5 Dynamic theories	11
2.5.1 Natural frequencies and shapes of bridge	11
2.5.2 Basic resonance concept	13
2.5.3 Resonance between moving load and simplified beam bridge model	15
2.6 FEM Modelling of rail-vehicle system	15
2.6.1 Modelling of railway vehicles	16
2.6.1.1 Moving vertical forces model	16
2.6.1.2 Advanced models	16
2.6.1.3 Models proposed in Eurocodes	16
2.6.2 Track model	16
3 Literature Review of regulations regarding lateral railway bridge dynamics in 1991-2	19
3.1 Factors influencing dynamic behaviour	19
3.2 Requirements for railway bridge verification	20
3.3 Horizontal transverse dynamic effects	20
3.3.1 Nosing force	20
3.3.2 Verification of the Limit States	21
3.3.3 Serviceability limit states - traffic safety	21
3.3.3.1 Transverse deformations and vibrations	21
3.4 Conclusion	22

4 Investigation of report series created by D181 Committee Group	23
4.1 Introduction	23
4.1.1 Structure of report series	23
4.1.2 Items of interests in report series	23
4.2 Investigation of DT329	24
4.2.1 Methodology of Parametric Research DT329	24
4.2.2 Modelling	24
4.2.2.1 Model of bridge	24
4.2.2.2 Bridge parameters	25
4.2.2.3 Vehicle parameters	25
4.2.2.4 Track	26
4.2.2.5 Contact data	26
4.2.2.6 Data produced	26
4.2.3 Investigation of resonance phenomenon studied in DT329	27
4.2.3.1 Resonance caused by axle repeat pattern	27
4.2.3.2 Resonance caused by kinematic movement of trains	27
4.2.3.3 Apparent shift in resonance frequency	28
4.3 Investigation of RP6	29
4.3.1 Debate on proposed 1.2Hz criterion	29
4.3.2 Lateral forces on railway bridges	30
4.3.2.1 Basic characteristics of lateral force on railway bridges	30
4.3.2.2 Refining of lateral force model	31
4.3.2.3 Application of lateral force model	33
4.4 Conclusion of D181 report series	34
5 Study on vehicle wavelength	35
5.1 Effects investigated in wavelength study	35
5.2 Speed range of dynamic consideration	35
5.3 Equivalent conicity used in this study	36
5.4 Study on frequency of Klingel movement	36
5.5 Comparison between Klingle movement and train kinematic movement studied in D181 DT329	36
5.6 Assess of frequency bandwidth based on realistic data of Dutch Rail/Vehicle	37
5.7 Study on frequency caused by axle repeat pattern	38
5.8 Conclusion of wavelength study	39
6 Fundamental of analytical approach to be adopted in practical checking method	41
6.1 Introduction	41
6.2 Overview	41
6.3 The model, its assumptions and field of application	41
6.4 Solution deduction	42
6.5 Damping	44
6.6 Script structure	45
6.7 Comparison between analytical model and DT329 simulation results	45
6.7.1 First attempt	45
6.7.2 Second attempt	46
6.7.2.1 Third attempt	48
6.7.3 Alternative load model	49
6.8 Alternative analytical model for longer span bridges	50
6.9 Parametric research	51
6.9.1 Mass	51
6.9.2 Stiffness	51

6.9.3	Speed	52
6.9.4	Conclusion	53
7	New practical method for checking lateral dynamic response of railway bridges	56
7.1	Introduction	56
7.2	Overview of this chapter	56
7.3	Development of refined load model	57
7.3.1	Introduction to the analytical model to be used in pair with equivalent force amplitude	57
7.3.2	Finding equivalent lateral force amplitude for specific cases	58
7.3.3	Key parameter for equivalent force amplitude and hypothesis expression for refined load model	59
7.4	Verification of the method	61
7.5	Finalizing the method for practical usage	61
8	Recommendations on improvement on Eurocode	64
8.0.1	Add reference	64
8.0.2	Improve criteria for lateral bridge dynamics	64
8.0.3	Requirements for traffic safety(horizontal)	64
8.0.4	Requirements for traffic safety on derailment: Railway vehicle derailment mechanism and safety criteria	64
8.0.4.1	Flange climb derailment	65
8.0.4.2	Derailment caused by gauge widening and rail rollover	65
8.0.4.3	Derailment caused by track panel shift	66
8.0.4.4	Derailment caused by vehicle lateral instability	67
8.0.5	Requirements for traffic serviceability(horizontal)	68
9	Conclusion	69
Appendices		70
A	Plots and diagrams used in D181 DT 329	71
B	Speeds which do not require dynamic compatibility checks	87
C	MU-Groups and MU-Classes	90
C.1	Definition	90
C.1.1	Train parameters of MU-Class CB_1	90
C.1.2	Train parameters of MU-Class CB_2	90
C.1.3	Train parameters of MU-Class AB_1	90
C.1.4	Train parameters of MU-Class AB_2	91
C.1.5	Train parameters of MU-Class AB_3	91
C.1.6	Train parameters of MU-Class AB_4	91
C.1.7	Train parameters of MU-Class SA_1	91
C.1.8	Train parameters of MU-Class SA_2	91
D	Regression commands for R console	94
E	Matlab scripts	95
E.1	fog.m	95
E.2	Speedenvelop.m	97
E.3	Spanenvelop.m	97
E.4	Stiffenvelop.m	98

E.5	Massenvelop.m	99
F	Train vehicles	100
F.1	Locomotives	100
F.1.1	4-axle locomotives	100
F.1.2	6-axle locomotives	100
F.2	Trains in Netherlands	100

Chapter 1

INTRODUCTION

1.1 Summary of topic

The lateral dynamic behaviour of steel railway bridges are minimally discussed in Eurocodes and designers lack knowledge of background of criteria proposed in the code. For example, there is one criterion in Eurocode requiring railway bridges should have a lateral natural frequency higher than 1.2Hz. However, this criterion is becoming more and more unsuitable because longer span provides lower natural frequencies. For bridges having span more than 100m, it is almost guaranteed that the first lateral natural frequency of the bridge fall below 1.2Hz, unable to meet the requirement of Eurocode.

Criteria on lateral dynamics of railway bridges are complicated if taking vehicle systems and interaction into account. Designers need a better knowledge on railway dynamics and a tool in calculating the lateral dynamic behaviour of the whole system. This tool needs to be simple to meet the engineering needs.

1.2 Motivation of the thesis

1.3 Objectives and research question

The main goal of this thesis is to discuss the sufficiency and reliability of current criteria regarding lateral dynamics of steel railway bridges that exist in Eurocode 1991-2. Original reports where criteria were proposed will be reviewed to reveal the background of them to Eurocode users.

Depending on the output of previous step, if the current requirements/criteria show lack of reliability/sufficiency of Eurocode 1991-2, further recommendation will be made for revising or amending current Eurocode.

This report also aims to providing knowledge of railway bridge dynamics to Eurocode users. The dynamics of railway bridge concerns cross-field knowledge, including intelligence of railway tracks/ vehicles/ bridge structures, etc. Some of them are essential to dynamics problem but unfamiliar to Eurocode users. Thus the report is willing to convey users the reason and importance of dynamic concerns of railway bridges.

1.4 Main steps

In order to provide a better tool for designers when they encounter lateral dynamic problems on steel railway bridges, following objectives are made:

1. Literature research of dynamic actions as well as their criteria on railway bridges, rails and train vehicles in order to give a better understanding of the background of the criteria which is unclear to the designers. Study the dynamic behaviour of these system respectively. Then discuss their effects when combined.
2. Find the original reports which proposed 1.2Hz criterion but assess the content of these reports.
3. Study wavelength range of trains running in the Netherlands.
4. Develop a analytical model for simple calculating time-history of the dynamic response of the bridge under train vehicle load.
5. Conduct parametric research using the analytical model developed in previous step. Propose design strategy based on this parametric research.

1.5 Outline of the report

The report is created in following structure:

1. Literature study on basic concepts of railway bridge dynamics.
2. Deep investigation of EN1991-2 supporting research report series
3. Wavelength study
4. Development of analytical model
5. Parametric research based on analytical model
6. Design strategies for railway bridge dynamics
7. Suggestions for Eurocode

Chapter 2

Basic concepts of railway bridge dynamics

In this chapter some basic concepts of railway bridge dynamics will be described in order to provide preliminary relevant knowledge for following chapters. The knowledge will be introduced in the order of railway related only to bridge related.

2.1 Sources induce transverse dynamic reactions

According to [20][12][10], following sources are identified:

- Horizontal track irregularities
- Sinusoidal motion of conical wheels along cylindrical rail heads
- Centrifugal forces on curved tracks
- Train switches

2.2 Wheel-Rail Interface

2.2.1 Wheelset and track dimensions

Generally the track gauge is used as a distance measured between the two rails, more specifically the distance between the inside of the railheads measured 14mm below the surface of the rail. By choosing 14 mm the measurement is less influenced by lipping or lateral wear on the rail head and by the radius $r = 13$ mm of the rail head face. On normal track the gauge is 1435^{+10}_{-3} mm with a maximum gradient of 1:3000. For new track, however, NS apply the following standards:

1. Mean gauge per 200 m: 1435^{+10}_{-1} mm
2. Standard deviation within a 200 m section less than 1 mm

2.2.2 Conicity and Equivalent Conicity of Wheels

Originally conical tire profiles with an inclination of 1:20 were used. Since a centrally applied load on the railhead is desired, a rail inclination of 1:20, as shown in Figure 2.1, was also selected; this for instance still applies to NS profile NP 46. UIC 54 rail usually has an inclination of 1:40. This inclination matches the S 1002 worn wheel profile which is in general use in Europe. During manufacturing the tires are given a profile which matches the average shape cause by wear. In contrast to the straight conical profile this has a hollow form.

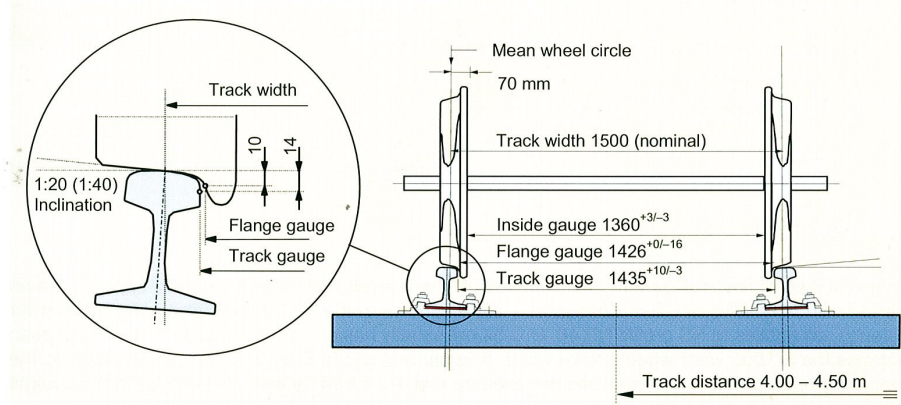


Figure 2.1: Wheelset and track dimensions for straight normal gauge track. Extracted from [9, p.17]

It is clear that regarding a worn profile the conicity depends on the actual shape of the rail head and tire, including any wear, track gauge, and rail inclination. Likewise, elastic deformation of the wheelset and rail fastenings plays a role.

Generally, the effective or equivalent conicity is defined as:

$$\gamma_e = \frac{\Delta r}{2y} = \frac{r_1 - r_2}{2y}$$

Here $r_1 - r_2$ is the instantaneous difference in rolling radius of the wheel treads; generally speaking this is a non-linear function of the lateral displacement y of the wheelset with respect to the central position. The difference between conical and worn profiles is given in Figure 2.2. To enable numerical comparisons γ_e is determined at a certain lateral displacement $y = \bar{y}$.

2.2.3 Worn wheel profiles

A perfectly conical wheel profile is unstable as far as its shape is concerned, but will take on a shape that is stable as the effect of wear.

Practical research has shown that over a period of time wheel profiles stabilise with wear at an equivalent conicity of 0.2 to 0.3. With regards to running stability, the equivalent conicity must remain below 0.4 and to ensure the centering effect it must be greater than 0.1.

With a conical profile the conicity is constant and above equation becomes:

$$\gamma_e = \frac{\Delta r}{2y} = \frac{(r + \gamma y) - (r - \gamma y)}{2y} = \gamma$$

2.2.4 Lateral Track Irregularities

This section describes allowable lateral track irregularities defined in EN13848-5[2].

Lateral alignment irregularities was defined in EN13838-1. It states: "Deviation y_p in y-direction of consecutive positions of point P... on any rail, expressed as an excursion from the mean horizontal position (reference line) covering the wavelength ranges stipulated below and calculated from successive measurements ...". See Figure 2.3.

For lateral deviations, the following wavelengths shall be considered: $D1 = 3 - 25m$, $D2 = 25 - 70m$ and $D3 = 70 - 200m$.

Table 2.1 defines the allowable standard deviation for lateral track irregularities. Lateral track irregularity has great influence on vehicle's lateral dynamic behaviour.

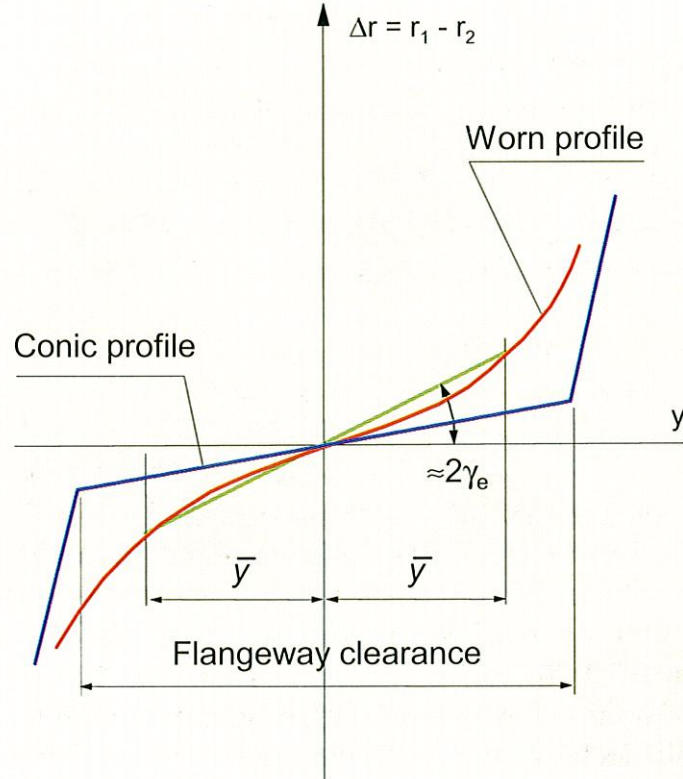


Figure 2.2: $y - \Delta r$ curves. Difference between conical and worn wheel profiles. Extracted from [9, p. 2.4]

2.3 Lateral movement of a wheelset on straight track

2.3.1 Theory according to Klingel

If a wheelset with conical tire profiles is laterally displaced from central position, this displacement is counteracted due to different rolling radii of the wheels. This results in a periodical movement of the wheelset which was described by Klingel in 1883 and is therefore often referred to as the Klingel movement. When analysing the case, the wheelset is modelled as a biconus travelling on an ideally straight track as shown in Figure 2.4

The Klingel movement is therefore purely a kinematic movement in which forces play no part in the derivation. As a result, Figure 2.5 visualizes the Klingel movement. The lateral displacement y is a harmonic, undamped function of the distance co-ordinate x as long as the amplitude moves within the flangeway clearance fwc . This is illustrated in Figure 2.6.

Introducing the speed, the time domain frequency of the Klingel movement is:

$$f = \frac{V}{L_k}$$

and hence the maximum lateral acceleration can be calculated as:

$$\ddot{y}_{max} = 4\pi^2 y_0 \frac{v^2}{L_k^2}$$

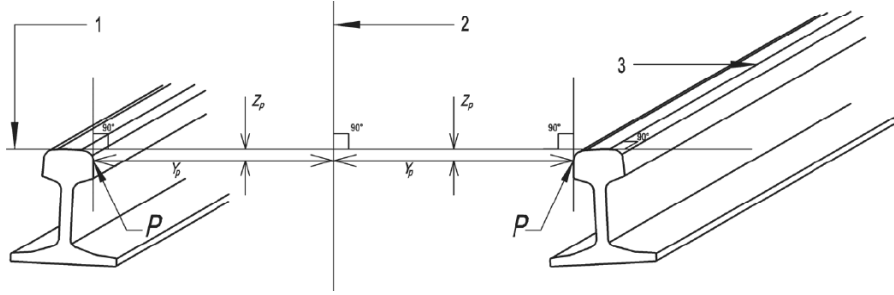


Figure 2.3: Lateral deviation definition. Lateral deviations y_p for each rail with 1: running surface, 2: reference line and 3: centre line of running table

Table 2.1: Alignment - AL - Standard deviation. Extracted from [2, Table B.6]

Speed(km/h)	Standard deviation(mm)
$V \leq 90$	1.5 to 1.8
$80 < V \leq 120$	1.2 to 1.5
$120 < V \leq 160$	1.0 to 1.3
$160 < V \leq 230$	0.8 to 1.1
$230 < V \leq 300$	0.7 to 1.0

If the frequency f coincides with one of the natural frequencies of the rolling stock, the vehicle ride becomes unstable. The lateral acceleration, which is a measure of the forces, shows the adverse effect of high speed and/or small wavelength. A conicity, for example, of 1:40 in comparison with 1:20 therefore gives a greater wavelength and a lower lateral acceleration at the same speed. The progressively increasing conicity in the case of worn profiles due to increasing lateral axle movement, therefore, has an adverse effect in this respect.

2.3.2 Hunting movement

It should be noted that the Klingel theory is simple and instructive but does not include the effect of coupled axes, mas forces, and adhesion forces. In reality, the amplitude y_0 of the Klingel movement is dependent on alignment, dynamic vehicle behaviour, and the speed of the rolling stock.

Generally speaking, y_0 due to slip will increase with speed until it is equal to half the flangeway clearance. Flanging then occurs as a result of which the axle will rebound.

This means that the lateral movement takes on a completely different behaviour which is known as hunting. As shown in the drawing in Figure 2.7 the movement changes from a harmonic to a zig-zag shape. The wavelength becomes shorter and the frequency increases quickly until it is in the critical range for the rolling stock and resonance occurs.

This phenomenon is shown in Figure 2.8. The bogie design, as far as conicity and flangeway clearance are concerned, must be such that stable running is always guaranteed for the speed range in which the vehicle is to be used.

2.4 Single and two-point contact between wheel and rail

In the case of single-point contact, according to Figure, wheel load and lateral force act on the same point. This situation occurs when using worn wheel profiles. In the case of two-point contact, shown in Figure, the application points do not coincide.

Flanging occurs in the situation of double contact.

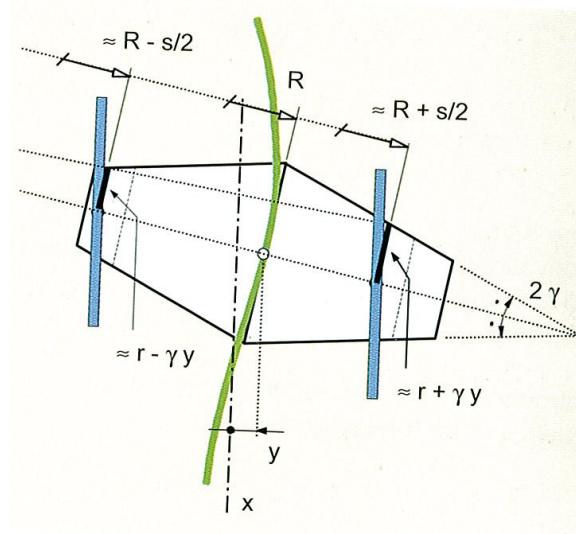


Figure 2.4: Wheelset biconus in general position. Extracted from [9, Figure 2.2]

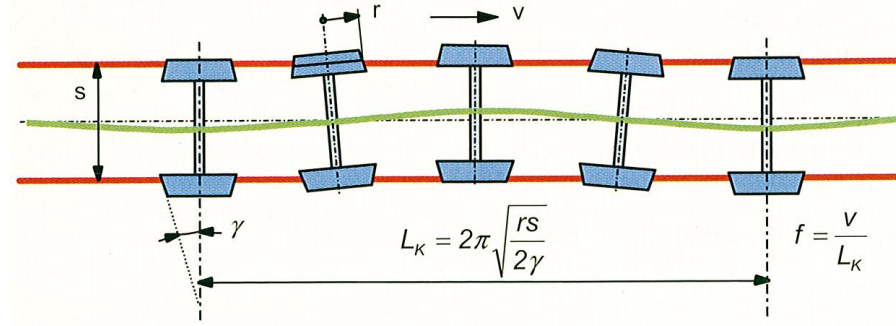


Figure 2.5: Klingel movement. Extracted from [9, Figure 2.3]

2.5 Dynamic theories

2.5.1 Natural frequencies and shapes of bridge

Undamped Euler-Bernoulli beam theory is adopted to obtain natural wave shapes and frequencies of a bridge structure. This theory is the simplest bridge dynamic model which assumes that the bridge behaves as a vibrating uniform beam.

The bridge is simply supported at both ends, and the stiffness is specified as a deflection at the mid span per unit span length arising from a static point load of 100kN at mid span.

The equation of vibration of a uniform beam is:

$$\frac{\partial^2 y}{\partial t^2} + a^2 \frac{\partial^4 y}{\partial x^4} = 0$$

where:

y = deflection of beam

x = coordinates along longitudinal axis

t = time

$a^2 = EI/m$

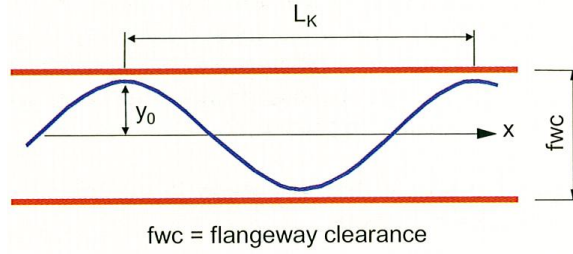


Figure 2.6: Undisturbed lateral movement of a wheelset. Extracted from [9, Figure 2.4]

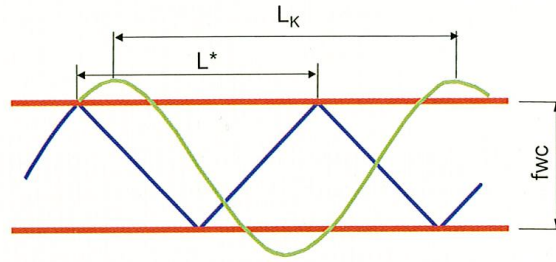


Figure 2.7: Influence of flanging on lateral wheelset movement. Extracted from [9, Figure 2.5]

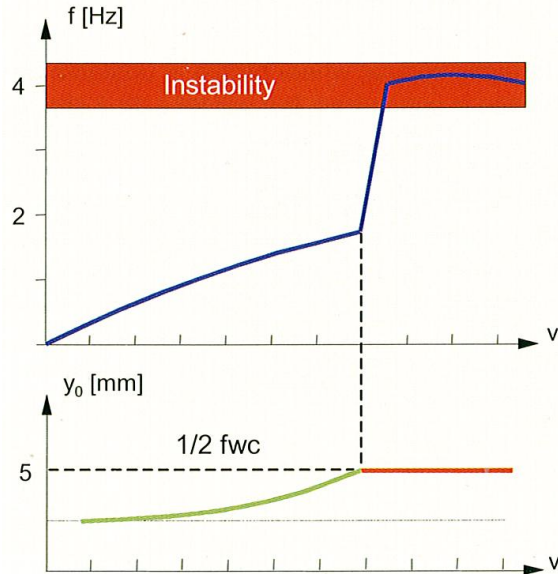
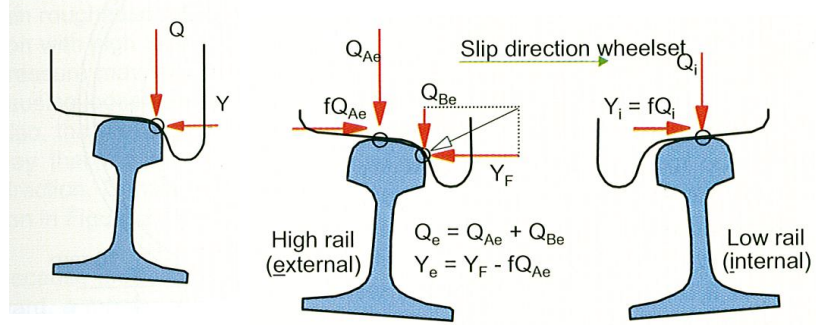


Figure 2.8: Increase in amplitude and frequency with speed and the development of instability. Extracted from [9, Figure 2.6]

EI = flexural rigidity
and, m = mass per unit length
The general solution is:

$$y(x, t) = (A \cos pt + B \sin pt)(C \cos kx + D \sin kx + F \cosh kx + G \sinh kx)$$



(a) Single contact point

Extracted from [9, Figure 2.13]

$$Q_e = Q_{Ae} + Q_{Be}$$

$$Y_e = Y_F - fQ_{Ae}$$

(b) Double contact point. Forces on rails in case of lateral slip in curves. Extracted from [9, Figure 2.14]

which consists of independent time and distance parts. The distance dependent part of the solution gives the family of mode shapes which the beam will exhibit. Thus, generally, a beam has mode shapes which satisfy:

$$y(x) = C \cos kx + D \sin kx + F \cosh kx + G \sinh kx$$

For a beam which is simply supported at either end the general solution simplifies, giving a family of normalized amplitude mode shapes as follows:

$$y_r = \sin \frac{r\pi x}{L}$$

for $r = 1, 2, 3, \dots, n$ and $L = \text{spanlength}$

with corresponding angular frequencies, ω_r , of:

$$\omega_r = \frac{r^2\pi^2}{L^2} \sqrt{\frac{EI}{m}}$$

thus natural frequencies f_r of beam, are:

$$f_r = \frac{r^2\pi}{2L^2} \sqrt{\frac{EI}{m}}$$

2.5.2 Basic resonance concept

The most simplest resonance scenario happens at a one degree-of-freedom mass-spring system loaded by a force whose frequency coincides with the natural frequency of mass-spring system.

Assume there is a simple one degree-of-freedom mass-spring system and an external force is acting on it. The force is given as $F(t) = F_0 \cos(\omega t)$. In this case the equation of motion takes the form

$$m\ddot{x} + kx = F_0 \cos(\omega t) \quad (2.1)$$

The general solution can be written as

$$x(t) = A \cos(\omega_n t) + B \sin(\omega_n t) + \frac{F_0}{k} \frac{1}{1 - \omega^2/\omega_n^2} \cos(\omega t) \quad (2.2)$$

where $\omega_n = 2\pi\sqrt{k/m}$

The unknown constants A and B depend on the initial conditions.

The steady-state solution is given as:

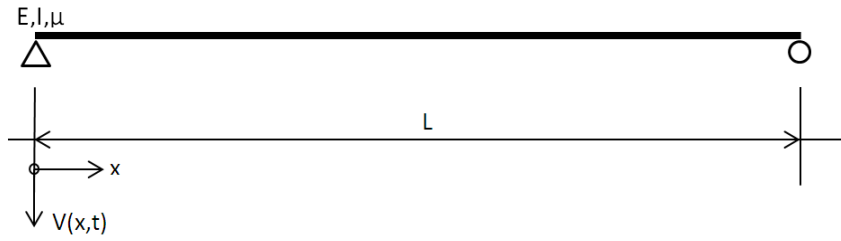


Figure 2.10: Mass beam model of span L

$$x_{steady} = X \cos(\omega t) = \frac{F_0}{k} \frac{1}{1 - \omega^2/\omega_n^2} \cos(\omega t) \quad (2.3)$$

The amplitude of vibrations of the mass-spring system is given by:

$$|X| = \left| \frac{F_0}{k} \frac{1}{1 - \omega^2/\omega_n^2} \right| \quad (2.4)$$

The amplitude-frequency dependencies is shown in 2.11

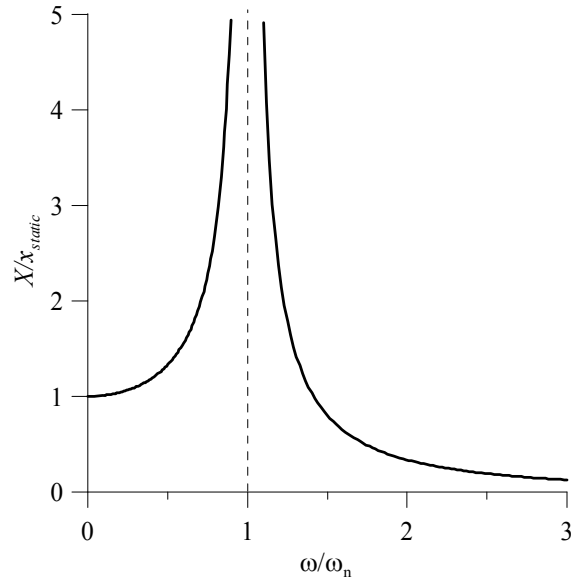


Figure 2.11: Amplitude-frequency characteristic. Extracted from [17, p. 2.2.2]

When the frequency of force equals frequency of mass-spring system, the amplitude of vibration is infinitely high. It means system becomes unstable and normally it's a dangerous sign. This phenomenon is called resonance. Resonance can happen if the frequency of excitation coincides with the natural frequency of the excited systems.

Resonance can also happen when a harmonic force is loaded on an Euler-Bernoulli beam. It can be loaded anywhere on the beam to produce resonance.

2.5.3 Resonance between moving load and simplified beam bridge model

It becomes a much more complicated problem when moving load is applied on an Euler-Bernoulli beam though analytical solution is still possible. Moving harmonic loads can represent, for instance, a component of the load transmitted to rails by moving trains. Thus it suits the aim of this thesis well.

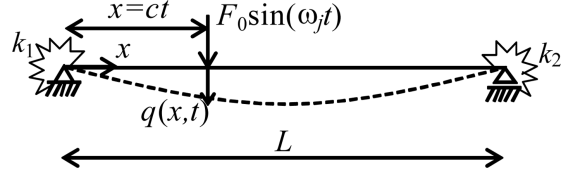


Figure 2.12: Schematic representation of a generic beam crossed by a harmonic load

In most cases force input are hard to determine because of the complicity of wheel-rail interaction. But, in the context of lateral dynamics, the process can be simplified by adopting nosing forces.

Giuseppe Piccardo [18] has provided following solutions:

The deflection $q(x, t)$ of a Euler-Bernoulli prismatic beam to a harmonic load moving with a constant speed c (Figure 6.1) is described by the well-known field equation

$$\mu \frac{\partial^2 q(x, t)}{\partial t^2} + \chi \frac{\partial q(x, t)}{\partial t} + EJ \frac{\partial^4 q(x, t)}{\partial x^4} = F_0 \sin(\Omega t) \delta(x - ct)[H(t) - H(t - L/c)]$$

where μ is the mass per unit length, χ is the damping coefficient, EJ is the flexural stiffness, F_0 and Ω are, respectively, the amplitude and the circular frequency of the moving load, δ is the Dirac delta function, H is the Heaviside step function, L is the beam span length.

By using convolution integral, the solution can be expressed as:

$$\begin{aligned} \tilde{p}(\tilde{t}) = & \varepsilon \exp(-\varepsilon \xi^* \tilde{t}) \left\{ \left[\int_0^{\tilde{t}} \sin(\tilde{\Omega} \tilde{\tau}) \phi_j(\varepsilon \Omega_c^* \tilde{\tau}) \exp(\xi^* \tilde{t} \tilde{a} u) \cos(\tilde{\tau}) \right] \sin(\tilde{t}) \right. \\ & \left. - \left[\int_0^{\tilde{t}} \sin(\tilde{\Omega} \tilde{\tau}) \phi_j(\varepsilon \Omega_c^* \tilde{\tau}) \exp(\xi^* \tilde{t} \tilde{a} u) \cos(\tilde{\tau}) \right] \cos(\tilde{t}) \right\} \end{aligned} \quad (2.5)$$

Under the hypothesis that $\tilde{\Omega} = 1$ (i.e., perfect resonance), Eq. 2.5 can be rewritten as follows

$$\begin{aligned} \tilde{p}(\tilde{t}) = & \varepsilon \exp(-\varepsilon \xi^* \tilde{t}) \left\{ - \left[\frac{1}{2} \int_0^{\tilde{t}} \phi_j(\varepsilon \Omega_c^* \exp(\varepsilon \xi^* \tilde{t} \tilde{a} u d \tilde{\tau})) \right] \cos(\tilde{t}) \right. \\ & + \left[\frac{1}{2} \int_0^{\tilde{t}} \sin(2\tilde{\tau}) \phi_j(\varepsilon \Omega_c^* \exp(\varepsilon \xi^* \tilde{t} \tilde{a} u d \tilde{\tau})) \right] \sin(\tilde{t}) \\ & \left. + \left[\frac{1}{2} \int_0^{\tilde{t}} \cos(2\tilde{\tau}) \phi_j(\varepsilon \Omega_c^* \exp(\varepsilon \xi^* \tilde{t} \tilde{a} u d \tilde{\tau})) \right] \cos(\tilde{t}) \right\} \end{aligned} \quad (2.6)$$

This equation can be solved numerically.

2.6 FEM Modelling of rail-vehicle system

2.6.1 Modelling of railway vehicles

According to Newton's law, 2 basic load effects are produced by moving train: vertical forces due to vehicle weight, and inertia effects caused by vehicle acceleration. The loads on a railway bridge are very complex problems thus in engineering practice, loads are often simplified. But, the simplification depends on the purpose of the analysis.

2.6.1.1 Moving vertical forces model

If the inertia effects are neglected, loads of the moving trains can be modelled as moving vertical forces. For example, load diagram for type TALGO trains is shown in Figure 2.13 proposed by [19].

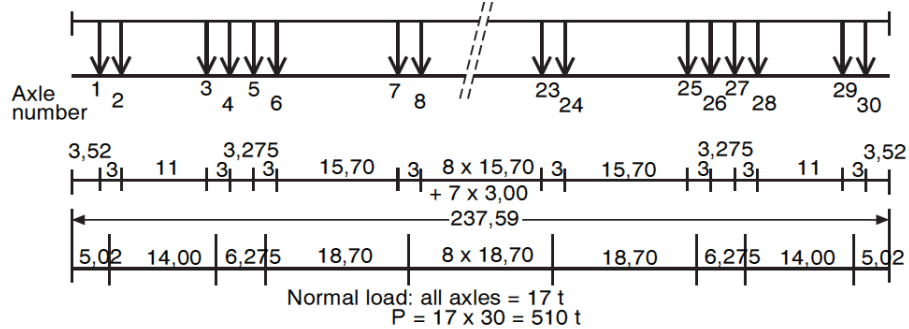


Figure 2.13: Moving vertical force model for TALGO trains

2.6.1.2 Advanced models

Nowadays more and more models have been proposed to meet different requirements of railway bridge dynamic analysis. The complexity of these models differs from each other but they are all more complicated than moving vertical forces models. For example, vehicle-bridge interaction model takes vehicle suspension system into account, which gives an alternative for discovering resonance effects between bridge and the vehicle suspension systems.

See Figure 2.14 for an example of advanced model.

2.6.1.3 Models proposed in Eurocodes

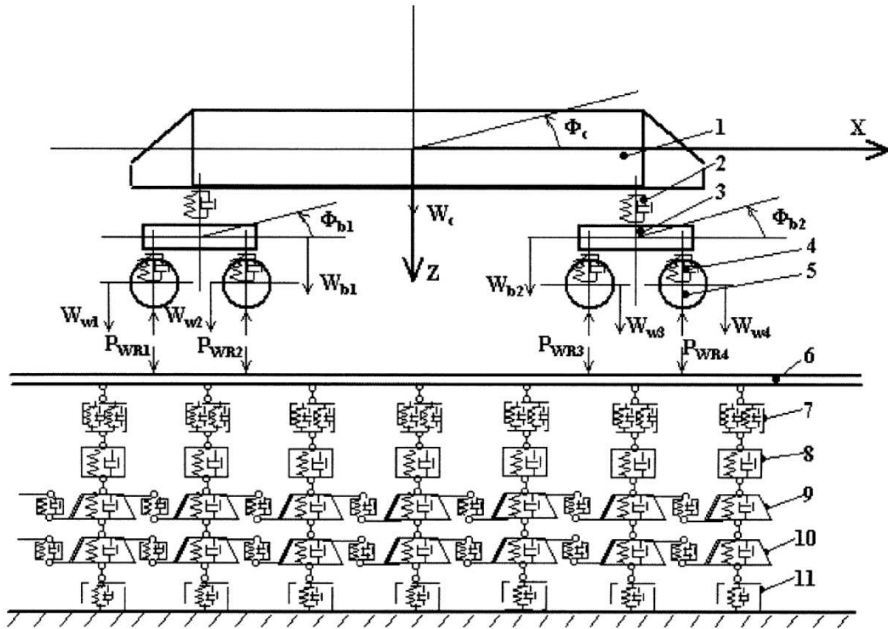
See Chapter ??

2.6.2 Track model

Proposed in [19, A.6.1.3], the track is represented by Timoshenko beam elements for the rails and takes account of the rail/sleeper fastening characteristics as well as the ballast(if one exists).

"A sleeper is generally represented by two beam elements, with two covering the rail and one used for the deck. Sleepers and ballast are modelled as concentrated masses. They are linked to the nodes of the rail and the bridge by a parallel spring and damper system. The track can be modelled to any length on both side of the bridges, where the stiffening effect of the bridge has to be taken into account. The effects of track distribution are not considered. Each vehicle is able to absorb the kinetic energy of the bridge and it is for this reason that, at resonance, the deflections and accelerations of the bridge obtained with this model are lower than those obtained with a live load diagram."

The most complete model for analysing train/track/bridge interaction is shown in Figure



- 1 – Wagon Body (M_c – mass, J_c – inertial moment),
- 2 – Secondary Suspension (K_{sc} – stiffness coefficient, C_{sc} – damping coefficient),
- 3 – Bogie (M_b – mass, J_b – inertial moment),
- 4 – Primary Suspension (K_{pr} – stiffness coefficient, C_{pr} – damping coefficient),
- 5 – Wheelset (M_w – mass),
- 6 – Rail (Timoshenko Beam)
- 7 – Fastener and Pad (K_f , K_p – stiffness coefficients, C_f , C_p – damping coefficients),
- 8 – Sleeper (M_s – mass, K_{sl} – stiffness coefficient, C_{sl} – damping coefficient),
- 9 – Ballast (M_{bl} – mass, K_{bl} – stiffness coefficient, C_{bl} – damping coefficient),
- 10 – Subballast (M_{sb} – mass, K_{sb} – stiffness coefficient, C_{sb} – damping coefficient),
- 11 – Subgrade (K_{sg} – stiffness coefficient, C_{sg} – damping coefficient).

Figure 2.14: A dynamic model for the vertical interaction of the rail track and wagon system. Proposed in [21]

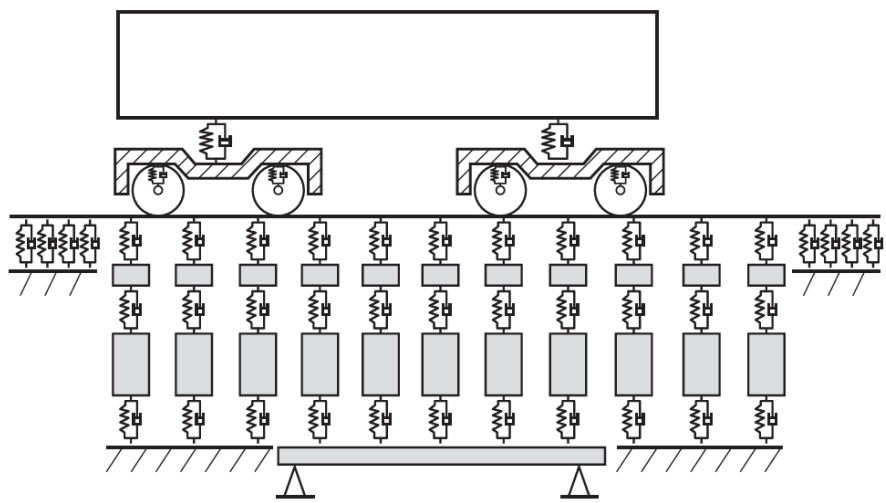


Figure 2.15: Diagram of the dynamic train-track-bridge model. Extracted from [19, Fig. 15]

Chapter 3

Literature Review of regulations regarding lateral railway bridge dynamics in 1991-2

Eurocode 1990 and Eurocode 1991-2 and their corresponding National Annex are primary codes to be fulfilled through out the whole process of conducting a railway bridge in Netherlands. It is of great importance to study dynamic effect on railway bridges due to increasing usage of public train service. What's more, as the need on capacity of railway service increase, high-speed train dynamic loading becomes a more general issue in the design of railway bridges. It is common knowledge that bridge structures loaded by high-speed trains have bigger chance of resonance, as well as of being required to be dynamic analysed in designing process.

Unfortunately in Chapter 6.4 of Eurocode NEN-EN 1991-2-2003, the description of various subjects is vague including general procedures of conducting a dynamic analyses and methods of additional dynamic analysing calculating, etc. The following paragraphs aim to summarize Chapter 6.4 of Eurocode 1991-2 [10], in order to give a better interpretation.

This literature research will be done by reviewing both physics knowledge and engineering standards.

3.1 Factors influencing dynamic behaviour

As stated in [10, p. 6.4.2] there are 11 factors influencing dynamic behaviour of a railway bridge. The principal factors which influence dynamic behaviour are:

- the speed of traffic across the bridge
- the span L of the element and the influence line length for deflection of the element being considered
- the mass of the structure
- the natural frequencies of the whole structure and relevant elements of the structure and the associated mode shapes (eigenforms) along the line of the track
- the number of axles, axle loads and the spacing of axles
- the damping of the structure
- vertical irregularities in the track
- the unsprung/sprung mass and suspension characteristics of the vehicle
- the presence of regularly spaced supports of the deck slab and/or track (cross girders, sleepers etc.)
- vehicle imperfections (wheel flats, out of round wheels, suspension defects etc.)

- the dynamic characteristics of the track (ballast, sleepers, track components etc.)
- Other factors may include:
1. The track number of the bridge and their alignment.
 2. Multiple trains running on bridge simultaneously.
 3. Track alignment

3.2 Requirements for railway bridge verification

[14] propose following requirements

1. Checks on bridge deformations shall be performed for traffic safety purposes for the following items:
 - vertical accelerations of the deck
 - vertical deflection of the deck throughout each span
 - unrestrained uplift at the bearings(to avoid premature bearing failure)
 - vertical deflection of the end of the deck beyond bearings(to avoid destabilising the track, limit uplift forces on rail fastening systems and limit additional rail stresses)
 - twist of the deck measured along the centre line of each track on the approaches to a bridge and across a bridge(to minimise the risk of train derailment)
 - rotation of the ends of each deck about a transverse axis or the relative total rotation between adjacent deck ends(to limit additional rail stresses, limit uplift forces on rail fastening systems and limit angular discontinuity at expansion devices and switch blades)
 - longitudinal displacement of the end of the upper surface of the deck due to longitudinal displacement and rotation of the deck end(to limit additional rail stresses and minimise disturbance to track ballast and adjacent track formation)
 - **horizontal transverse deflection(to ensure acceptable horizontal track radii)**
 - **horizontal rotation of a deck about a vertical axis at ends of a deck (to ensure acceptable horizontal track geometry and passenger comfort)**
 - **limits on the first natural frequency of lateral vibration of the span to avoid the occurrence of resonance between the lateral motion of vehicles on their suspension and the bridge**
2. Checks on bridge deformations should be performed for passenger comfort, i.e. vertical deflection of the deck to limit coach body acceleration in accordance with A2.4.4.3[14]
3. The limits given in A2.4.4.2 and A2.4.4.3[14] take into account the mitigating effects of track maintenance (for example to overcome the effects of the settlement of foundations, creep, etc.)

3.3 Horizontal transverse dynamic effects

There's only one criterion in the Eurocodes mentioned that the bridge's first lateral natural frequency should no lower than 1.2 Hz.

However, as more and more long-span bridges are built nowadays, this requirement is not valid for more bridges. This is because, in general, the lateral natural frequency of a bridge decreases when span increases. For bridges with span longer than 100m, there's few bridge can have a lateral frequency higher than 1.2Hz, according to senior engineers' designing experience.

So it is vital to discuss horizontal dynamic effects for the sake of longer span bridges. In addition, study the requirements for horizontal vibration of railway bridges to make the results of dynamic analysis usable.

3.3.1 Nosing force

Nosing force is defined in Eurocode 1991-2. Its original background can be found in [5, Proposed criteria]. It is defined as a representation of actions, in combine with actions like vertical loads,

dynamic effects, centrifugal forces, traction and braking forces, etc.

The evidence of RP6 is the background of nosing force in EN1991-2 is the following repeating literature:

In [10, p. 6.5.2]:

(1)P The nosing force shall be taken as a concentrated force acting horizontally, at the top of the rails, perpendicular to the centre-line of track. It shall be applied on both straight track....

In [5, 4.1B]:

These forces shall be applied at the top of the rails in the most unfavourable position and acting horizontally, perpendicular to the track centreline...

With another statement also helps proofing RP6 is the background of nosing force in EN1991-2 in [5, 4:Draft Recommendations]:

These can therefore be expressed as follows: (Article **6.5.2** of ENV 1991-3 of 1994)...

ENV 1991-3 was renamed to EN 1991-2 in 2003.

Originally in [5, 4:Draft Recommendations], nosing forces was defined as lateral forces from vehicle/bridge interaction as a result of **hunting**.

The characteristic value of the nosing force shall be taken as $Q_{sk} = 100kN$. It shall not be multiplied by the factor Φ ([10, p. 6.45]) or by the factor f in [10, p. 6.51].

The characteristic value of the nosing force should be multiplied by the factor α in accordance with [10, p. 6.3.2] for values of $\alpha \geq 1$

The nosing force shall always be combined with a vertical traffic load.

A detailed analysis on the background of nosing force will be given in Section 4.3.2

3.3.2 Verification of the Limit States

[10, p. 6.4.6.5] proposes following principles to be followed during design:

To ensure traffic safety:

1. The verification of maximum peak deck acceleration shall be regarded as a traffic safety requirement checked at the serviceability limit state for the prevention of track instability
2. The dynamic enhancement of load effects shall be allowed for by multiplying the static loading by the dynamic factor Φ defined in [10, p. 6.4.5]. If a dynamic analysis is necessary, the results of the dynamic analysis shall be compared with the results of the static analysis enhanced by Φ (and if required multiplied by α in accordance with [10, p. 6.3.2]) and the most unfavourable load effects shall be used for the bridge design.
3. If a dynamic analysis is necessary, a check shall be carried out according to [10, p. 6.4.6.6] to establish whether the additional fatigue loading at high speeds and at resonance is covered by consideration of the stresses due to load effects from $\Phi \times LM71$ (and if required $\Phi \times LoadModelSW/0$ for continuous structures and classified vertical load in accordance with [10, 6.3.2(3)] where required). The most adverse fatigue loading shall be used in the design.

3.3.3 Serviceability limit states - traffic safety

3.3.3.1 Transverse deformations and vibrations

[8, A2.4.4.2.4] proposed that transverse deformation and vibration of the deck shall be checked for characteristic combinations of Load Model 71 and SW/0 as appropriate multiplied by the dynamic factor ϕ and α (or real train with the relevant dynamic factor if appropriate), wind loads, nosing force, centrifugal forces in accordance with [10, p. 6] and the effect of a transverse temperature differential across the bridge.

The transverse deflection δ_h at the top of the deck should be limited to ensure:

1. a horizontal angle of rotation of the end of a deck about a vertical axis not greater than the values given in Table. 3.1 , or
2. the change of radius of the track across a deck is not greater than the values in Table. 3.1 , or
3. at the end of a deck the differential transverse deflection between the deck and adjacent track formation or between adjacent decks does not exceed the specified value

Speed range V(km/h)	Maximum horizontal rotation(radian)	Maximum change of radius of curvature	
		Single deck	Multi-deck bridge
$V \leq 120$	α_1	r_1	r_4
$120 \leq V \leq 200$	α_2	r_2	r_5
$V > 200$	α_3	r_3	r_6

NOTE 1 The change of the radius of curvature may be determined using:

$$r = \frac{L^2}{8\delta_h}$$

NOTE 2 The transverse deformation includes the deformation of the bridge deck and the substructure(including piers, piles and foundations).

NOTE 3 The values for the set of α_i and r_i may be defined in the National Annex. The recommended values are:

$$\begin{aligned} \alpha_1 &= 0.0035; \alpha_2 = 0.0020; \alpha_3 = 0.0015; \\ r_1 &= 1700; r_2 = 6000; r_3 = 14000; \\ r_4 &= 3500; r_5 = 9500; r_6 = 17500 \end{aligned}$$

Table 3.1: Maximum horizontal rotation and maximum change of radius of curvature

The first natural frequency of lateral vibration of a span should not be less than f_{h0} . The value for f_{h0} may be defined in the National Annex. The recommended value is: $f_{h0} = 1.2\text{Hz}$

Evidence of [5] is the origin of [10, A.2.4.4.2.4(3)] is found in [5, p4.2: Lateral Frequencies]:

In order to avoid the phenomena of lateral resonance in vehicles, the first natural frequency of lateral vibration of the span f_{lt} such that:

$$f_{lt} \geq 1.2\text{Hz}$$

Until now there's no further instructions in EN1991-2 for bridges which can not pass 1.2Hz criterion. However, for bridges longer than 100 meters, they are almost guaranteed to fail 1.2Hz criterion. In order to solve this problem, a detailed analysis is conducted in Sec.4.3.1

3.4 Conclusion

There are altogether two regulations regarding lateral dynamics of railway bridges in EN1991-2. They are:

1. Nosing force(action)
2. 1.2Hz criterion

These two regulations have the same background documents: D181 report series. The analysis of D181 report series will be carried out in following chapter.

Chapter 4

Investigation of report series created by D181 Committee Group

4.1 Introduction

D181 Committee Group is created by UIC, in order to investigate Lateral Forces on Railway Bridges. Some of the proposed criteria in reports created by this committee group are adopted by Eurocode Committee to created Eurocode 1991-2. The goal of this investigation is to summarize the research done by D181 report series and give further conclusion.

The investigation will be done in following aspects:

1. Investigation of DT329
2. Investigation of RP6
3. Conclusion of D181 report series

4.1.1 Structure of report series

Reports involved in the series are listed below in the order of publishing time:

1. RP 1: Summaries of national standards and literature survey
2. RP 2: Submitted programs and example of application
3. RP 3: Dynamic measurements on the steel bridge over the Brenta river on the MilanVenice line at 234 + 0.963 km
4. RP 4: Dynamic measurements on steel bridges over the Vh river by Sala on the MarcheggSzob line at 117 748 km
5. DT 312: Etude de l'influence de la frquence du filtre sur les valeurs mesures des forces verticales et latrales sur les rails
6. RP 5: Dynamic measurements on the metal arched bridge on PKP
7. DT 313: Analyse des dformations latrales d'un pont souple (cas du PONT de LIXHE) Ligne SNCB de TONGRESMONTZEN par J.J. REBER SBB Bau GD
8. DT 329: Parametric study Part 1: Parametric study Initial phase (September 1994) Part 2: Parametric study Phase 2 (February 1995) Authors: L.T. James and G.A. Scott
9. RP 6: Final Report

In this thesis DT 329 and RP 6 are obtained and studied, but other reports in English version are not available to the researcher.

4.1.2 Items of interests in report series

1. Resonance mechanisms studied. They are discussed in DT329. See Section 4.2.3

2. The proposed 1.2 Hz Criterion and its background. It is discussed in RP6. See Section 4.3.1
3. Lateral forces(Nosing force) on the bridges. See Section 4.3.2

4.2 Investigation of DT329

4.2.1 Methodology of Parametric Research DT329

The DT329 research was conducted in two phases. It is noted that all studies were done using VAMPIRE software. The reliability of simulation has been discussed and confirmed in previous reports.

In the initial phase 11 sets of bridge parameters were selected for the simulation. 52 combinations of bridge parameters and train configurations were examined. The goal of the initial phase is to filter out most influencing parameters for bridge dynamics.

In the secondary phase, the influence of selected parameters were categorized into 3 cases. They include:

1. the influence of multiple span bridges (viaducts)
2. the influence of track quality
3. the influence of stiffness/span/frequency on the resonant behaviour of the bridge

They were studied by using the same simulation method used in initial research phase.

4.2.2 Modelling

A special version of VAMPIRE with bridge module implemented was used to run simulation analysis.

For an overview of modelling setup in both research phases, see Figure 4.1. Following paragraphs will give details of modelling.

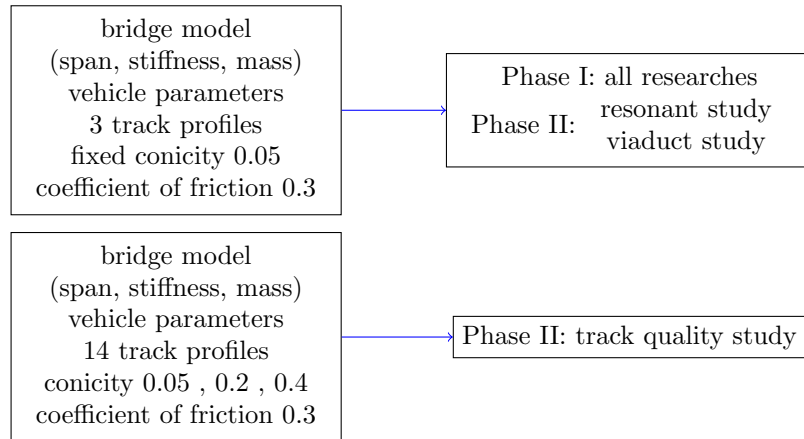


Figure 4.1: Overview of modelling setups for different studies conducted in DT329

4.2.2.1 Model of bridge

The bridge cases were modelled by assuming the bridges to behave as simply supported uniform beams. Transverse beam theory was then used to determine the frequencies and mode shapes of vibration for a given combination of span, mass per unit length and flexural rigidity. The modal information for the bridge was then used in a 'Normal Modes' analysis of the bridge.

For each case, all lateral modes of vibration up to and including 20 Hz were used. In order to prevent this artificially over-simplifying the model, if fewer than five modes were 20 Hz or less, all of the first five were used.

4.2.2.2 Bridge parameters

The spans considered were: 20 m, 33 m, 54 m, 90 m and 120 m. The flexibilities, defined as deflection of mid span over span length due to a static point load of 100 kN at mid span, are: 1/4000, 1/10000, and 1/20000. The mass per unit lengths required are: 2 tonnes/m, 6 tonnes/m, and 10 tonnes/m.

For the initial phase, see Figure 4.2 for a selection of eleven of the possible combinations examined.

Span	Flexibility	Mass/Length	Cases
20	1/10000	6	36-40, 52
33	1/10000	6	41-43
54	1/4000	2	16-20
54	1/4000	10	21-25
54	1/10000	2	1-5
54	1/10000	6	6-10
54	1/10000	10	11-15
54	1/20000	2	26-30
54	1/20000	10	31-35
90	1/10000	6	44-46
120	1/10000	6	47-51

Figure 4.2: Bridge parameter combination

4.2.2.3 Vehicle parameters

Three train types are considered: a typical freight train, a typical standard passenger train, and a typical high speed passenger train. Appendix.A details the parameters used to construct each model. In general, each model consists of a locomotive and a number of identical vehicles appropriate to the train type. The total number of axles in each train is 24. Although effects on the train are only examined on the first vehicle of each type, extra vehicles are added to the train to see what cumulative effects occur to the bridge.

The freight train consists of a British Railways Class 56 locomotive and nine UIC wagons. This has a total length of 131.56 m, which assumes a nominal vehicle coupling distance of 4 m. Runs at 60 km/h and 100 km/h are required.

The standard passenger train consists of an E444 locomotive and five UIC coaches. This has a total length of 143.8 m. It is based on one of two train models used as part of the study of the FS Bridge discussed in report RP 3 of the Committee, differing only by the addition of three extra coaches. This is required to run at 160 km/h and 200 km/h.

The high speed passenger train consists of an ETR500 locomotive and five ETR500 coaches, having a total length of 145.8 m. It is based on the other FS bridge study train model mentioned above, differing from the original by an additional three ETR500 coaches. It is required to run at 300 km/h and 350 km/h.

4.2.2.4 Track

For initial study phase, the track samples used were consistent with each train type. PSD plots of each are shown in Figures A.13 to A.15. Sample TRACKFRT.DAT was used for all analysis runs for the freight train. This is measured data from a typical BR freight line. Sample TRACKPNT.DAT was used for the standard passenger train analysis runs. This is measured data from a part of the BR East Coast main line. Sample TRACKPH.DAT was used for high speed passenger train analysis runs. This is measured data from a typical DB high speed line.

Samples of 500 m were chosen so that there would be 100 m before the bridge and at least 100 m after the bridge for all combinations of span and train length. The initial 100 m is required to check vehicle behaviour on the track irregularity alone, and the portion after the train has left the bridge is required to check that the bridge vibrations decay.

For secondary study phase, the track data used to excite the mathematical models was taken from the British Rail Research library of measured track data. For the viaduct and resonance investigations, the track files used were the same as those used in the first part of the study. For the investigation of the influence of track quality, additional track data was used so as to give the widest possible range of realistic track qualities.

4.2.2.5 Contact data

For each run the same contact data was used, consisting of rails inclined at 1:20, and wheel profiles of conicity of 0.05 (based on standard British Rail 113A rails and PI wheel profiles). The coefficient of friction applied was 0.3.

4.2.2.6 Data produced

For every analysis run the following results were obtained at intervals of 0.01 seconds.

BRIDGE DATA:

Lateral displacement at mid span Lateral acceleration at mid span

VEHICLE LATERAL ACCELERATION DATA:

Loco body at leading pivot

Leading coach/wagon body at leading pivot/axle

Loco leading bogie

Leading coach/wagon leading bogie/axle

TOTAL LATERAL FORCE DATA:

Loco leading bogie

Leading coach/wagon leading bogie/axle

LATERAL FORCES ON INDIVIDUAL WHEELS

Leading coach/wagon, first axle, left and right wheels

Leading coach/wagon, second axle, left and right wheels

Loco, first axle, left and right wheels

Loco, second axle, left and right wheels

In addition, for freight train runs, since the locomotive has two bogies of three axles, the forces on the individual wheels of the third axle were also produced.

Peak values for each of the outputs produced for the required ranges were obtained. For bridge outputs, peak values were taken for the period where any part of the train was on the bridge. For loco and leading coach/wagon outputs, peak values were taken whilst the vehicle in question was in contact with the bridge.

Peak values for each output were then read into a spread sheet where they could be compared more easily to check for emerging trends. The spread sheet has been partially automated to produce graphs of a single output for each train type for a single varying bridge parameter, for given values of the other bridge parameters. Figures 4 to 30([4]) show typical plots which have been produced in this manner.

4.2.3 Investigation of resonance phenomenon studied in DT329

2 types of resonance were studied in DT329, including:

1. Resonance caused by axle repeat pattern
2. Resonance caused by kinematic movement

The summary of these resonances effects are presented in following paragraphs.

Frequency shift phenomenon is an important characteristics observed from resonance effects lists above. It is explained in Section 4.2.3.3

4.2.3.1 Resonance caused by axle repeat pattern

Axle repeat patterns are wavelength phenomena - regardless of vehicle speed, the repeat length is constant. However, since frequency is speed divided by wavelength, the frequency of the axle repeat patterns vary with train speed. A table of axle repeat pattern lengths, and typical frequencies arising from train speed are given in Figure.A.1

By running train at different speeds shows resonance is possible between train and bridge if the axle passing frequency coincides with the first lateral bridge mode. The effect occurring in bridge lateral displacement over a limited frequency range around the resonance frequency.

However, the speed on theory which should yield resonance effect may be different from the speed that actually triggered resonance.

4.2.3.2 Resonance caused by kinematic movement of trains

Kinematic wavelength also gives rise to frequencies which vary with speed for the same reason. For first lateral bending mode coincidence with kinematic frequency, the kinematic wavelength of each train type had to be established, by running each train at a range of typical operating speeds over a discrete lateral irregularity, and examining the frequency content of the lateral wheel motion. The resulting wavelength ranges are tabulated in Table.A.2. See Figure 4.3 for an overview of workflow of this study.

The most likely possible resonance in the initial studies to be of this type was between the passenger train at 200 km/h (55.556 m/s) on passenger track and BR PI wheel profiles, and a span of 54 m, stiffness 1/10000, mass/length of 6 tonnes/m. This combination was examined by varying the speed between 55.556 - 64.6 m/s over the span, and by varying the stiffness of the span between 117000 and 1112000 running the train at 55.556 m/s. Another combination was examined - the ETR500 train running between 65 - 80 m/s on high speed track and BR PI wheel profiles, for a span of 38 m, stiffness 1110000, and mass/length 10 tonne/m; the span in this case was chosen to coincide with the kinematic wavelength of the coaches.

Coincidence of vehicle kinematic frequency with bridge first lateral bending mode may cause resonance to occur over a broad range of frequencies to a less pronounced effect than coincidence of axle passing frequencies. Evidence of coincidence of kinematic wavelength with length of span has been found in the lateral acceleration of bridges, but was not demonstrated in the lateral bridge displacement in the cases examined. For short kinematic wavelengths, this effect could not be seen, possibly because of lack of time for the bridge to respond.

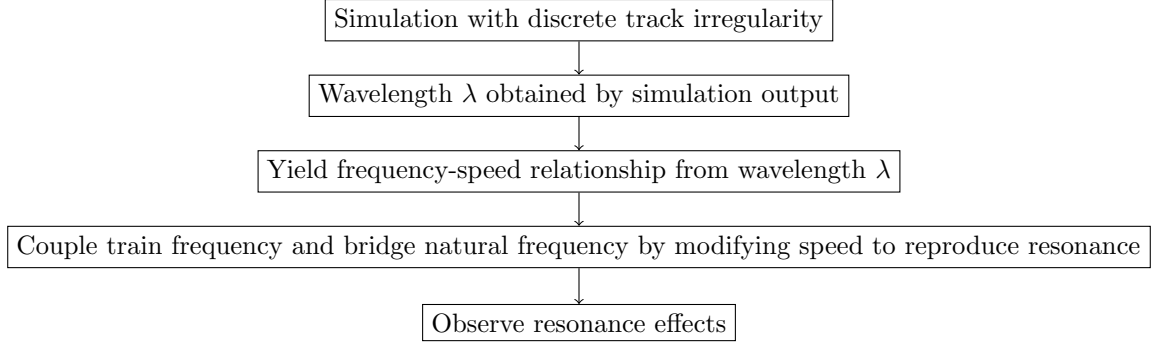


Figure 4.3: Workflow of kinematic resonance research

4.2.3.3 Apparent shift in resonance frequency

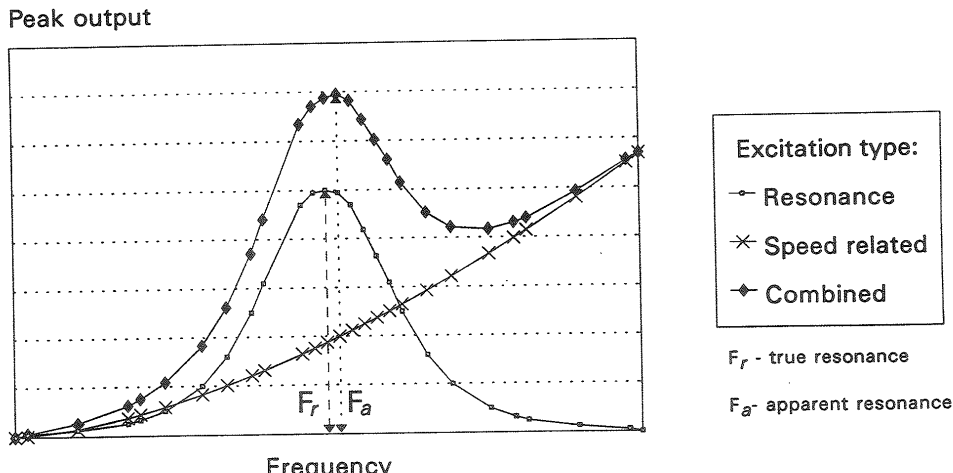
It is frequently observed in the output of both resonance effects that apparent resonance happens at some frequencies higher than frequencies calculated on theory. This is explained in following quote on [4, Page 13, Secondary Phase]. However, the explanation wasn't verified by further studies. They can only be treated as hypothesis.

Although the peak mid span displacement was expected to occur at 28.5 mis, it can be seen that for the runs with just the coaches that the peak occurs at about 32 m/s. This is confirmed to be a resonance-type effect rather than a discrete event in the time histories of the runs, a selection of which are shown in Figure C6(Original report), of which an extract of 100-285m follows as Figure C7(Original report). This speed is mid way between axle passing frequency coinciding with first bending mode of the bridge, and kinematic frequency coinciding with the first bending mode. So, the apparent shift in resonant frequency may be due to a combination of these effects (see discussion of kinematic frequency resonance results). However, an alternative explanation may be that as track forces generally increase with speed, the deflection of the span would be expected to increase. If this effect continued through a resonant band, the peak displacement would appear greater at a speed slightly above that calculated for resonance, as sketched in Figure 4.4.

In the sketch of possible explanation of apparent shift in resonant frequency(Figure 4.4), the combined effect is the superposition of both resonance effect and speed-related effect. Speed-related effect simply increase when speed increase regardless of resonance. Speed is linear to frequency. Thus speed-related effect also simply increase when frequency increases. Resonance effect has an impact where frequency of train and bridge coincides. Speed-related effects is the cause for the frequency shift of combined peak output.

Both explanations indicate that apparent resonance frequency can hardly be predicted. Apparent frequency may even shift into domain lower than theory frequency.

Sketch of Possible Explanation of Apparent Shift in Resonant Frequency



ERRI D181 PARAMETER STUDY
DJ/82879/D001
British Rail Research

Figure C8

Figure 4.4: Sketch of Possible Explanation for Apparent Shift in Resonant Frequency. Extract from [4, Appendix 2]

4.3 Investigation of RP6

4.3.1 Debate on proposed 1.2Hz criterion

The value of frequency limit, 1.2Hz is explained in [5, p3.2: Criterion 2]:

To avoid the occurrence of resonance in the lateral motion of the vehicles due to the lateral motion of the bridge, a limit value lower than the first natural frequency f_{1t} of the lateral vibration of the span studied should be fixed. The natural frequency for lateral movements is between 0.5 and 0.7 Hz for coaches and between 0.7 and 1 Hz for locomotives. We therefore propose a safety margin $F_{lt} \geq 1.2\text{Hz}$

The original author of report RP6 Graham Scott was contacted to reveal the background of 'natural frequency for lateral movements'. Mr.Scott is still in charge of the development of software VAMPIRE and he's still active in the field. Unfortunately he was unable to remember what did 'natural frequency for lateral movements' stand for in previous quotes since it was written nearly 20 years ago. He passed me to his colleague Alan Minnis for further questions. Mr.Minnis stated following:

Looking at the values I think they would refer to typical rigid body modes of a vehicle. These are independent of speed and a typical passenger coach with air suspension will have a lower sway frequency of around 0.6Hz which is within 0.5-0.7Hz. Locomotives tend to have a slightly stiffer suspension hence the slightly higher frequency range.

Mr. Minnis statements, combined with results yielded in supporting parametric report DT329 proves 1.2Hz criterion is aiming to avoid occurrence of resonance. But this isn't a feasible strategy in following reasons:

1. The resonance between rigid body mode of train and first lateral vibration mode of the bridge has never been discussed in all D181 report series. No research proofed this kind of resonance can be critical in real life scenario.
2. There are lots of evidence can be found in report DT329, showing resonance can happen on a bridge with a first lateral natural frequency even higher than 1.2Hz, which is self-conflicting with 1.2Hz criterion. In fact, the resonance could happen at any frequency on theory. However, the magnitude of resonance effect ranges from less pronounced to more pronounced from case to case.

For example, [4, Page 14, Phase II] shows resonance occurs on 1.71Hz:

The first lateral bending mode of this bridge is at 1. 71 Hz. The kinematic wavelength of the passenger coaches is around 34-38 m, giving a kinematic frequency range of 1.46 - 1.63Hz. Speeds of 58.14 m/s(1.53-1.71 Hz) and 64.6m/s(1.7-1.9Hz) were also done. The mid span lateral displacement for each of the time histories are shown in Figure C12(Original report). The slowest speed appears to show the greatest resonance.

4.3.2 Lateral forces on railway bridges

4.3.2.1 Basic characteristics of lateral force on railway bridges

It is concluded in initial phase of the study that presence of the bridge doesn't influence the track forces and track quality is a major factor in determining the lateral forces generated by a particular train on [4, Page 7, Secondary Phase]

From the initial study [1], it was concluded that the track quality on a bridge is a major factor in determining the lateral forces generated by a particular train. The D181 Committee therefore asked BRR to determine the peak track forces generated over a wide range of track qualities.

The length of a bridge is small compared to the overall length of a railway track and so track quality on a single bridge may not be representative of that on other bridges on the same route. However the initial study concluded that, in general, the lateral track forces are not influenced by the presence of the bridge.

The resonance effects mentioned in the previous sections were only observed in deflection and acceleration domain due to the reason that the presence of the bridge doesn't influence the track forces.

Influence on the total lateral force as a result of hunting of single vehicle bodies were examined. Three parameters were involved in this parametric research. They were vehicle speed, track irregularities deviation and wheel conicity.

Vehicle speed plays a key role. When speed is 60 km/h for freight trains, in the response output, there is very limited influence by increasing both track deviation and conicity. Different conicity tends to yield same force output. Same as track deviation. See Figure B1.

When speed increases, output of different conicity on same track deviation is more scattered. Similarly, increased deviation yields greater output. They are two basic trends observed in all output data.

However, it is uncertain which conicity will yield greater output compared to other 2 conicity setups. Surprisingly, in some cases, best maintained wheel profile (effective conicity 0.05) generates greater output than poorly maintained wheels (effective conicity 0.4). See Figure B2. The most

obvious case of this kind is freight train running at 100 km/h on track with 5.7mm (approximate) deviation.

Different from conicity, the influence of increasing track deviation is simply predictable. Research report DT329 provided approximate linear function for relationship between lateral force and track deviation. These linear functions can be extracted from plots B1-B30 of DT329.

Since peak force output of 120 km/h freight train and 200 km/h passenger train are close(2% difference), it is reasonable to conclude that passenger train tends to yield smaller result than freight train at same speed. This is probably due to passenger trains have more sophisticated suspension system designed to suppress lateral motion of the vehicle. Unfortunately, only one speed of 200km/h configuration was available in DT329. But since freight train yields greater output, it is conservative for designer to adopt force output of freight trains for speeds of 60km/h, 100km/h, 120km/h.

It is worthy to point out a suspicious mistake of DT329 in Table.4.1. Report claimed that output data were filtered by statistical analysis. The peak lateral track force was determined from a statistical analysis of lateral track forces as $M \pm 3\sigma$ where M is the mean lateral force value over the segment and σ is the standard deviation over the segment. It does not give a true maximum lateral force but on which is greater than 99.5% of all force values. It is obvious in Table.4.1 that output data of 160kN for freight train wagon was not filtered by statistical analysis. It is the greatest value among all raw output data of freight train running at 100 km/h. See Figure B7. This data of 160kN also illustrates that peak forces will be influenced by discrete features in the track geometry which may not be reflected thoroughly in the standard deviation. This thesis report suggest substitute 160kN with 80kN(value by approximate observation). See Table.[note1]4.1

Table 4.1: Peak Lateral Track Force Over All Track Qualities. Extracted From [4, Tab. B1]

Peak lateral force(kN)	Locomotive	Total	Coach/Wagon	Total
Freight 60 km/h	50		60	110
Freight 100 km/h	90		160(80) ¹	250(170) ¹
Freight 120 km/h	75		110	185
Passenger 200 km/h	140		50	190
High Speed 350 km/h	125		125	250
Passenger 200 km/h(worn wheels)	190		80	270
High Speed 350 km/h(worn wheels)	330		225	555

Note1: Force value 160kN for wagon of freight train running at 100 km/h is not representative. But it is not filtered by statistical analysis. It is advised to substitute 160kN with 80kN. 80kN is obtained by approximate observation of [4, Figure B7]. As a result, total force is reduced from 250kN to 170kN.

Speed and track quality are two most sensitive parameters. Control of track quality is more advisable compared to control of wheel conicity due to the reason that influence of track quality deviation is simply approximate linear to force output, whereas influence of wheel conicity has an unpredictable characteristic. Moreover, track quality can be controlled by using a maintenance regime.

4.3.2.2 Refining of lateral force model

Figure.4.5 is created to plot total peak force illustrated in Table.4.1. 5 sets of data available were used to create the plot. 3 of them are data of freight train running at 60km/h, 100km/h and 120km/h. The other 2 sets of data are passenger train running at 200km/h and high speed train running at 350km/h respectively. Data produced with worn wheels profiles are neglected because they are not representative for normally maintained railway vehicles. Adjacent points were connected by solid

lines. Different colour stands for different train types. Red lines and dots stand for freight trains. Blue stands for passenger trains and black stands for high speed trains.

It is indicated that freight trains tends to have the biggest lateral force on track compared to other two kind of trains. And high speed train has lowest lateral force on track. This can be explained by freight trains possessing the most stiff suspension systems, while high speed trains possessing complicated suspension system to suppress lateral motion.

It can also be concluded that the relationship between lateral force and speed is not linear. As a general phenomenon observed, force increment decreases as speed increases. Regressions were made to better illustrate the trend of lateral force increment. Please note these regressions are only sufficient within the speed range plotted.

The first regression made was on freight train because it has the most sets of data. The form of function should satisfy:

1. 0kN lateral force when speed is 0km/h
2. Simply increasing in value but generally decreasing in increment

Finally function form $F = a * v^b$ is selected because its satisfying characteristics. R language was used to perform regression process. The regression result is also in good likelihood with original data. Achieved convergence tolerance was 2.868e-06. The result is presented in Formula.4.1. See Appendix.D for code.

$$F_{lf} = 5.2064 \cdot v^{0.7495} \quad (4.1)$$

Since 1 set of data is available for passenger train, Formula.4.1 is scaled by a constant factor to create regression for passenger trains. Please note that this regression can not be verified because lack of data. However, since freight train has a greater lateral force then passenger train, it is conservative to adopt lateral force of freight train when calculating consequences related to passenger trains. It is still reasonable to adopt this regression since passenger trains are just simply less stiff than freight trains.

Unfortunately, conducting such transient simulations is extremely time and resource consuming. It is impossible for this thesis to carry out more simulations to verify the sufficiency of following scaled regression. More data on passenger train and high speed train is recommended to be produced by future researches.

The scale factor k_{pf} is obtained by comparing force value yielded by Formula.4.1 at 200km/h and original passenger train force(190kN) data at 200km/h.

$$k_{pf} = \frac{190}{a_{lf} \cdot 200^{b_{lf}}}$$

$$a_{lp} = a_{lf} \cdot k_{pf}$$

merge above two equations, yield

$$a_{lp} = \frac{190}{200^{b_{lf}}} = \frac{190}{200^{0.7495}} \approx 3.58$$

and

$$F_{lp} = a_{lp} \cdot v^{0.7495}$$

thus

$$F_{lp} = 3.58 \cdot v^{0.7495} \quad (4.2)$$

Lateral force for high speed train were obtained in same manner. The scale factor k_{hf} is obtained by comparing force value yielded by Formula.4.1 at 350km/h and original high speed train force(250kN) data at 350km/h.

$$k_{hf} = \frac{250}{a_{lf} \cdot 350^{b_{lf}}}$$

$$a_{lh} = a_{lf} \cdot k_{hf}$$

merge above two equations, yield

$$a_{lh} = \frac{250}{350^{b_{lf}}} = \frac{250}{350^{0.7495}} \approx 3.10$$

and

$$F_{lh} = a_{lh} \cdot v^{0.7495}$$

thus

$$F_{lh} = 3.10 \cdot v^{0.7495} \quad (4.3)$$

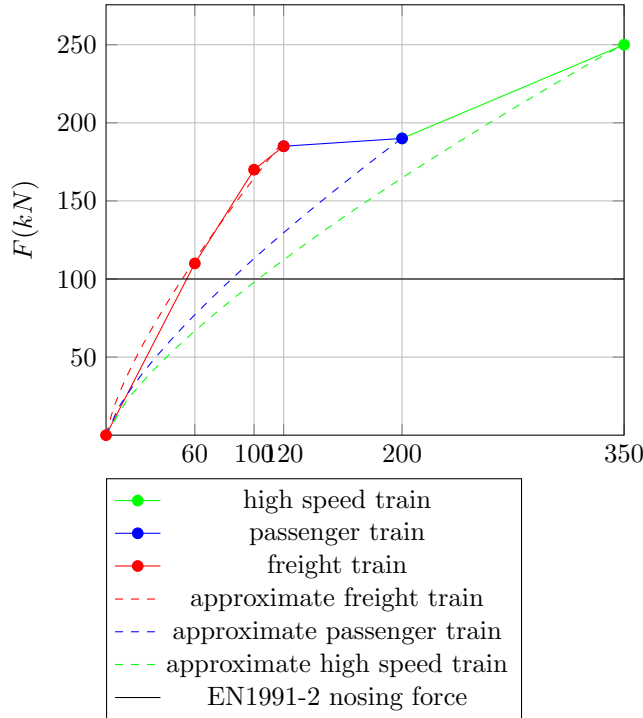


Figure 4.5: Total peak lateral track forces over all track qualities(worn profile scenario neglected)

4.3.2.3 Application of lateral force model

Formula 4.1, 4.2 and 4.3 can be used as load forces for different design scenario. However, these loads are normally higher than the load defined in EN1991-2[10, 6.5.2 Nosing force]. EN 1991-2 states that the characteristic value of the nosing force shall be taken as $Q_s k = 100\text{kN}$.

It is worthy to note that although in RP6[5, Proposed criteria] several load model with loading magnitude ranging from 70 kN to 270 kN were originally proposed, EN1991-2 uses a single characteristic value of 100 kN for all design scenarios.

Since no document has explained this modification, this is probably due to the consideration of lower track irregularity deviation during the creation of EN1991-2.

As explained in previous chapter, peak force is generally linear to track standard deviation. Most of the peak lateral force described in DT329 was obtained on track with 7mm standard deviation, while EN13848-5[2] allows much lower track standard deviation defined in Table 2.1. This means peak lateral force on tracks(if maintained according to Eurocode regulations) is also much smaller than peak force obtained in DT329.

EN1991-2 states the usage of nosing force. See 3.3.1. Moreover, since loading model is obtained in Figure.4.5, a response solution of the bridge can also be obtained.

This can be done by using the solution in 2.5.3 and substitute peak force into the formula as the amplitude of harmonic force F . Development of this method is presented in Chapter.

It should be noted that the proposed model in RP6, as well as modified model in EN1991-2, is based on the investigation of first two traction units of the train. It is suspected that when bridge is longer, more traction units can run on the bridge simultaneously, introducing bigger force to the bridge. This can lead to a problem that EN1991-2 is non-conservative in the magnitude of nosing force when applied to longer bridges. However, this suspecting hypothesis is not verified in this chapter.

4.4 Conclusion of D181 report series

The report series managed to create load models for lateral dynamics railway effects. It is worthy to note that the lateral force on the track wasn't influenced by the presence of the bridge. The major influencing parameter for lateral force is track quality and conicity of the wheel profile.

The resonance phenomenon was successfully reproduced and observed, though its only visible in deflection and acceleration domain. A basic characteristic of resonance, regardless of the type of resonance, is that apparent resonance frequency will shift from resonance frequency calculated on theory. The shift is unpredictable in the sense of both direction and magnitude. The effect related to speed start to creep in when speed is higher, making the effect of resonance less pronounced in higher speed(Figure 4.4).

Please note that every bridge will always have resonance with running train because axle repeat pattern and kinematic movement are both wavelength phenomenon, which means there is always a speed of train yielding a vibration frequency coincides with the first lateral natural frequency of bridge. However, the effect of resonance happening on long-span bridge is usually unpronounced since the speed of the train is low as 2.5m/s to 14m/s when resonance occurs.

Some of the conclusion and proposed criteria in RP6 were adopted in Eurocode 1991-2. One of them is 1.2Hz criterion. It was adopted without amending. The other one is lateral force models. They were adopted in a different name as 'nosing force' in [10, A6.5.2].

The 1.2Hz criterion was under debate and proofed unreliable in fulfilling its original intention, avoiding occurrence of resonance. There is no research in D181 report series supporting this criterion, nor there exists literature behind the natural frequency of vehicles. This criterion ignored the fact of future bridge designs with long span would certainly have a natural frequency lower than 1.2 Hz. It is advised that Eurocode review this criterion and revise it.

Chapter 5

Study on vehicle wavelength

5.1 Effects investigated in wavelength study

Effects investigated in this report will be the same effects investigated in DT 329, which is described in Sec.???. However, according to the statement in Sec.2.3[Summary of results] in the same report,

Even when the axle repeat frequency matches the first lateral bending mode of each span, there is no evidence that the resonant behaviour of the span and train has any effect on subsequent spans, since the resonant effects do not appear to grow from span to span.

the third investigated resonance effect 'coincidence between the length of the span and the kinematic wavelength of the trailing vehicles' is neglected in this thesis.

5.2 Speed range of dynamic consideration

The thesis will focus on normal speed trains because IV-Groep is only interested in normal speed train lines, which its projects are being built for. Higher boundary is set according to maximum speed allowed on Dutch railways, while lower boundary is set according to an estimation. The reason for a lower boundary speed is that dynamics issues for railway infrastructures increase with respect to vehicle speed, which means generally less concern is needed when the speed of train is low. It's certain that there exists a threshold of speed for every type of train that dynamic behaviour of them start to be a problem to concern but this threshold of speed varies from different scenarios. Till now no solid research can give a value to this threshold of speed so this is why estimation of lowest speed is adopted.

My assumption of lower boundary of speed for consideration is 120 km/h. This is still very conservative because according to logic diagram Eurocode 1991-2[10], dynamic check is always needed when $V \geq 200\text{km/h}$ for vertical direction. Under same speed, the kinematic energy passed to bridge by running vehicle in vertical direction is apparently higher than that in lateral direction on a straight track. So it is believed that in lateral direction, the threshold will be even higher than 200 km/h according to Eurocode 1991-2. Value 120 km/h is taken according to [11, Appendix F]: *Speeds which do not require dynamic compatibility checks* where 120 km/h is the lowest speed can be found in the table, excluding special vehicle. This table is attached in this thesis in Appendix.B.

Upper boundary for consideration:

Normal trains running on Dutch railway has a speed limit of 160 km/h so the upper boundary for speed is set to 160 km/h, which is also 44.44 m/s.

$$V_{max} = 44.44\text{m/s}$$

Lower boundary for consideration:

$$V_{min} = 33.33m/s$$

However, it is strongly advised that future research investigate the lowest speed threshold for dynamic for consideration for train vehicles in the Netherlands due to the fact that the lower boundary used in this thesis is an assumption.

5.3 Equivalent conicity used in this study

According to [9, Section.2.6],

Practical research has shown that over a period of time wheel profiles stabilise with wear at an equivalent conicity of 0.2 to 0.3. With regards to running stability, the equivalent conicity must remain below 0.4 and to ensure the centering effect it must be greater than 0.1.

conicity range will be 0.2 to 0.3.

It is suggested that vehicle maintenance sector ensure wheels of train wheels stay in the safe zone of conicity.

5.4 Study on frequency of Klingel movement

Klingel movement is proposed by Klingel which can well predict the moving trend of a single wheelset on a straight railway track. However, the kinematic movement of a certain wheelset assembled into a running train is different from the movement of a single free wheelset. This is due to multiple bodies interact with each other, introducing more complicated mechanism in wheel/rail interaction.

This parametric study focuses on Klingel movement of a single wheelset. First part of the parametric study will try to discuss the relationship of Kiingle frequency of a wheelset and kinematic movement frequency of a whole train. Second part of the parametric study will use realistic data of Dutch railway/vehilces to assess the frequency bandwidth of Dutch native trains.

Parametric to be studied:

Speed of train, radius of the wheel and conicity of the wheel.

Gauge distance is fixed to 1435mm according to UIC standard.

Frequency is linear to speed if other parameters are fixed.

5.5 Comparison between Klingle movement and train kinematic movement studied in D181 DT329

By comparing the result from above parametric study and kinematic wavelength obtained by D181, presented as table.C2 in original report, parametric study results show close prediction for kinematic wavelength of freight train locomotive/coach/wagon. It's because freight train suspension system is simpler and stiffer compared to passenger train's, making the behaviour of train acts more similar to the behaviour of a single wheelset of bigger mass. However, results of wavelength of single wheelset is 33% shorter than kinematic wavelength of train because suspension system of passenger coaches are much more sophisticated. The wavelength of passenger coach is highly related to the characteristics of its suspension systems. These data is often difficult to obtain.

The train parameter used in this part of parametric study is attached in the Appendix.C.

Table 5.1: Add caption

	Gauge	BWD	Radius	Conicity	Wavelength_0()	Wavelength	Freq
BR CLASS 56 LOCOMOTIVE	1435	1500	290	0.0500	12.8175	18.5418	
FS E444 LOCOMOTIVE	1435	1500	550	0.0500	17.6517	25.5349	
FS ETR500 LOCOMOTIVE	1435	1500	550	0.0500	17.6517	25.5349	
UIC FREIGHT WAGON (LADEN)	1435	1500	460	0.0500	16.1430	23.3524	
FS ETR500 COACH	1435	1500	440	0.0500	15.7882	22.8391	
UIC COACH	1435	1500	445	0.0500	15.8776	22.9685	
	1435	1500	500	0.0250	23.8016	34.4313	
	1435	1500	500	0.2000	8.4151	12.1733	
	1435	1500	500	0.3000	6.8709	9.9395	
	1435	1500	460	0.0250	22.8297	33.0253	
	1435	1500	460	0.2000	8.0715	11.6762	
	1435	1500	460	0.3000	6.5904	9.5336	

5.6 Assess of frequency bandwidth based on realistic data of Dutch Rail/Vehicle

The wavelength of passenger coach is highly related to the characteristics of its suspension systems. These data is often difficult to obtain. To establish an easy approach, wavelength of passenger train calculated in this section will be multiplied by an amplification factor of 1.5. This value is obtain by train wavelength/wheelset wavelength ratio in previous parametric study. Please note this factor is an estimation. However, wavelength of freight train is not modified due to the conclusion that freight train's suspension system is stiff enough for the Klingel movement of a single wheelset to describe the kinematic movement of a whole freight train.

However, future research is highly recommended to be conducted to study the kinematic wavelength of complete vehicles in the Netherlands, using realistic data of their suspension systems.

Klingel's formula: Klingel has done experiments and has given that the wavelength of a single wheelset:

$$\lambda_0 = 2\pi \sqrt{\frac{rG}{2\gamma}}$$

where:

G = Dynamic Gauge

r = Dynamic Wheels Radius

g = Conicity

For 2 wheelsets connected by a bogie:

$$\lambda = \lambda_0 \sqrt{1 + \left(\frac{I}{G}\right)^2}$$

where:

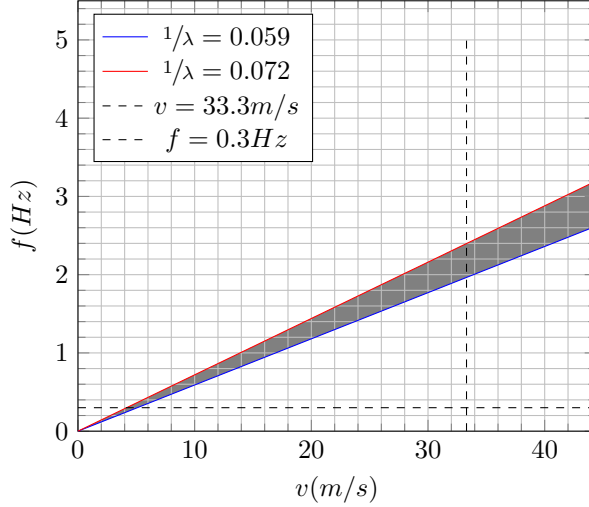
I = Rigid wheel base

Thus range of λ is obtained by inputting data discussed in previous sections of this chapter.

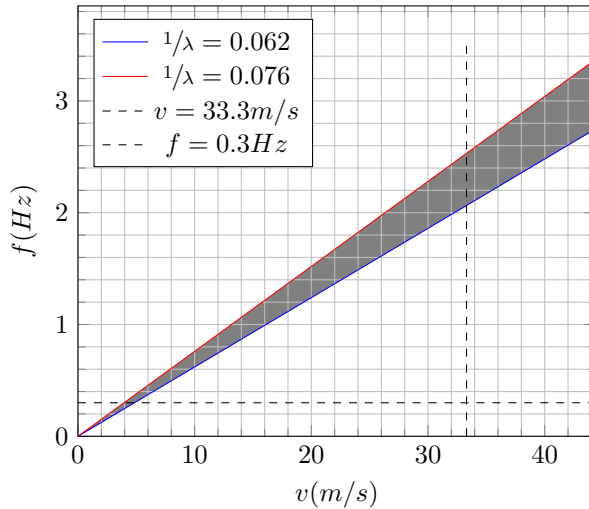
Following plots are generated according to linear relationship between frequency and speed:

$$f = v \frac{1}{\lambda}$$

Lateral frequency of freight train with respect to speed



Lateral frequency of passenger train with respect to speed



5.7 Study on frequency caused by axle repeat pattern

Following wavelength of axle repeat pattern is obtained by extracting MU standards in [11]. Detailed information can be found in Appendix.C

Range of wavelength(m) of first repeat pattern mode:

$$\lambda_{1stRepeat} \in (9.2, 9.8) \cup (12.8, 13.5) \cup (14.9, 16) \cup (17, 17.5) \cup (18.7, 19.5) \cup (23.8, 27.5)$$

Range of wavelength(m) of second repeat pattern mode:

$$\lambda_{2ndRepeat} \in (18.4, 19.6) \cup (25.6, 27) \cup (29.8, 32) \cup (34, 35) \cup (37.4, 39) \cup (37.6, 55)$$

Table 5.2: Wavelength of axle repeat pattern(m)

Type	L_coa min	L_coa max	2*L_coa min	2*L_coa max
CB_1	23.8	25.3	47.6	50.6
CB_2	25.3	27.5	50.6	55
AB_1	14.9	16	29.8	32
AB_2	18.8	19.5	37.6	39
AB_3	17	17.5	34	35
AB_4	18.7	19.2	37.4	38.4
SA_1	9.2	9.8	18.4	19.6
SA_2	12.8	13.5	25.6	27

Range of frequency(Hz) yielded by dividing 1m/s with wavelength of first repeat pattern mode:

$$\frac{1}{\lambda_{1stRepeat}} \in (0.036, 0.042) \cup (0.051, 0.053) \cup (0.057, 0.059) \cup (0.063, 0.067) \cup (0.074, 0.078) \cup (0.102, 0.109)$$

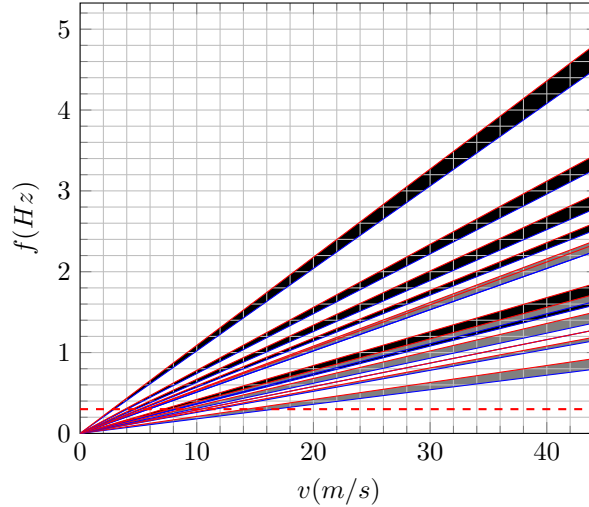
Range of frequency(Hz) yielded by dividing 1m/s with wavelength of second repeat pattern mode:

$$\frac{1}{\lambda_{2ndRepeat}} \in (0.018, 0.021) \cup (0.026, 0.027) \cup (0.029, 0.029) \cup (0.031, 0.034) \cup (0.037, 0.039) \cup (0.051, 0.054)$$

Following plot is generated according to linear relationship between frequency and speed:

$$f = v \frac{1}{\lambda_{repeat}}$$

Two repeat pattern frequencies with respect to speed



5.8 Conclusion of wavelength study

This wavelength study illustrates a tool of obtaining danger zone for train speed for a specific bridge first lateral natural frequency.

For example, if a bridge has a first lateral natural frequency of 0.3Hz:

1. To avoid resonance between freight train and bridge caused by kinematic frequency coincidence, speed of train should be regulated above 4m/s
2. To avoid resonance between passenger train and bridge caused by kinematic frequency coincidence, speed of train should be regulated above 5m/s
3. To avoid resonance caused by axle repeat pattern, speed of train should be regulated above 16m/s

As a conclusion, if the speed of train is regulated above 16m/s, there won't be resonance between bridge and train.

Chapter 6

Fundamental of analytical approach to be adopted in practical checking method

6.1 Introduction

This chapter aims to give a preliminary knowledge of a selected analytical model that simulates the perfect resonance scenario for railway bridge under lateral dynamic load. The knowledge contains the simplified model itself, its assumptions, field of application and explicit solutions.

The output response of the solution to the analytical model is able to provide the maximum bridge response in worst case scenario. Thus it is sufficient to be adopted in practical purposes for verifications of lateral railway bridge dynamics.

6.2 Overview

To give a clear view of this chapter, following overview is created:

1. The model, its assumptions and field of application.
2. Procedure of solution deduction
3. Damping

6.3 The model, its assumptions and field of application

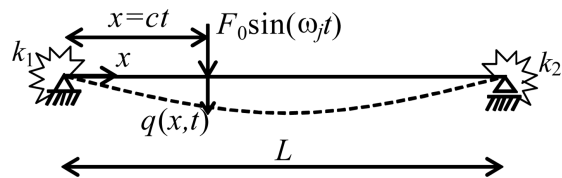


Figure 6.1: Schematic representation of a generic beam crossed by a harmonic load

Presented in Figure 6.1, the model features a simply supported beam which is the simplification of bridge structure and a moving harmonic load introducing resonant dynamic effects caused by the presence of moving train.

The beam is assumed to be uniform in both geometry and material. The stiffness of the beam is the equivalent uniform lateral bending stiffness of the bridge.

The load is moving in the same speed as the train. The magnitude of load amplitude in going to be discussed in the following chapter. And the load's self vibration frequency is equal to the first natural lateral bending frequency of the beam.

This model is valid for single span railway bridges that has a sinuous first natural lateral vibration shape.

6.4 Solution deduction

Solution provided by Fryba[13] is used to analyse the problem. A harmonic moving along a beam is a fundamental dynamics topic and was first solved by S.P.Timoshenko. Fryba further deduced the basic results, and set them forth in the form of useful formulae. This model is used to simulate a perfect resonance scenario which yields conservative results for designing and checking of the dynamics behaviour of the bridge. Deduction procedure is extracted from [13, Section II.2.1] and presented below.

The solution of the problem of a harmonic concentrated force moving at constant speed c over a simply supported beam with span l is carried out under the same assumptions as that discussed in Chap. 1. The time-variable concentrated force is of the form

$$P(t) = Q \sin \Omega t \quad (6.1)$$

where Q is the amplitude and Ω is the circular frequency of the harmonic force. Vibration of the beam is then described by the equation

$$EJ \frac{\partial^4 v(x, t)}{\partial x^4} + \mu \frac{\partial^2 v(x, t)}{\partial t^2} + 2\mu\omega_b \frac{\partial v(x, t)}{\partial t} = \delta(x - ct)Q \sin \Omega t \quad (6.2)$$

by the boundary conditions (1.2) and by the initial conditions (1.3). The symbols used in 6.2 have the same meaning as those of Chap. 1.

Eq.6.2 together with conditions (1.2) and (1.3) will again be solved by the method of integral transformations. Following the Fourier sine transformation according to (1.9), Eqs.6.2 and (1.2) give

$$\frac{d^2 V(j, t)}{dt^2} + 2\omega_b \frac{dV(j, t)}{dt} + \omega_{(j)}^2 V(j, t) = \frac{Q}{\mu} \sin \Omega t \sin j\omega t \quad (6.3)$$

Solving the above with (1.3) by the Laplace-Carson transformation (1.15) - making use of Eq.(27.24) in doing so and of the notation

$$r_1 = \Omega + j\omega; \quad r_2 = \Omega - j\omega \quad (6.4)$$

we get

$$V^*(j, p) = \frac{Q}{2\mu} \left(\frac{1}{p^2 + r_2^2} - \frac{1}{p^2 + r_1^2} \right) \frac{p^2}{(p + \omega_b)^2 + \omega_{(j)}'^2} \quad (6.5)$$

After inverse transformations of Eq.6.5 according to (27.24) and (1.9) the required result for $t \leq T$ is

$$\begin{aligned}
v(x, t) = & \sum_{j=1}^{\infty} \frac{Q}{\mu l} \left\{ \frac{1}{(\omega_{(j)}^2 - r_2^2) + 4\omega_b^2 r_2^2} [(\omega_j^2 - r_2^2)] (\cos r_2 t - e^{-\omega_b t} \cos \omega_{(j)}' t) \right. \\
& + 2\omega_b r_2 \sin r_2 t - \frac{\omega_b}{\omega_{(j)}'} (\omega_{(j)}^2 + r_2^2) e^{-\omega_b t} \sin \omega_{(j)}' t] \\
& - \frac{1}{(\omega_{(j)}^2 - r_1^2)^2 + 4\omega_b^2 r_1^2} [(\omega_{(j)}^2 - r_1^2) (\cos r_1 t - e^{-\omega_b t} \cos \omega_{(j)}' t) + 2\omega_b r_1 \sin r_1 t \\
& \left. - \frac{\omega_b}{\omega_{(j)}'} (\omega_{(j)}^2 + r_1^2) e^{-\omega_b t} \sin \omega_{(j)}' t] \right\} \sin \frac{j\pi x}{l}
\end{aligned} \tag{6.6}$$

We shall now simplify Eq.6.6 to fit the case most frequently met with in practical applications. Thus, for example, it is entirely satisfactory to use only the first of its terms ($j = 1$); further, as we know from Chap. 1, parameters α and β are usually much smaller than 1 ($\alpha = \omega/\omega_{(1)} \ll 1$, $\beta = \omega_b/\omega_{(1)} \ll 1$). And finally, since in practice a harmonic force is always accompanied by a constant force P , we shall introduce in 6.6 also the deflection v_0 according to (1.21). Following these simplifications Eq.(2.6) takes on the form

$$\begin{aligned}
v(x, t) = & v_0 \frac{Q \omega_{(1)}^2}{p \Omega^2} \frac{1}{(\frac{\omega_{(1)}^2}{\Omega^2} - 1)^2 + 4(\frac{\omega^2}{\Omega^2} + \frac{\omega_b^2}{\Omega^2})} \left\{ \left[\left(\frac{\omega_{(1)}^2}{\Omega^2} - 1 \right)^2 \right. \right. \\
& + 4 \frac{\omega_b^2}{\Omega^2}]^{1/2} \sin(\Omega t + \varphi) \sin \omega t \\
& \left. \left. + 2 \frac{\omega}{\Omega} (\cos \Omega t \cos \omega t - e^{-\omega_b t} \cos \omega_{(1)} t) \right\} \sin \frac{\pi x}{l}
\end{aligned} \tag{6.7}$$

where

$$\tan \varphi = - \frac{2\omega_b/\Omega}{\omega_{(1)}^2/\Omega^2 - 1} \tag{6.8}$$

The beam reaches the state of highest dynamic stressing in the region of resonance, i.e. whenever Ω is close or just equal to $\omega_{(1)}$, i.e.

$$\Omega = \omega_{(1)} \tag{6.9}$$

In such a case Eq.6.7 can further be simplified to

$$v(x, t) = v_0 \frac{Q\omega_{(1)}}{2P} \frac{\cos \omega_{(1)} t}{\omega^2 + \omega_b^2} [\omega (\cos \omega t - e^{-\omega_b t}) - \omega_b \sin \omega t] \sin \frac{\pi x}{l} \tag{6.10}$$

According to (1.21)

$$v_0 = \frac{Pl^3}{48EJ} \approx \frac{2P}{\mu l \omega_{(1)}^2} = \frac{2Pl^3}{\pi^4 E J} \tag{6.11}$$

substitute v_0 into Eq.6.10

$$v(x, t) = \frac{l^3 Q \omega_{(1)}}{\pi^4 E J} \frac{\cos \omega_{(1)} t}{\omega^2 + \omega_b^2} [\omega (\cos \omega t - e^{-\omega_b t}) - \omega_b \sin \omega t] \sin \frac{\pi x}{l} \tag{6.12}$$

And the mid-span response time-history for deflection is :

$$v(l/2, t) = \frac{l^3 Q \omega_{(1)}}{\pi^4 E J} \frac{\cos \omega_{(1)} t}{\omega^2 + \omega_b^2} [\omega(\cos \omega t - e^{-\omega_b t}) - \omega_b \sin \omega t] \quad (6.13)$$

Above expression is the ready-to-use expression being adopted in practical checking method to be discussed in following chapter.

6.5 Damping

Damping is an important parameter influencing the dynamic behaviour of a structure. 6.2 uses a different form of damping expression ω_b , which can be converted from normal damping coefficient. Equation of motion using damping coefficient:

$$E J \frac{\partial^4 v(x, t)}{\partial x^4} + \mu \frac{\partial^2 v(x, t)}{\partial t^2} + \chi \frac{\partial v(x, t)}{\partial t} = \delta(x - ct) Q \sin \Omega t \quad (6.14)$$

where χ stands for damping coefficient. By comparing 6.14 and 6.2:

$$\omega_b = \frac{\chi}{2\mu} \quad (6.15)$$

where:

ω_b : circular frequency of damping

χ : damping coefficient

μ : mass per unit length of the bridge

also, in [1, Page.704] it is mentioned that:

The external and internal damping of the beam are assumed to be proportional to the mass and stiffness of the beam respectively,i.e., $r_a = \gamma_1 \mu ..$, where γ_1 and γ_2 are proportionality constants.

thus:

$$\omega_b = \frac{\gamma_1}{2} \quad (6.16)$$

and it is mentioned in [1, Eq.8] that:

$$\zeta = \frac{\gamma_1}{\omega_1}$$

so:

$$\gamma_1 = \zeta \omega_1$$

so:

$$\omega_b = \frac{1}{2} \zeta \omega_1 = \frac{1}{2} \frac{\zeta \pi^2}{l^2} \sqrt{\frac{EJ}{\mu}}$$

where ζ is the structure damping ratio stated in EN1991-

Adopting $\zeta = 0.001$ for steel railway bridges. This ζ value is used among all DT329 simulations run files. See Figure.B.3 for example.

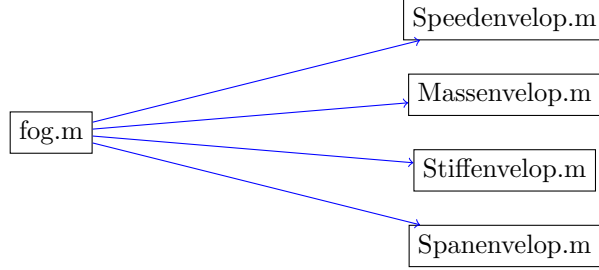


Figure 6.2: Overview of script structure

6.6 Script structure

In order to conduct the study efficiently, scripts in Matlab language are written to automate research procedure. See Appendix.E for codes.

fog.m is the core file for response calculation. This file is responsible for receiving bridge/train parameter input and yield time-history response for mid-span of the bridge. It also handles conversion of force amplitude from train speed. Calculation of bridge stiffness is also implemented, making it easier to input stiffness representing routine used in DT329.

Other scripts files are written to iterate *fog.m* in different parameters in order to conduct parametric study.

Read comments between the code for detailed explanation. **remember to add comment**

6.7 Comparison between analytical model and DT329 simulation results

Several resonance phenomenon were produced during DT329 resonance study. By comparing with the output of reproduced resonance in DT329, the analytical model can be verified.

6.7.1 First attempt

It can be observed in Figure.7.1 that the greatest resonance happened at train running at $14m/s$, on a bridge with following parameters: $l = 54m$, $EJ = 2.43e10Nm^2$, $\mu = 6000kg/m$. Displacement is approximately $15mm$ and acceleration is approximately $1.0m/s^2$.

A analytical run is done using the exactly same bridge parameters and using the load model proposed in Figure.4.5.

Output is presented in Figure.6.4. Figure.6.4 shows the time-history of mid-span response under model moving at $14m/s$, with maximum deflection at $17.1mm$ and maximum acceleration at $0.97m/s^2$.

It can be concluded than analytical solution coincides well with the output of the simulations in the first comparison attempt because the output were close to each other and analytical output is slightly higher. This is acceptable because analytical model simulates a perfect resonance scenario while DT329 simulations takes multiple-axles into account. Axles may interfere with each other(different axle spacing) in the sense of harmoniously exciting the bridge, introducing disturbance into the development of resonance. So DT329 simulations are not perfect resonance scenarios and their output is supposed to be lower than analytical solutions.

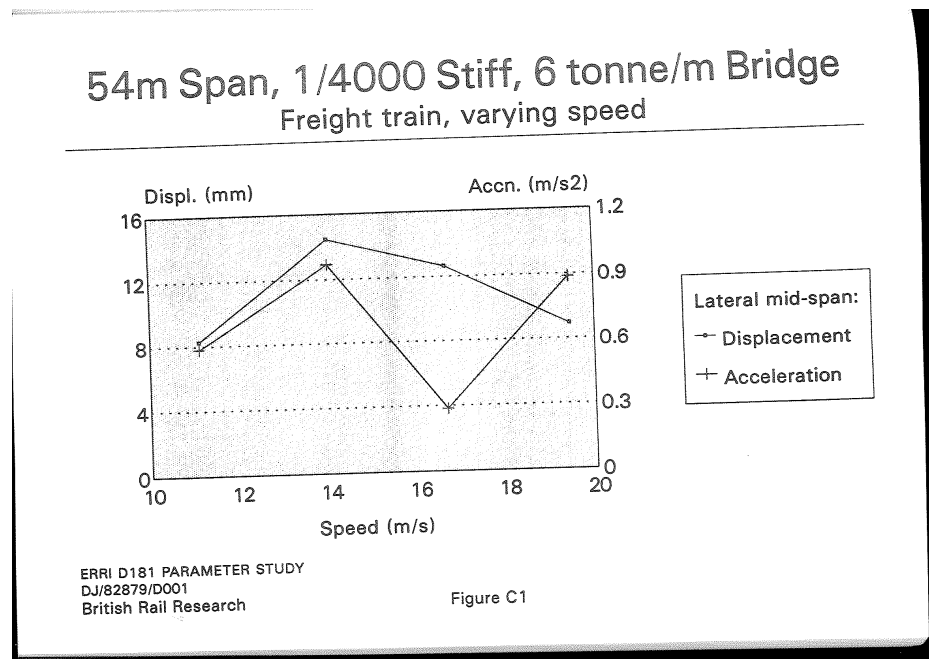


Figure 6.3: Figure C1 extracted from [4]

Max Deflection:0.0171666118764236, Max Acceleration:0.966456968399831

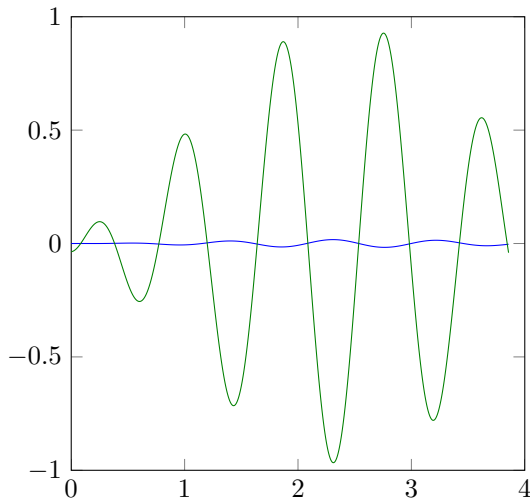


Figure 6.4: EJ243000000000L54mu6000c14.tikz

6.7.2 Second attempt

The second attempt of comparison is conducted by extracting data from Figure 7.2. The bridge parameters are $l = 54m$, $EJ = 2.43e10 Nm^2$, $\mu = 6000 kg/m$, train is running at $60 km/h$, converted to $16.67 m/s$.

Maximum displacement in simulation is approximately $12.5 mm$ and acceleration is approximately $0.3 m/s^2$. The acceleration value is surprisingly low with a step change. The reason causing this unexpected trend in acceleration is unknown, it is recommended to adopt $1.0 m/s$ as a more general

54m Span, 6 tonne/m Bridge, varying stiffness
 Freight train @ 60km/h
 (x axis not to scale)

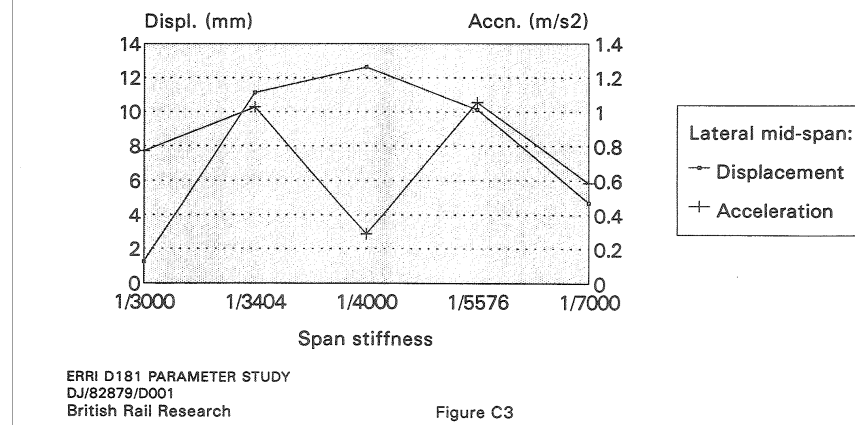


Figure 6.5: Figure C3 extracted from [4]

acceleration value. $1.0m/s$ is the acceleration for $1/3404$ stiffness and $1/5576$ stiffness. It can be seen that at these 2 stiffness, the resonance effect is already building up.

Max Deflection:0.0218101765059296, Max Acceleration:1.06144343401643

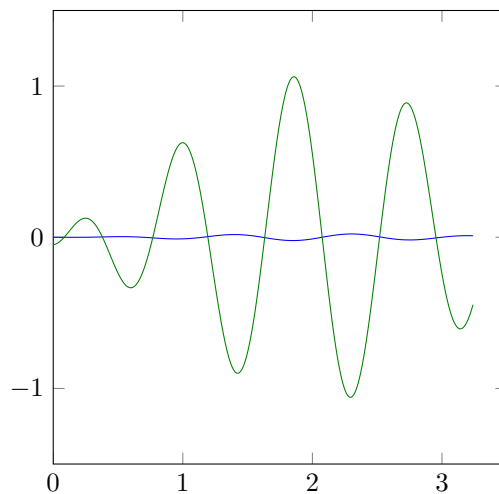


Figure 6.6: EJ24300000000L54mu6000c17.tikz

Analytical solution outputs maximum displacement $21.8mm$, and maximum deflection at $1.06m/s^2$. Analytical solution is still conservative compared to simulation results.

6.7.2.1 Third attempt

The third attempt is to reproduce the resonance on a longer bridge. The bridge parameters are $l = 120m$, $EJ = 3e11Nm^2$, $\mu = 6000kg/m$. Maximum displacement is approximate $17mm$ and maximum acceleration is approximate $1.0m/s^2$

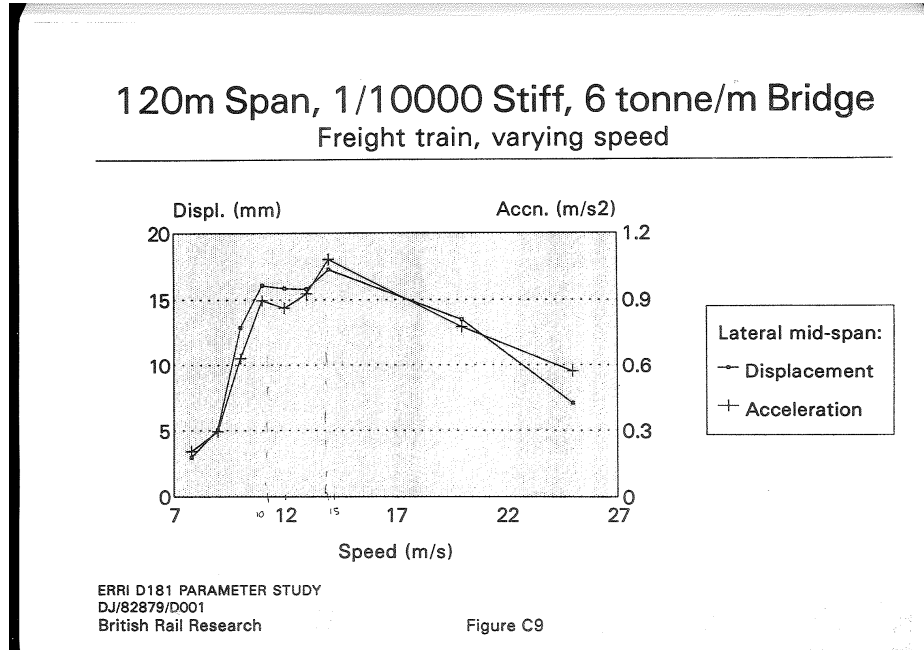


Figure 6.7: Figure C3 extracted from [4]

The analytical result if presented in Figure 6.8.

Max Deflection:0.00165451876202448, Max Acceleration:0.098608250658388

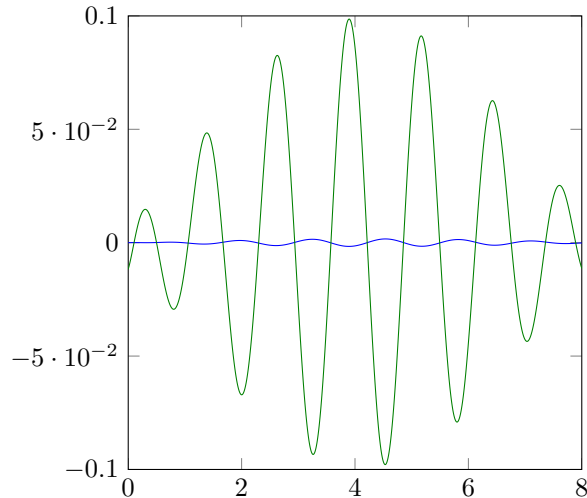


Figure 6.8: EJ3000000000000L120mu6000c15.tikz

The maximum displacement yielded from analytical solution is $1.65mm$ and maximum acceler-

ation is $0.099m/s^2$. Analytical solution is no longer valid in this because its output is dramatically smaller than DT329 simulations.

The only difference between 3rd attempt and other two attempts is the length of the bridge while other two attempts yield satisfying results. The reason for this is that force model is no longer valid when bridge is longer. Longer bridge can have more traction units running on it simultaneously, introducing greater lateral force to the bridge.

Several additional attempts of analytical calculation were done to see the magnitude of an equivalent lateral force sufficient in producing the same displacement($17mm$) as DT329 simulation does. These additional calculations were done by manually increasing the force input little by little. It is then found that an equivalent force of $1200kN$ is barely enough for reproduce such a displacement.

EN1991-2 states that nosing force has an characteristic value of $100kN$ while in this case an equivalent force of $1200kN$ is needed to reproduce $17mm$ displacement. What's more, trains running at higher speed, which is also completely possible, will result in even higher lateral force than $120kN$.

It can be concluded that the magnitude of nosing force defined in EN1991-2 is not conservative for the whole range of bridges, especially for long span bridges.

6.7.3 Alternative load model

An alternative load model can be found in [5, Figure.4.1] and it is extracted as Figure.6.9. Although this model is also proposed in RP6 but due to unknown reason it is not adopted in EN1991-2. This model is more accurate in the sense that it gives a more detailed relationship between lateral force and bridge length. This concept coincides and proofs the conclusion in previous section.

However, the background of this plot is also unknown. It is believed that data of track quality study of Parametric Study DT329[4] in phase II is used to create the plot but explanation is nowhere to be found. This plot is hardly usable for practical purposes but it is a good reference for a rough idea of lateral force induced by trains on a bridge with certain length.

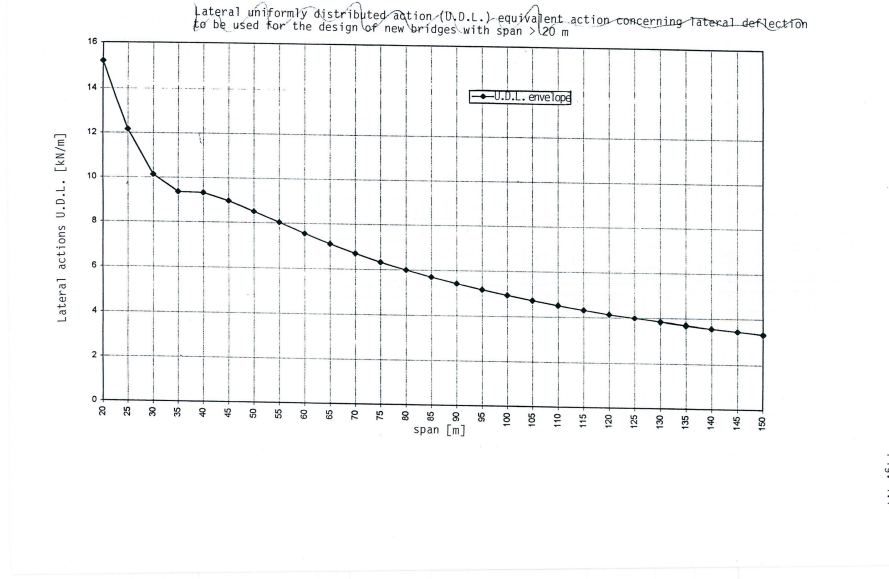


Figure 6.9: Lateral actions U.D.L. Extracted from [5, Figure.4.1]

To use this plot in analytical solution, an equivalent concentrated force needed to be converted from uniformly distributed force.

The deflection at mid-span of a simply supported beam loaded by uniformly distributed load q is

$$\delta = \frac{5}{384} \frac{ql \cdot l^3}{EI}$$

The deflection at mid-span of a simply supported beam loaded by concentrated force P at mid-span is

$$\delta = \frac{1}{48} \frac{P \cdot l^3}{EI}$$

Thus equivalent concentrated force P can be obtain by

$$P = \frac{1 \cdot 384}{48 \cdot 5} ql = \frac{5}{8} ql$$

For example, using the alternative load model in Figure.6.9, equivalent concentrated force for 120m bridge is $\frac{5}{8} \cdot 120m \cdot 4kN/m = 300kN$. It gives an conservative force output compared to 120kN.

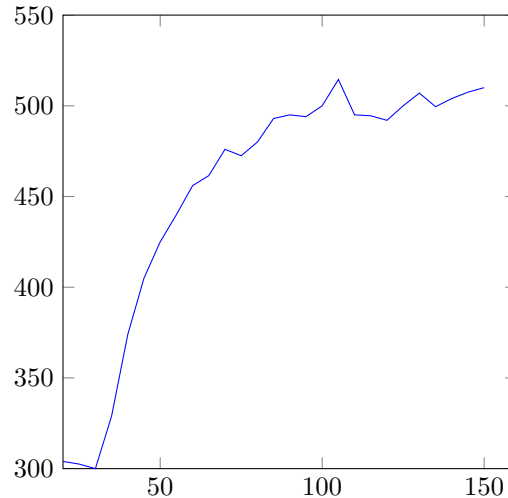


Figure 6.10: Total load verses span calculated from Figure.6.9

6.8 Alternative analytical model for longer span bridges

Moving continuous load model can be adopted.

Add deduction procedure

Solution:

$$v(x, t) = \frac{v_0}{2} (1 + \cos \omega t) \sin \frac{\pi x}{l} \quad (6.17)$$

Maximum deflection

$$v_{max} = v_0 \quad (6.18)$$

No dynamics amplification for longer span bridges. Calculate using alternative load model. This is because train speed is far lower than critical speed.

6.9 Parametric research

Since it is concluded in previous chapter that load model is no longer valid when span is large, this parametric research will focus on stiffness of the bridge and mass of the bridge. Length of the bridge will be fixed at 54m.

6.9.1 Mass

The first parameter examined is mass. *Massenvelop.m* is run to iterate calculation. Mass were checked from 1000kg/m to 12000kg/m. Other parameters were $l = 54m$, $EJ = 2.43e10Nm^2$, $mu = 6000kg/m$. The output are presented in Figure.6.11 as deflection and Figure.6.12 as acceleration.

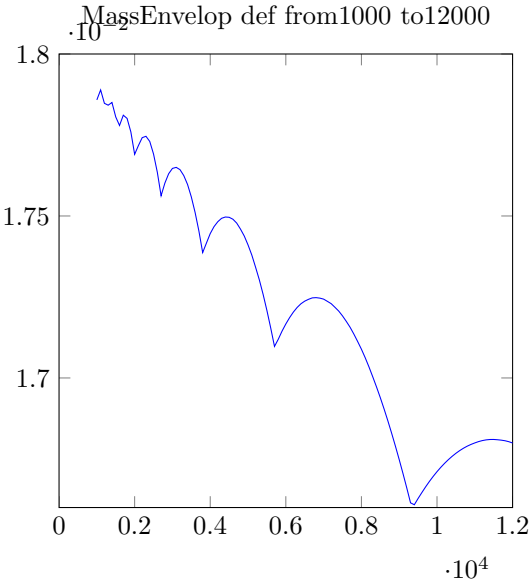


Figure 6.11: medefEJ24300000000L54c14min1000max12000.tikz

Increased mass generally decreases deflection in trend but with a lengthening periodic sinuous wave shape. Further (linear)regression on deflection can be made from peaks.

The acceleration simply decreases as mass increases.

6.9.2 Stiffness

The next parameter examined is stiffness. *Speedenvelop.m* is run to iterate calculation. Stiffness were checked from $2e10Nm^2$ to $3e11Nm^2$. Other parameters are $l = 54m$, $mu = 4000kg/m$, $c = 14m/s$. The output is presented in Figure.6.13 as deflection and Figure.6.14 as acceleration.

In addition, dynamic coefficient is plotted in Figure.6.15. Dynamic coefficient becomes relevant in stiffness case. This is because stiffness is relevant to static deflection. Static deflection decreases as stiffness increases.

The dynamic coefficient is an indication for the amplification level of resonance effect. Usually symbolized as δ , dynamic coefficient is simply the ratio of the maximum dynamic deflection to the static deflection at mid-span of a beam:

$$\delta = \frac{MAXv(l/2, t)}{v_0}$$

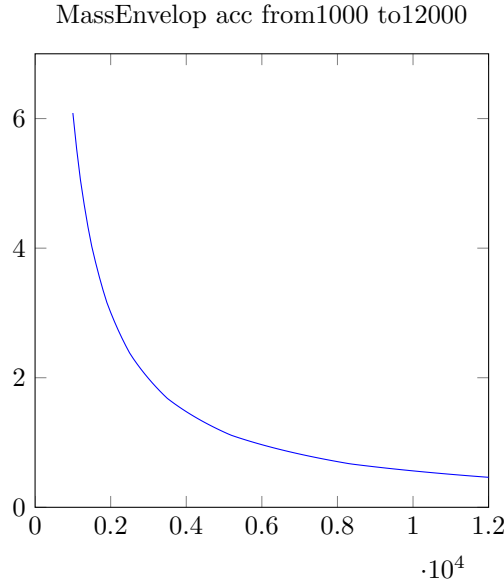


Figure 6.12: meaccEJ24300000000L54c14min1000max12000.tikz

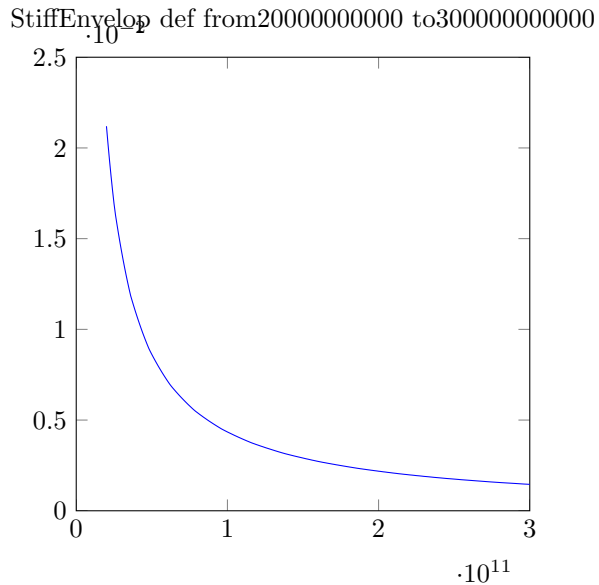


Figure 6.13: stedefmin20000000000max3000000000000L54c14mu4000.tikz

6.9.3 Speed

The next parameter examined is speed. *Speedenvelop.m* is run to iterate calculation. Stiffness were checked from $1m/s$ to $30m/s$. Other parameters are $l = 54m$, $\mu = 4000kg/m$, $EJ = 3e10Nm^2$. The output is presented in Figure 6.16 as deflection and Figure 6.16 as acceleration.

It can be seen that increasing speed increases both maximum deflection and maximum acceleration.

StiffEnvelop acc from200000000000 to300000000000

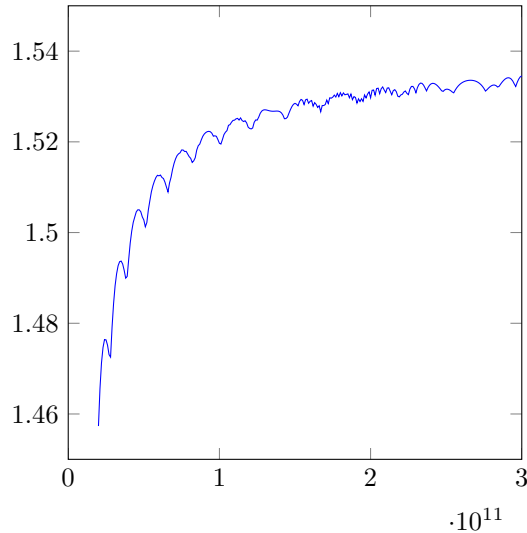


Figure 6.14: steaccmin20000000000max300000000000L54c14mu4000

StiffEnvelop dc from200000000000 to300000000000

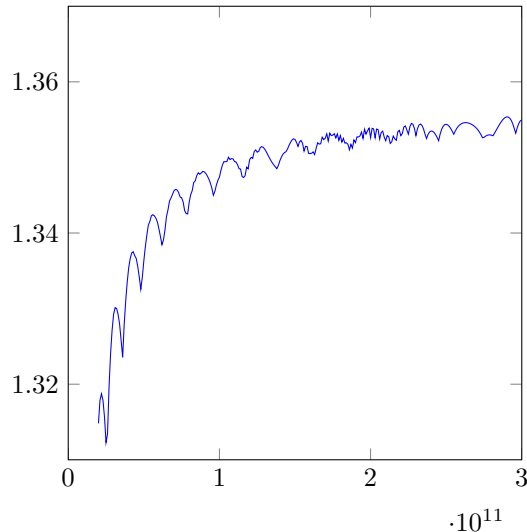


Figure 6.15: steacomin20000000000max300000000000L54c14mu4000

6.9.4 Conclusion

An analytical method for calculating resonance response at mid-span of the bridge is developed on the basis of load model obtained in previous chapters. But it's no suitable for longer span bridges because load model is no longer valid. For longer span bridges, it is advised to use an alternative load model and a different analytical solution.

Parametric research shows that speed, mass and stiffness all have remarkable effects on the response of the bridge. However, as an easier way of controlling, speed of the train also has the simplest relationship with response of the bridge. Although increased speed provides less time for

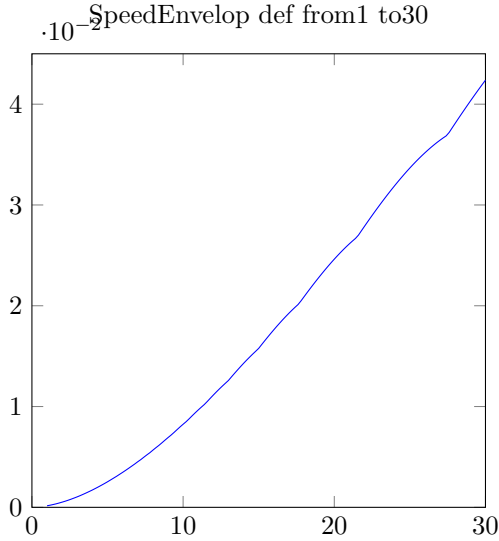


Figure 6.16: speedefEJ30000000000L54min1max30mu4000

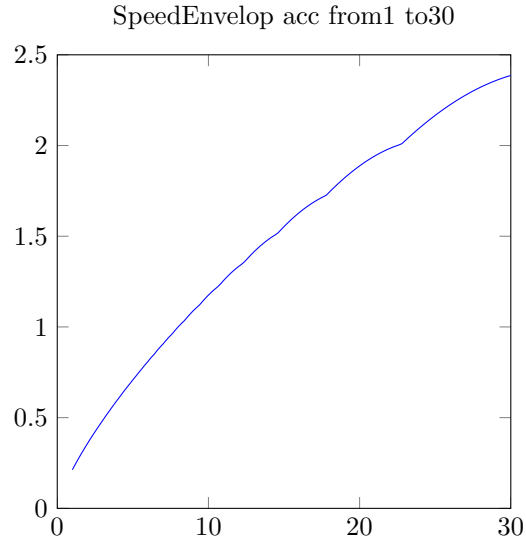


Figure 6.17: speaccEJ30000000000L54min1max30mu4000.tikz

resonance effect to build up, its increased lateral force is more dominating.

However, setting up additional speed limit for trains may not be favoured by train operators. Increasing stiffness also provides a reliable decrement in lateral deflection but it can be less effective when original stiffness is already high. Also, increasing stiffness can increase lateral acceleration for a slight effect. This increased acceleration could be critical because for most of time, passenger comfort can be the governing criterion for bridge dynamics design. And passenger comfort criterion is regard to lateral accelerations. In addition, dynamic coefficient also increases when stiffness increase.

Controlling mass, on the other hand, can be adopted when running out of options because although increasing mass generally decreases deflection, but due to its sinuous characteristics(Figure.6.11), deflection can increase if not handled properly. It's worth noting that using mass as a way of controlling acceleration is reliable.

Length in practical is not flexible so it's not listed as a way of controlling.
Thus, ways of controlling deflection in more preferable order is

$$\text{speed} > \text{stiffness} > \text{mass}$$

Ways of controlling acceleration in more preferable order is

$$\text{speed} > \text{mass} > \text{stiffness}$$

Chapter 7

New practical method for checking lateral dynamic response of railway bridges

7.1 Introduction

This chapter proposes a new method for checking lateral dynamic response of railway bridges. This method aims to provide an engineering solution for checking the deflection and acceleration of railway bridges under horizontal dynamic train load. The method features the combined usage of a simplified analytical structure model and a more refined lateral force model. The analytical structure model simulates a perfect resonance scenario for the target bridge. And the refined load model, which is a concentrated harmonic moving load, represents the lateral dynamic effects that occur because of the passing of the train. The combination of these two analytical elements will generate a resonance response conservative compared to the simulation output in DT329 because varies types of disturbance were included in these simulation runs.

The analytical structure model and its explicit solution has already been worked out in previous chapter. Thus the main objective of this chapter is finding a better lateral force load model because current existing ones are too conservative(see Section.7.3). The refined load model shall be able to be adopted universally for all regular train types. Once this load model is obtained and verified, it is then possible to take advantage of the combination of the load model and analytical solution for practical designing purposes.

7.2 Overview of this chapter

To give a clear overview of this chapter, procedure of development of the method is given as following:

1. *Developing:* Develop a more practical load model to be used in pair with the analytical model introduced in previous chapter. See Section.7.3
 - 1.1. Introduction to the usage of analytical model.
 - 1.2. Find the analytical equivalent nosing forces amplitude for freight trains in 3 different cases presented in DT329 resonance research simulation. The equivalent nosing force amplitude is the exact force amplitude to be substituted into analytical model as lateral harmonic force input, yielding the same response in DT329 simulation output. See Section.7.3.2
 - 1.3. Find regular pattern and key parameter for the magnitude of nosing forces amplitude for freight trains. See Section.7.3.3

- 1.4. Develop a conservative load model based on observed pattern of nosing force of freight trains. This load model is conservative because of the research result of DT329, that freight trains generates greater lateral force on track compare to passenger trains and high speed trains. See Section.7.3.3
2. *Verifying:* Validate the feasibility of combined usage of conservative load model and analytical model
3. *Finalizing:* Illustrate the usage of the method by applying it on a real railway bridge

7.3 Development of refined load model

The load model provided in EN1991-2(nosing force) and D181 RP6(proposed criteria) are too conservative. The reason is that these forces are obtained by simulations ran on poorest maintained tracks with $7mm$ track irregularity standard deviation. In fact tracks are allowed to have lateral irregularities up to $1.8mm$ according to EN13848(Section.2.2.4). So existing lateral force models are enormous compared to real-life scenario.

In addition, the existing load models are representative for hunting effects[5, Proposed criteria]. However, according to [16], although affected by varies parameters, critical speed for hunting effect is normally at 120km/h for modern railway vehicle and tracks. So at least for trains running slower than 120km/h , it can be conclude that hunting is not occurring. And their lateral force should be much less than the force magnitude mentioned in either EN1991-2 or D181 RP6.

Thus these existing load models are too big and not suitable for the analytical solution. A more precise load model is needed for coupled usage for analytical solution.

7.3.1 Introduction to the analytical model to be used in pair with equivalent force amplitude

The analytical model itself and its explicit expression have already been introduced and described in previous chapter. This section will give a overview on the input parameters of both VAMPIRE simulation and analytical model. This is not only due to the fact that VAMPIRE simulation was proved by D181 committee to be in close prediction with situ measurements, but also because in following sections VAMPIRE simulation results will be used as reference comparison data for the development of analytical model's pairing load model.

Table 7.1: Comparison between input parameters of DT329 VAMPIRE simulations and analytical model

	Simulation	Analytical model
Bridge structure	simply supported beam	simply supported beam
Span	Yes	Yes
Stiffness	Yes	Yes
Mass	Yes	Yes
Damping	Yes	Yes
Train	complete train as mass spring system	single moving harmonic load
Train Speed	Yes	Yes
Track irregularities	Yes	No
Wheel profile	Yes	No
Wheel-rail interaction	Yes	No

As demonstrated in Table.7.1, while input parameters for simulation are complicated, analytical model possesses less input parameters.

The single moving harmonic load in analytical model shall be capable of providing dynamic effect caused by train speed, track irregularities, wheel profile and wheel-rail interaction to the analytical model. Correct single moving harmonic load input shall yield the same result as VAMPIRE simulation provided that same span, stiffness, mass and damping value are adopted in both two calculating methods.

Thus finding the correct expression for the harmonic moving force is vital to the analytical model. The harmonic moving force has 3 parameters: speed c , frequency Ω and amplitude Q . Since speed c simply equals to train speed and frequency Ω equals to the first natural bending frequency of the beam ω_1 , the amplitude of the harmonic force remains to be researched. Further development of the amplitude expression will be discussed in following sections.

7.3.2 Finding equivalent lateral force amplitude for specific cases

In this section, equivalent lateral force amplitudes for analytical solution are obtained. The equivalent lateral force amplitude does not represent real force magnitude in rail/wheel interaction, but a force amplitude that yields same result as VAMPIRE simulations using same input parameters if substituted into analytical solution. So this lateral force amplitude may not be correct if adopted in other structure models. On the other hand, analytical solution may yield imprecise results if not substituted with this exact equivalent force amplitude. They can only be used in pair with each other.

Thus in order to perform the comparison mentioned above, both input and output data of DT 329 VAMPIRE simulations are selected as reference data. The input data will be substituted into analytical model and the output data of VAMPIRE simulation will be compared with output of analytical model.

3 sets of reference data are extracted from DT329 report. They are C1,C3,C9 in Figure.7.1,7.2 and 7.3 respectively. These data are all resonance study so they are qualified to be used as reference data. Please note that C1,C3,C9 were all done on freight trains on same track sample. Finally 3 equivalent forces are collected from these 3 test samples to see regular pattern and relevant parameters for freight trains.

By observing Eq.6.13, it is concluded that force amplitude is an independent variable and perfectly linear to the analytical output. Thus the equivalent force is obtained by inputting bridge parameters and train speed into the analytical solution Eq.6.13 and manually increasing the force amplitude little by little until the peak response output reaches the same magnitude of peak simulation output. The parameters used and their corresponding results are presented in Table.7.2.

Table 7.2: Parameter setups and equivalent force amplitude for C1,C3,C9

	C1	C3	C9
Stiffness(δ_0/l)	1/4000	1/4000	1/10000
Span(m)	54m	54	120
Mass per unit length(kg/m)	6000	6000	6000
Speed of train(m/s)	14	16.67(60km/h)	14
Damping ratio	1%	1%	1%
Train type	Freight	Freight	Freight
Track	Coupled freight track	Coupled freight track	Coupled freight track
Equivalent load amplitude(kN)	14	15	14

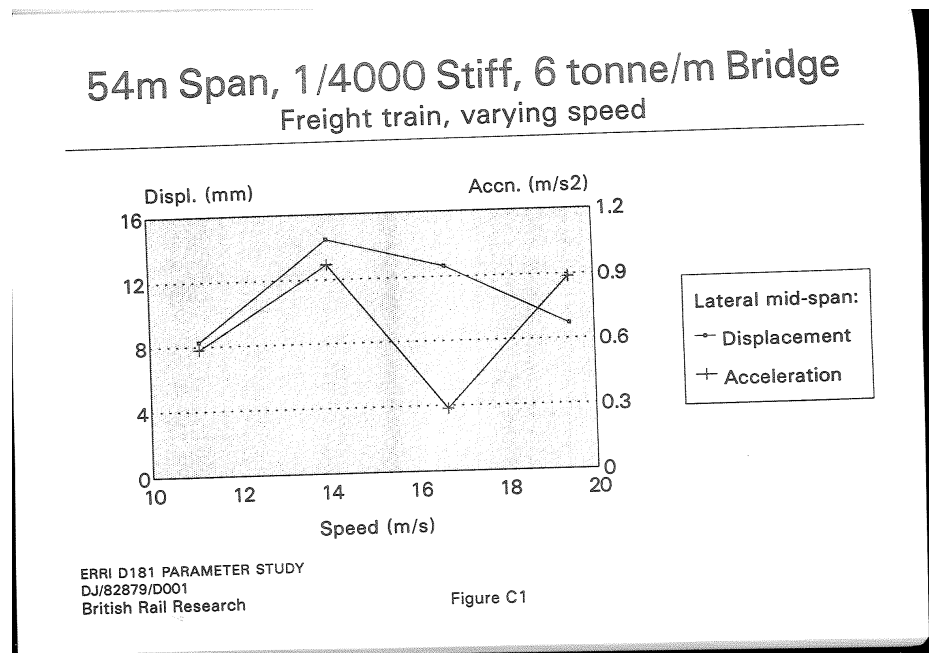


Figure 7.1: Figure C1 extracted from [4]

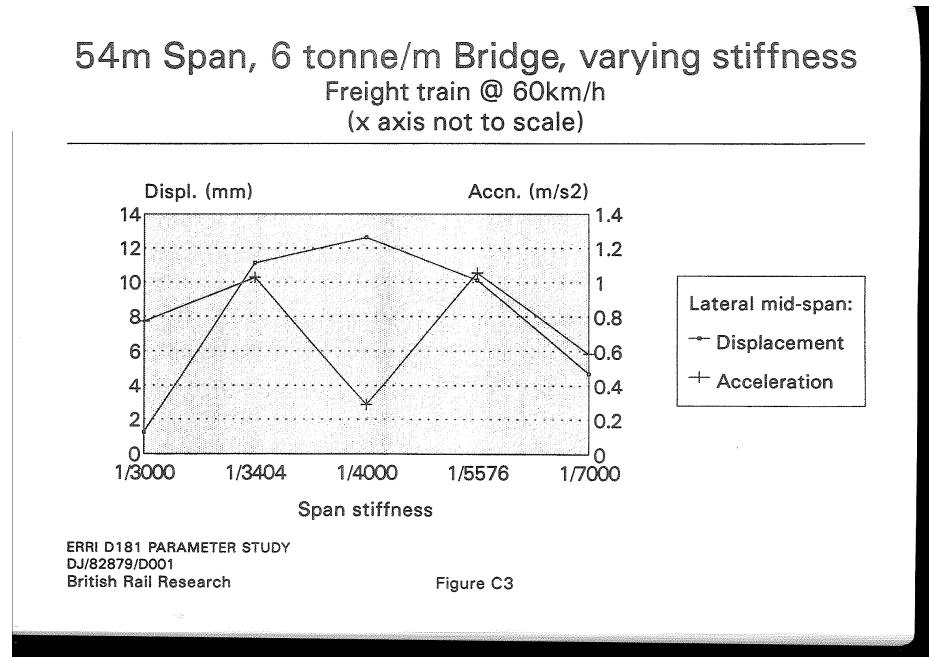


Figure 7.2: Figure C3 extracted from [4]

7.3.3 Key parameter for equivalent force amplitude and hypothesis expression for refined load model

By observing the equivalent load amplitude illustrated in Table 7.2, it is found that the equivalent load amplitude yielded by analytical solution meets the general principle of lateral track force

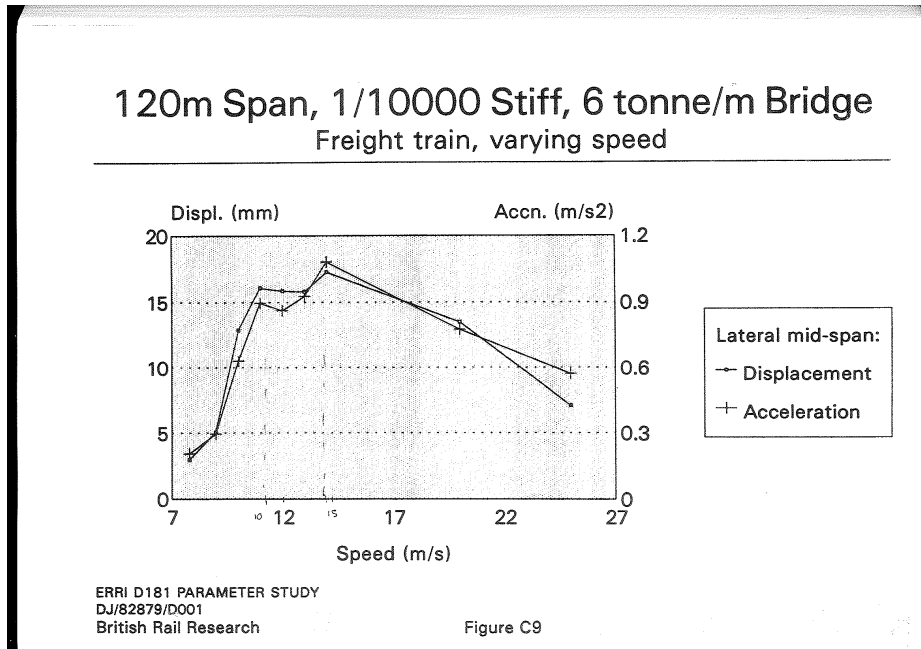


Figure 7.3: Figure C9 extracted from [4]

concluded by DT329 track quality research. The general principle is that the lateral force is only relevant to speed if track quality and wheel conicity are fixed. And lateral force is irrelevant to the bridge parameters.

Because equivalent force amplitude meets the general lateral force principle, it is further expected that the equivalent force amplitude also has a similar form of force-speed relationship of DT329 VAMPIRE simulations. Due to the lack of reference data, it is impossible to make a reliable regression. Only a hypothesis expression can be created by scaling Eq.4.1 to 14kN at 14m/s(reference data set C1). Please note only C1 was used in creating the hypothesis expression so C3 and C9 remains available for the verification.

$$Q = 1928 \times c^{0.7495} \quad (7.1)$$

where:

Q : equivalent force amplitude(N)

c: speed of the train(m/s)

This scaling is reasonable because: according to the conclusion of DT329 track quality research, lateral forces generated on 7mm standard deviation tracks has a certain relationship with speed(Eq.4.1). And it is also concluded that at same speed, lateral forces are linear to the track stand deviation. Thus, since all 3 reference data are run on the same track, force output of analytical model at each speed(14m/s and 16.67m/s) could be scaled from Eq.4.1 's results at these speeds. Furthermore, a scale factor is then applied on Eq.4.1 to reflect the scaling to the whole speed domain and this yields above equation.

As a conclusion, this hypothesis expression is obtained by processing the output of VAMPIRE simulation on freight trains and coupled freight track(poorer than passenger line and high speed line). So it is in closest prediction in the effects generated by freight trains. However, since passenger trains and high speed trains yields lower lateral force compared with freight trains, this hypothesis expression remains conservative for all train types.

7.4 Verification of the method

In this section the combined usage of analytical model and hypothesis expression for equivalent force amplitude is examined and verified. A matlab script is written to function the analytical model with hypothesis expression for equivalent load amplitude implemented. Now that force amplitude Q is a function of speed, there's no longer necessary to input the force amplitude manually. To verify the correctness of combined usage of these two elements, other reference data from resonance research in DT329 are selected.

To assure conservative comparison, only axle repeat pattern resonance results are selected because their output are more pronounced than kinematic resonance effect. Altogether 5 sets of reference data are selected. They include 2 reference data for freight trains(C3,C9), 2 reference data for passenger train(C12,C13) and 1 reference data for high-speed train(C14). Due to the fact that freight trains yield greater force than the other two types of trains, the analytical result should be conservative for the latter 3 cases. Since the output of C3 and C9 are already presented in Table.7.2 so they are not being presented with other 3 sets of data this time. The bridge parameters and trains speed involved in these 3 cases(C12,C13,C14) are input into the analytical solution to yield analytical results.

Table 7.3: Comparison of results of simulation output and analytical output using refined load model

	C12	C13	C14
Stiffness(δ_0/t)	1/10000	1/12000	1/10000
Span(m)	54	54	38
Mass per unit length(kg/m)	6000	6000	10000
Speed of train(m/s)	55.6	55.6	65
Damping ratio	1%	1%	1%
Train type	Passenger	Passenger	High speed
Track	Passenger Track	Passenger Track	High speed track
Peak Simulation displacement(mm)	1.48	1.41	0.117
Peak Analytical displacement(mm)	6.6	5.8	3.0

In Table.7.3 the parameters involved in these 3 cases and their corresponding peak analytical results as well as peak simulation results are presented.

To clearer illustrate the comparison of both peak results from simulation and analytical, Figure.7.4 is created with rearranged x-axis order to make the descending trend more obvious. Please note all data sets except for C1 are valid for verification(C1 is used in creation of expression).

It can be seen that analytical results always keep a conservative margin above the simulation results. As expected, margins for C12,C13,C14 are bigger compared to C9,C1,C3 proofs that the analytical solution becomes more conservative if adopted to passenger train and high-speed train. What's more, the descending trend of analytical results follows the descending trend of simulation results perfectly regardless of train types. Thus considering these reasons, the analytical solution is sufficient for universal application on all train types.

7.5 Finalizing the method for practical usage

In practical usage, the speed that generates the highest peak response is unknown. Thus it is necessary to obtain the peak response for all speeds within the possible speed range. This is done by iterating the existing Matlab script with different speed. The increment in speed iteration is set in a way that ensures at least 1000 runs are done to guarantee precession. An example is illustrated as follows to show the usage on a real bridge project.

For an arch railway bridge located near Amsterdam, possessing following parameters:

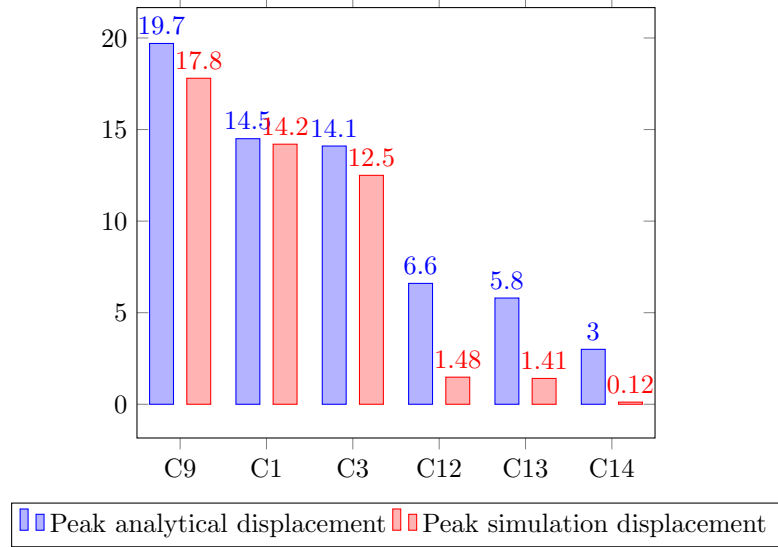


Figure 7.4: Comparison between peak simulation result and peak analytical result

$L = 255m$, $m = 5222e3kg$, $\mu = 2.0478e4kg/m$, $EJ = 6.56e12Nm^2$
to test through a speed range of $1m/s - 30m/s$

Before beginning the calculation, make sure you have fog.m and Speedenvelop.m in your current working directory. By inputting following command in Matlab console,

`Speedenvelop(6.56e12,255,2.0478e4,1,30,0.01)`

the envelop for displacement is generated and illustrated in Figure.7.5

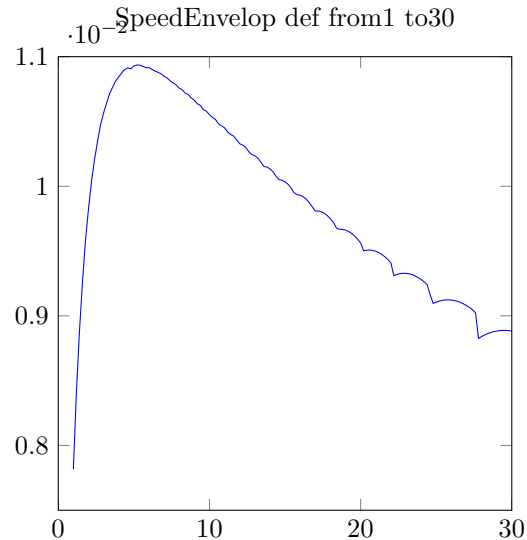


Figure 7.5: spedefEJ6560000000000L255min1max30mu20478

The plot shows that the critical speed appears at approximately $5m/s$ and corresponding peak deflection response is approximately $11mm$.

Since the relationship between end support rotation angle and mid-span deflection is widely known as:

$$\varphi = \frac{3}{L} \cdot \delta_0$$

and rotation is yielded as:

$$\varphi = \frac{3}{255} \times 0.011 = 0.00013$$

This value is much lower than the rotation value regulated in EN1991-2. See Section 3.3.3.1 for criteria details.

Thus the conclusion can be made that this bridge is safe subjected to lateral dynamic load.

However, if encountering unfavourable peak result, a filter can be applied on the train speed to further cut off the peak response. In previous chapter it has been already concluded that all resonance effects between train and bridge are wavelength phenomenon. In order to couple frequency with bridge's first natural bending frequency, the train needs to operate at a certain speed range.

For example, assuming the train's wavelength is 20m-40m, including both axle repeat wavelength and kinematic wavelength.

The natural frequency of the bridge in this example is

$$f_1 = \frac{\pi}{2l^2} \sqrt{\frac{EJ}{\mu}} = \frac{\pi}{2 \times 255^2} \sqrt{\frac{6.56e12}{1.0478e4}} = 0.4Hz$$

so the possible resonance speed is obtained by multiplying wavelength range with natural frequency, yielding: 8m/s and 16m/s

The maximum response in deflection is lowered to 1.05 mm. The filter is more effective if the natural frequency of the bridge is higher.

Chapter 8

Recommendations on improvement on Eurocode

8.0.1 Add reference

Please

8.0.2 Improve criteria for lateral bridge dynamics

Following sections provides several orientations for improving criteria for lateral bridge dynamics in terms of safety and serviceability of running stock.

8.0.3 Requirements for traffic safety(horizontal)

Requirements other than bridge first lateral frequency higher than 1.2Hz. Since there's no further requirements mentioned by Eurocode, following requirements are gathered from other European codes, eg. British standards, UIC leaflet, etc.

- Requirements regarding traffic safety for vehicles
 - (a) Guiding Force: [3] , [7] and[6] propose safty limitations against railway vehicle overturning. From[7] the maximum guiding force for a vehicle with a load per axle of 170kN(AVE) is 66kN per axle and 48kN per axle for a vehicle with a load per axle of 112kN(ICE2). For the R1 freight wagon(load per axle of 245kN), the maximum guiding force per axle is 78kN.
 - (b) Maximum lateral acceleration of the railway vehicle: proposed by [23]
- Requirements regarding safety for bridge
 - [14] A2.4.4.1(2): Horizontal transverse deflection(to ensure acceptable horizontal track radii) and horizontal rotation of a deck about a vertical axis at ends of a deck(to ensure acceptable acceptable horizontal track geometry and passenger comfort)

8.0.4 Requirements for traffic safety on derailment: Railway vehicle derailment mechanism and safety criteria

Derailment mechanisms

1. vehicle resonant response
2. lateral instability
3. vehicle overturning
4. vertical wheel unloading
5. flange climb

6. rail roll-over
7. track panel shift
8. longitudinal train forces

The four types of derailment: flange climb derailment, derailment caused by gauge widening and rail roll-over, derailment caused by track panel shift, derailment cause by vehicle lateral instability have a common cause of high lateral force at the wheel-rail interface. According to [15, Chapter 8, IV] any conditions that lead to high lateral forces or lead to lower the ability of the system to sustain the force should be corrected.

8.0.4.1 Flange climb derailment

Wheel flange climb derailments are caused by wheels climbing onto the top of the railhead then further running over the rail. Wheel climb derailments generally occur in situations where the wheel experiences a high lateral force combined with circumstances where the vertical force is reduced on the flanging wheel. The high lateral force is usually induced by a large wheelset angle-of-attack. The vertical force on the flanging wheel can be reduced significantly on bogies having poor vertical wheel load equalisations, such as when negotiating rough track, large track twist, or when the car is experiencing roll resonances.

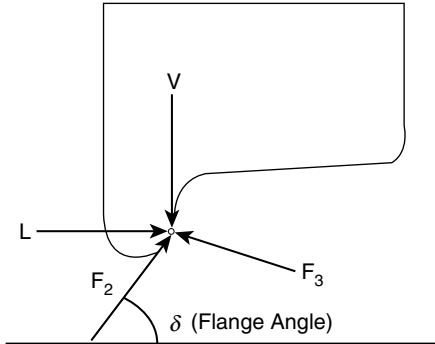


Figure 8.1: Forces at flange contact location. Extracted from [15, Figure8.4]

The criterion L/V ratio can be expressed as:

$$\frac{L}{V} = \frac{\tan \delta - \frac{F_2}{F_3}}{1 + \frac{F_2}{F_3} \tan \delta} \quad (8.1)$$

Nadal's famous L/V ratio limiting criterion, given by Equation.8.2, was proposed for the saturated condition $F_2/F_3 = \mu$

$$\frac{L}{V} = \frac{\tan \delta - \mu}{1 + \mu \tan \delta} \quad (8.2)$$

8.0.4.2 Derailment caused by gauge widening and rail rollover

Derailments caused by gauge widening usually involve a combination of wide gauges and large lateral rail deflections(rail roll), as shown in Figure8.2. Large lateral forces from the wheels act to spread the rails in curves. Both rails may experience significant lateral translation and/or railhead roll, which often cause the nonflanging wheel to drop between rails.

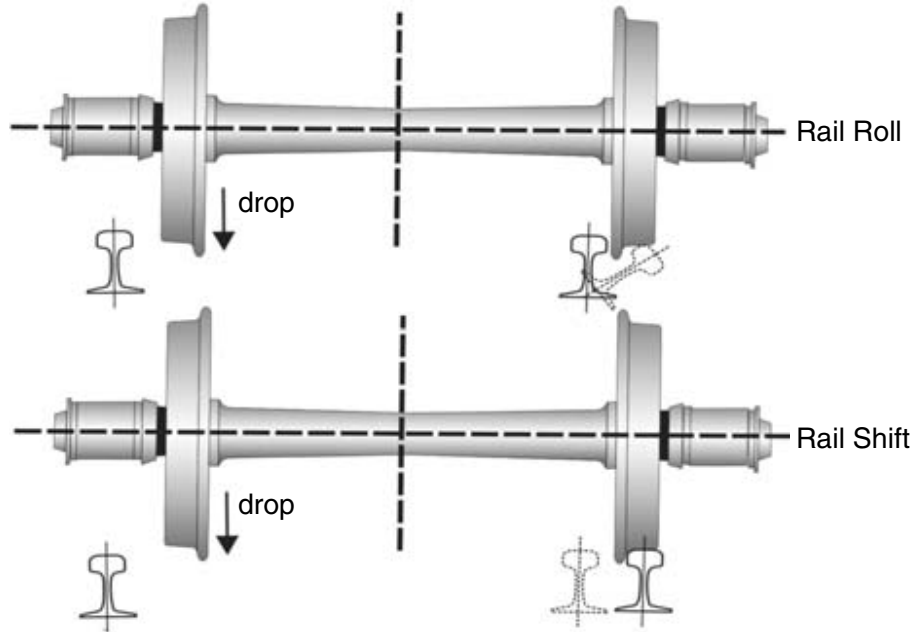


Figure 8.2: Gauge widening derailment. Extracted from [15, Figure8.18]

AAR Chapter XI rail roll criterion The AAR Chapter XI rail roll criterion is established by using the L/V ratio. The roll moment about the pivot point is given by,

$$M = Vd - Lh \quad (8.3)$$

under an equilibrium condition, just before the rail starts to roll, M approaches to zero, then,

$$\frac{L}{V} = \frac{d}{h} \quad (8.4)$$

This L/V ratio is considered as the critical value to evaluate the risk of rail roll. When the L/V ratio is larger than the ratio of d/h , the risk of rail roll becomes high. The critical L/V ratio for rail roll can vary from above 0.6 for contact at the gauge side to approximately 0.2 when the contact position is at the far-field side based on the dimension of the rails. This is because the distance d is reduced. Note that this L/V ratio is calculate assuming that neither the rail fasteners nor the torsional stiffness of the rail section provide any restraint.

8.0.4.3 Derailment caused by track panel shift

Track panel shift is the cumulative lateral displacement of the track panel, including rails, tie plates and ties, over the ballast, as shown in Figure8.3. A small shift of these components may not immediately cause the loss of guidance to bogies. However, as the situation gradually depreciates to a certain level, wheels could lose guidance and drop to the ground at some speed. The derailments caused by track panel usually result in one wheel falling between the rails and the other falling outside of the track.

Panel shift criterion Researched by the French National Railways suggested that the limiting lateral axle load can be defined in a general expression for preventing excessive track panel shift:

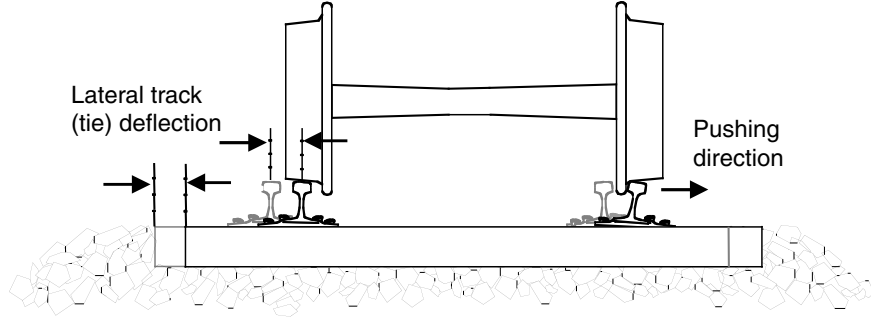


Figure 8.3: Lateral track panel shift. Extracted from [15, Figure8.27]

$$L_c = aV + b \quad (8.5)$$

where L_c is the critical lateral load and V is the vertical axle load. [15, Table 8.2] lists two groups of suggested values of a and b . It is possible that different values for a and b can be specified in different areas.

8.0.4.4 Derailment caused by vehicle lateral instability

On tangent track, the wheelset generally oscillates around the track centre due to any vehicle and track irregularities, as shown in Figure 8.4. This movement occurs because vehicle and track are never absolutely smooth and symmetric. This self-centring capability of a wheelset is induced by the coned shape of the wheel tread. However, as speed is increased, if the wheelset conicity is high, the lateral movement of wheelset, as well as the associated bogie and car body motion, can cause oscillations with large amplitude and a well-defined wavelength. The lateral movements are limited only by the contact of the wheel flanges with the rail. This vehicle dynamic response is also termed as vehicle hunting, and can produce high lateral forces to damage track to cause derailments.

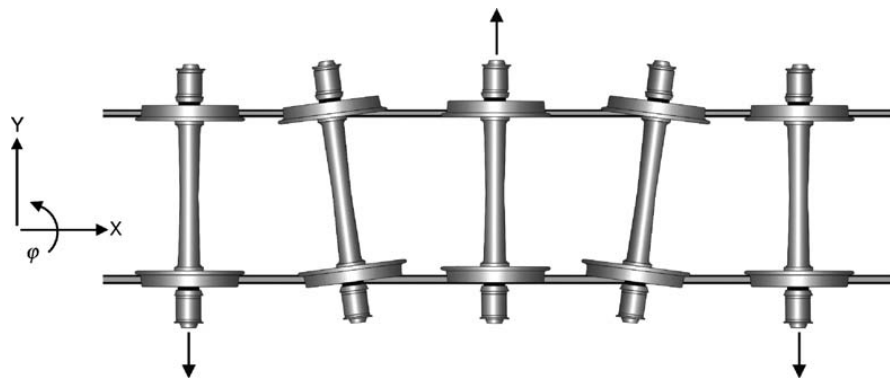


Figure 8.4: Wheelset oscillates around the track centre. Extracted from [15, Figure8.28]

Derailment cause by vehicle hunting can have derailment mechanisms of all four types discussed in the previous sections. The high lateral force induced from hunting may cause wheel flange climbing on the rail, gauge widening, rail roll-over, track panel shift, or combinations of these. The safety concerns for this type of derailment, usually occurring at higher speeds, make it an important area of study.

Hunting predominantly occurs in empty or lightweight vehicles. The critical hunting speed is highly dependent on the vehicle/track characteristics. Investigation of the critical speed for such a system with nonlinearities is to examine the vehicle response to a disturbance using a numerical solution of the equations of motion.

8.0.5 Requirements for traffic serviceability(horizontal)

The criteria Comfort Indexes for assessing ride comfort in railway vehicles proposed in [22]. This standard describes a methodology for assessing ride comfort as a function of longitudinal, vertical and transverse accelerations.

Comfort Index indicates the percentage of passengers experiencing discomfort in a specific situation. These indexes can be computed via empiric formula given in the standard, which depend on variables such as lateral acceleration, rate of change of acceleration and rolling velocity. All these values are filtered with a moving average filter that eliminates small wavelength components. Using this methodology for the computed worst-case situations, the comfort indexes have been found excellent, therefore no passenger should feel uncomfortable.

Chapter 9

Conclusion

2 proposed criteria in RP6[5] were adopted in Eurocode 1991-2. One of them is 1.2Hz criterion. It was adopted without amending. The other one is lateral force models. Loading models were adopted in a different name as 'nosing force' in [10, A6.5.2].

- The 1.2Hz criterion was aiming to avoid the occurrence of resonance between bridge first lateral vibration mode and vehicle sway mode, however, no research can be found among all D181 report series to support this hypothesis. This criterion was proposed without a valid background.
- Nosing force in EN1991-2 has a single characteristic value of 100kN, while RP6 proposes different values for different scenarios.

In addition, D181 did research on other 2 resonance phenomena, including axle repeat pattern resonance and kinematic movement resonance. Resonance was proved to be possible and was successfully reproduced using VAMPIRE software. These two resonance are wavelength phenomenon, meaning resonance can happen on any train/bridge combination.

Nosing force model was proposed by investigating the peak lateral force on first two traction units of the train in DT329. But this force is only representative for total peak lateral force for first two traction units of the running train. When the bridge is longer, larger total peak force could occur because more traction units will be expected to run on the bridge simultaneously.

The relationship between total peak lateral force of the first two traction units and speed is found by using the simulation output and regression approach. The lateral force is greatly dependant on track quality, train type and speed.

A analytical solution for calculating real-time responses of the bridge is also developed. The solution uses the regression force model found in previous chapters. It is shown that when bridge length is near 50m, analytical output is close to simulation output. However, when length is higher, the analytical output is getting smaller than simulation output. This is due to when bridge length is longer than the length of two traction units, the lateral force model is no longer valid.

From the analytical results it can also be conclude that design value(100kN) of nosing force in EN1991-2 can be non-conservative when bridge length is longer. Several designing strategy is proposed in controlling both dynamic deflection and dynamic acceleration.

Appendices

Appendix A

Plots and diagrams used in D181 DT 329

Freight train: Principle axle repeat patterns	dist m	Speed	
		60 km/h	100 km/h
wagon n axle 2 - wagon n+1 axle 1	4.00	4.17	6.94
wagon wheelbase	9.00	1.85	3.09
wagon n axle m - wagon n+1 axle m	13.0	1.28	2.14
wagon n axle m - wagon n+2 axle m	26.0	0.64	1.07
Passenger train: Principle axle repeat patterns	dist m	Speed	
		160 km/h	200 km/h
coach n axle 1 - 2, and coach n axle 3 - 4	2.56	17.36	21.70
coach n axle m - coach n+1 axle m	26.4	1.68	2.10
coach n axle m - coach n+2 axle m	52.8	0.84	1.05
ETR 500 train: Principle axle repeat patterns	dist m	Speed	
		300 km/h	350 km/h
coach n axle 1 - 2 and coach n axle 3 - 4	3.0	27.78	32.41
coach n axle m - coach n+1 axle m	26.1	3.19	3.72
coach n axle m - coach n+2 axle m	52.2	1.60	1.86
coach n axle m - coach n+3 axle m	69.3	1.20	1.40

Table A.1: Axle repeat patterns and typical frequencies. Extracted from [4, Appendix C]

Kinematic wavelength, m	Freight train	Passenger train	ETR500 train
Locomotive	39 - 45	32 - 38	39 - 45
Coach/wagon	24 - 39	34 - 38	36 - 40

Table A.2: Kinematic wavelength ranges per vehicle, with BR P1 profiles. Extracted from [4, Appendix C]

VEHICLE MODEL PARAMETER LISTS

VEHICLE TITLE BR CLASS 56 LOCOMOTIVE

MASSES & INERTIAS

Number of bogies	2
Number of axles (per bogie)	3
Body mass	81.2 Mg
Body roll inertia	107.0 Mgm ²
Body pitch inertia	1400.0 Mgm ²
Body yaw inertia	1400.0 Mgm ²
Bogie mass	5.6 Mg
Bogie roll inertia	5.0 Mgm ²
Bogie pitch inertia	21.6 Mgm ²
Bogie yaw inertia	21.6 Mgm ²
Wheelset mass	2.2 Mg
Wheelset roll and yaw inertia	2.7 Mgm ²

DIMENSIONS

Semi pivot spacing	5.19 m
Semi wheelbase	2.09 m
Wheel radius	0.57 m
Body centre of gravity height above rail level	1.85 m
Bogie centre of gravity height above rail level	0.86 m

PRIMARY SUSPENSION

Lateral stiffness (per axle)	0.1 MN/m
Vertical stiffness (per axle)	2.63 MN/m
Yaw stiffness (per axle)	29.0 MNm/r
Lateral damper rate (per axle)	- MNs/m
Vertical damper rate (per axle)	0.05 MNs/m
Vertical friction breakout (per axle)	- KN
Height above rail level of lateral springs	0.67 m
Lateral semi spacing of vertical springs	1.035 m
Height above rail level of lateral dampers	- m
Lateral semi spacing of vertical dampers	1.035 m
Lateral semi spacing of vertical friction	- m

Figure A.1: BR CLASS 56 LOCOMOTIVE. Extract from [4, Appendix 2]

Appendix 2

SECONDARY SUSPENSION

Lateral stiffness (per bogie)	0.77 MN/m
Vertical stiffness (per bogie)	2.72 MN/m
Roll bar stiffness (per bogie)	- MNm/r
Yaw stiffness (per bogie)	1.22 MNm/r
Lateral damper rate (per bogie)	0.084 MNs/m
Vertical damper rate (per bogie)	0.15 MNs/m
Yaw damper rate (per bogie)	0.055 MNms/r
Height above rail level of lateral springs	1.31 m
Lateral semi spacing of vertical springs	1.062 m
Height above rail level of lateral dampers	1.06 m
Lateral semi spacing of vertical dampers	1.062 m

Figure A.2: BR CLASS 56 LOCOMOTIVE. Extract from [4, Appendix 2]

Appendix 2

VEHICLE TITLE UIC FREIGHT WAGON (LADEN)

MASSES & INERTIAS

Number of bogies	-
Number of axles (per wagon)	2
Body mass	41.0 Mg
Body roll inertia	35.0 Mgm ²
Body pitch inertia	500.0 Mgm ²
Body yaw inertia	500.0 Mgm ²
Bogie mass	- Mg
Bogie roll inertia	- Mgm ²
Bogie pitch inertia	- Mgm ²
Bogie yaw inertia	- Mgm ²
Wheelset mass	2.0 Mg
Wheelset roll and yaw inertia	1.7 Mgm ²

DIMENSIONS

Semi pivot spacing	- m
Semi wheelbase	4.5 m
Wheel radius	0.46 m
Body centre of gravity height above rail level	1.5 m
Bogie centre of gravity height above rail level	- m

PRIMARY SUSPENSION

Lateral stiffness (per axle)	1.5 MN/m
Vertical stiffness (per axle)	2.6 MN/m
Yaw stiffness (per axle)	10.0 MNm/r
Lateral damper rate (per axle)	0.034 MNs/m
Vertical damper rate (per axle)	- MNs/m
Vertical friction breakout (per axle)	3.0 KN
Height above rail level of lateral springs	0.46 m
Lateral semi spacing of vertical springs	1.0 m
Height above rail level of lateral dampers	0.46 m
Lateral semi spacing of vertical dampers	- m
Lateral semi spacing of vertical friction	1.0 m

Figure A.3: UIC FREIGHT WAGON (LADEN). Extract from [4, Appendix 2]

SECONDARY SUSPENSION

Lateral stiffness (per bogie)	- MN/m
Vertical stiffness (per bogie)	- MN/m
Roll bar stiffness (per bogie)	- MNm/r
Yaw stiffness (per bogie)	- MNm/r
Lateral damper rate (per bogie)	- MNs/m
Vertical damper rate (per bogie)	- MNs/m
Yaw damper rate (per bogie)	- MNms/r
Height above rail level of lateral springs	- m
Lateral semi spacing of vertical springs	- m
Height above rail level of lateral dampers	- m
Lateral semi spacing of vertical dampers	- m

Figure A.4: UIC FREIGHT WAGON (LADEN). Extract from [4, Appendix 2]

Appendix 2

VEHICLE TITLE FS ETR500 LOCOMOTIVE

MASSES & INERTIAS

Number of bogies	2
Number of axles (per bogie)	2
Body mass	55.98 Mg
Body roll inertia	53.366 Mgm ²
Body pitch inertia	1643.0 Mgm ²
Body yaw inertia	1630.0 Mgm ²
Bogie mass	3.896 Mg
Bogie roll inertia	3.115 Mgm ²
Bogie pitch inertia	5.843 Mgm ²
Bogie yaw inertia	8.107 Mgm ²
Wheelset mass	2.059 Mg
Wheelset roll and yaw inertia	1.164 Mgm ²

DIMENSIONS

Semi pivot spacing	6.0 m
Semi wheelbase	1.5 m
Wheel radius	0.55 m
Body centre of gravity height above rail level	1.65 m
Bogie centre of gravity height above rail level	0.64 m

PRIMARY SUSPENSION

Lateral stiffness (per axle)	12.0 MN/m
Vertical stiffness (per axle)	3.55 MN/m
Yaw stiffness (per axle)	15.4 MNm/r
Lateral damper rate (per axle)	- MNs/m
Vertical damper rate (per axle)	0.3 MNs/m
Vertical friction breakout (per axle)	- KN
Height above rail level of lateral springs	0.55 m
Lateral semi spacing of vertical springs	1.03 m
Height above rail level of lateral dampers	- m
Lateral semi spacing of vertical dampers	1.2 m
Lateral semi spacing of vertical friction	- m

Figure A.5: FS ETR500 LOCOMOTIVE. Extract from [4, Appendix 2]

Appendix 2

SECONDARY SUSPENSION

Lateral stiffness (per bogie)	0.584 MN/m
Vertical stiffness (per bogie)	1.888 MN/m
Roll bar stiffness (per bogie)	1.0 MNm/r
Yaw stiffness (per bogie)	- MNm/r
Lateral damper rate (per bogie)	0.037 MNs/m
Vertical damper rate (per bogie)	0.145 MNs/m
Yaw damper rate (per bogie)	0.938 MNms/r
Height above rail level of lateral springs	0.95 m
Lateral semi spacing of vertical springs	1.03 m
Height above rail level of lateral dampers	0.73 m
Lateral semi spacing of vertical dampers	1.05 m

Figure A.6: FS ETR500 LOCOMOTIVE. Extract from [4, Appendix 2]

Appendix 2

VEHICLE TITLE FS ETR500 COACH

MASSES & INERTIAS

Number of bogies	2
Number of axles (per bogie)	2
Body mass	34.23 Mg
Body roll inertia	54.63 Mgm ²
Body pitch inertia	1821.0 Mgm ²
Body yaw inertia	1760.0 Mgm ²
Bogie mass	2.76 Mg
Bogie roll inertia	2.034 Mgm ²
Bogie pitch inertia	2.504 Mgm ²
Bogie yaw inertia	4.071 Mgm ²
Wheelset mass	1.58 Mg
Wheelset roll and yaw inertia	0.753 Mgm ²

DIMENSIONS

Semi pivot spacing	9.5 m
Semi wheelbase	1.5 m
Wheel radius	0.44 m
Body centre of gravity height above rail level	1.5 m
Bogie centre of gravity height above rail level	0.68 m

PRIMARY SUSPENSION

Lateral stiffness (per axle)	4.35 MN/m
Vertical stiffness (per axle)	1.61 MN/m
Yaw stiffness (per axle)	14.0 MNm/r
Lateral damper rate (per axle)	- MNs/m
Vertical damper rate (per axle)	0.015 MNs/m
Vertical friction breakout (per axle)	- KN
Height above rail level of lateral springs	0.44 m
Lateral semi spacing of vertical springs	0.96 m
Height above rail level of lateral dampers	- m
Lateral semi spacing of vertical dampers	0.96 m
Lateral semi spacing of vertical friction	- m

Figure A.7: FS ETR500 COACH. Extract from [4, Appendix 2]

Appendix 2

SECONDARY SUSPENSION

Lateral stiffness (per bogie)	0.256 MN/m
Vertical stiffness (per bogie)	0.722 MN/m
Roll bar stiffness (per bogie)	1.0 MNm/r
Yaw stiffness (per bogie)	- MNm/r
Lateral damper rate (per bogie)	0.04 MNs/m
Vertical damper rate (per bogie)	0.065 MNs/m
Yaw damper rate (per bogie)	0.70 MNms/r
Height above rail level of lateral springs	0.8 m
Lateral semi spacing of vertical springs	0.96 m
Height above rail level of lateral dampers	0.8 m
Lateral semi spacing of vertical dampers	1.2 m

Figure A.8: FS ETR500 COACH. Extract from [4, Appendix 2]

Appendix 2

VEHICLE TITLE FS E444 LOCOMOTIVE

MASSES & INERTIAS

Number of bogies	2
Number of axles (per bogie)	2
Body mass	64.6 Mg
Body roll inertia	53.366 Mgm ²
Body pitch inertia	1643.0 Mgm ²
Body yaw inertia	1630.0 Mgm ²
Bogie mass	4.0 Mg
Bogie roll inertia	3.115 Mgm ²
Bogie pitch inertia	5.843 Mgm ²
Bogie yaw inertia	8.107 Mgm ²
Wheelset mass	2.1 Mg
Wheelset roll and yaw inertia	1.164 Mgm ²

DIMENSIONS

Semi pivot spacing	4.5 m
Semi wheelbase	1.3 m
Wheel radius	0.55 m
Body centre of gravity height above rail level	1.65 m
Bogie centre of gravity height above rail level	0.64 m

PRIMARY SUSPENSION

Lateral stiffness (per axle)	12.0 MN/m
Vertical stiffness (per axle)	4.0 MN/m
Yaw stiffness (per axle)	15.4 MN/m
Lateral damper rate (per axle)	- MNs/m
Vertical damper rate (per axle)	0.03 MNs/m
Vertical friction breakout (per axle)	- KN
Height above rail level of lateral springs	0.55 m
Lateral semi spacing of vertical springs	1.03 m
Height above rail level of lateral dampers	- m
Lateral semi spacing of vertical dampers	1.2 m
Lateral semi spacing of vertical friction	- m

958223/01

9

Figure A.9: FS E444 LOCOMOTIVE. Extract from [4, Appendix 2]

Appendix 2

SECONDARY SUSPENSION

Lateral stiffness (per bogie)	1.0 MN/m
Vertical stiffness (per bogie)	2.1 N/m
Roll bar stiffness (per bogie)	1.0 Nm/r
Yaw stiffness (per bogie)	- Nm/r
Lateral damper rate (per bogie)	0.037 MNs/m
Vertical damper rate (per bogie)	0.145 MNs/m
Yaw damper rate (per bogie)	0.938 MNms/r
Height above rail level of lateral springs	0.95 m
Lateral semi spacing of vertical springs	1.03 m
Height above rail level of lateral dampers	0.73 m
Lateral semi spacing of vertical dampers	1.20 m

Figure A.10: FS E444 LOCOMOTIVE. Extract from [4, Appendix 2]

Appendix 2

VEHICLE TITLE UIC COACH

MASSES & INERTIAS

Number of bogies	2
Number of axles (per bogie)	2
Body mass	32.0 Mg
Body roll inertia	56.8 Mgm ²
Body pitch inertia	1970.0 Mgm ²
Body yaw inertia	1970.0 Mgm ²
Bogie mass	2.615 Mg
Bogie roll inertia	1.722 Mgm ²
Bogie pitch inertia	1.476 Mgm ²
Bogie yaw inertia	3.067 Mgm ²
Wheelset mass	1.70 Mg
Wheelset roll and yaw inertia	1.30 Mgm ²

DIMENSIONS

Semi pivot spacing	9.5 m
Semi wheelbase	1.28 m
Wheel radius	0.445 m
Body centre of gravity height above rail level	1.503 m
Bogie centre of gravity height above rail level	0.68 m

PRIMARY SUSPENSION

Lateral stiffness (per axle)	6.4 MN/m
Vertical stiffness (per axle)	1.46 MN/m
Yaw stiffness (per axle)	60.0 MNm/r
Lateral damper rate (per axle)	- MNs/m
Vertical damper rate (per axle)	0.005 MNs/m
Vertical friction breakout (per axle)	- KN
Height above rail level of lateral springs	0.445 m
Lateral semi spacing of vertical springs	1.0 m
Height above rail level of lateral dampers	- m
Lateral semi spacing of vertical dampers	1.0 m
Lateral semi spacing of vertical friction	- m

Figure A.11: UIC COACH. Extract from [4, Appendix 2]

Appendix 2

SECONDARY SUSPENSION

Lateral stiffness (per bogie)	0.32 MN/m
Vertical stiffness (per bogie)	0.86 MN/m
Roll bar stiffness (per bogie)	0.94 MNm/r
Yaw stiffness (per bogie)	- MNm/r
Lateral damper rate (per bogie)	0.059 MNs/m
Vertical damper rate (per bogie)	0.074 MNs/m
Yaw damper rate (per bogie)	0.591 MNms/r
Height above rail level of lateral springs	0.825 m
Lateral semi spacing of vertical springs	1.0 m
Height above rail level of lateral dampers	0.825 m
Lateral semi spacing of vertical dampers	1.3 m

Figure A.12: UIC COACH. Extract from [4, Appendix 2]

Freight track: Trackfrt. dat

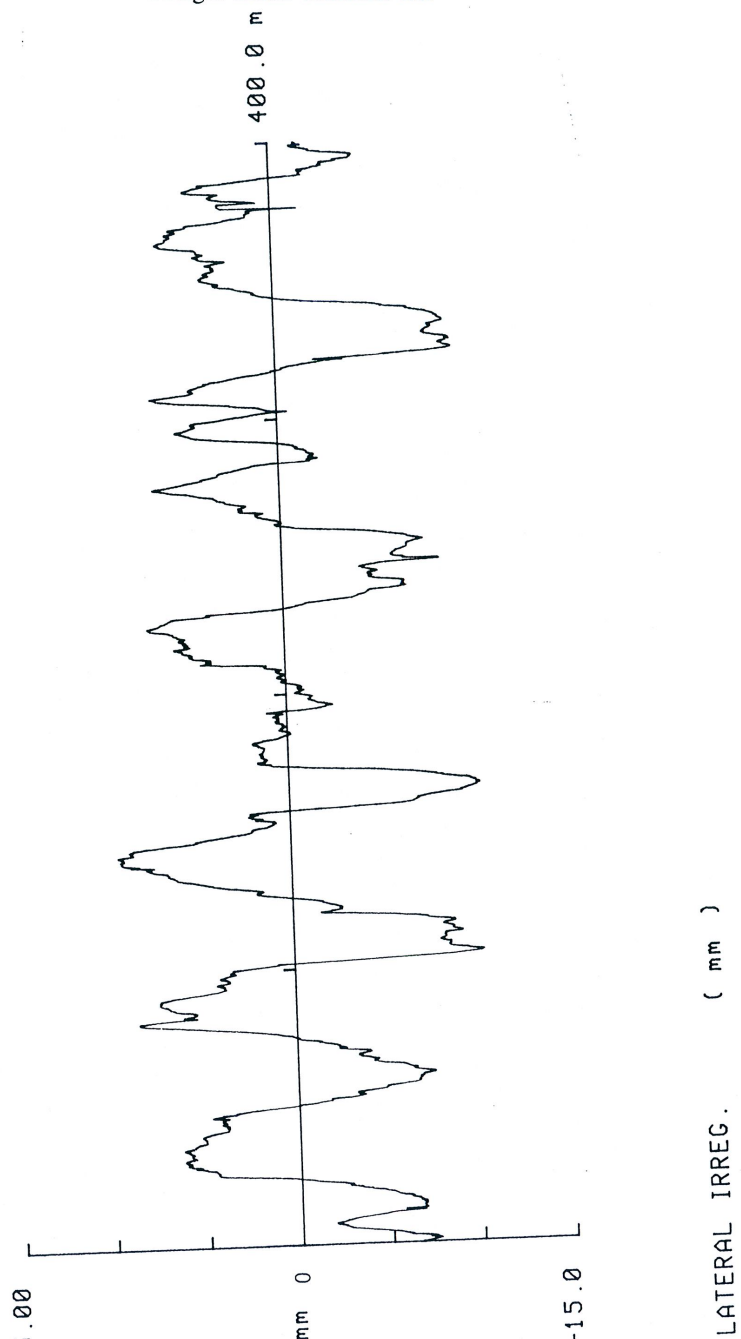
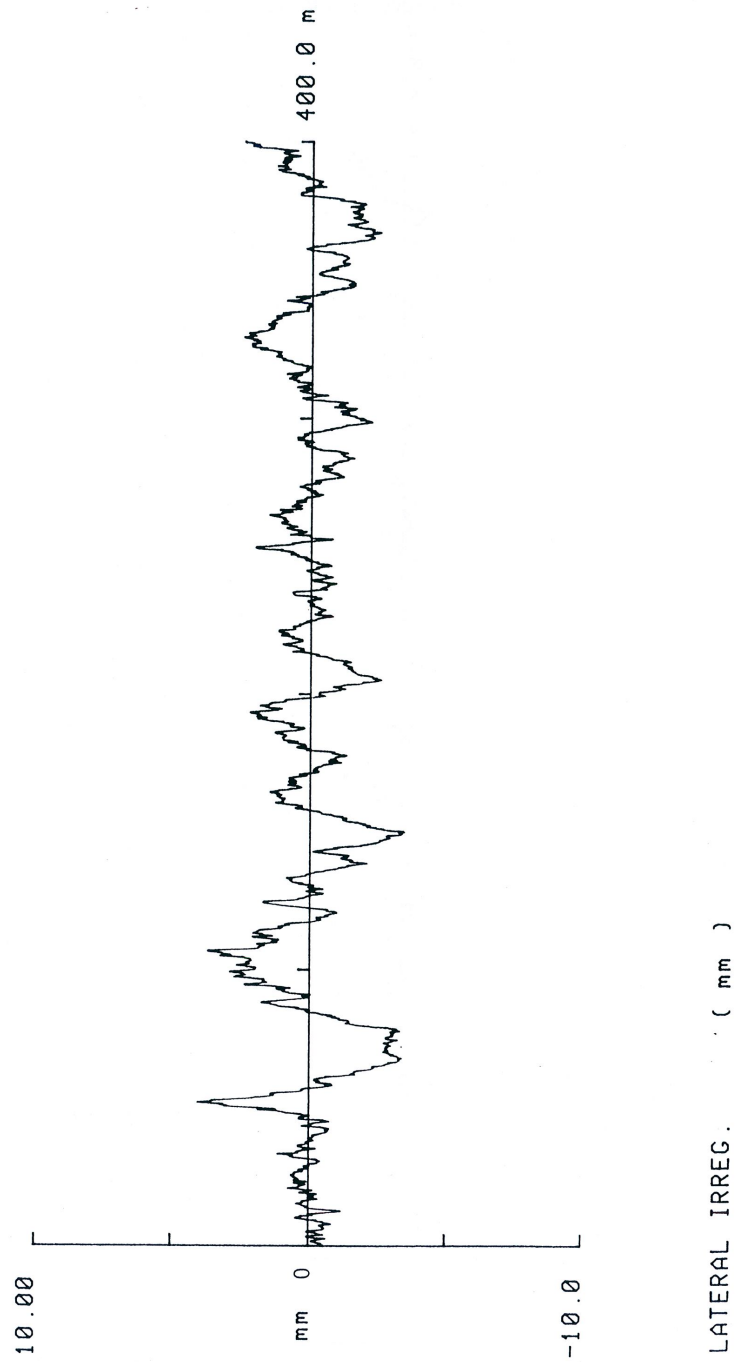


Figure A.13: Horizontal track irregularities for freight trains. Extract from [5, Figure 2.1]

Passenger track: Trackpn. dat



LATERAL IRREG. (mm)

63

Figure A.14: Horizontal track irregularities for standard passenger trains. Extract from [5, Figure 2.1]

ERRI D 181/RP 6	VAMPIRE HORIZONTAL TRACK IRREGULARITIES (HIGH-SPEED LINE)	Fig. 2.3
-----------------	---	----------

High speed track: Trackph. dat

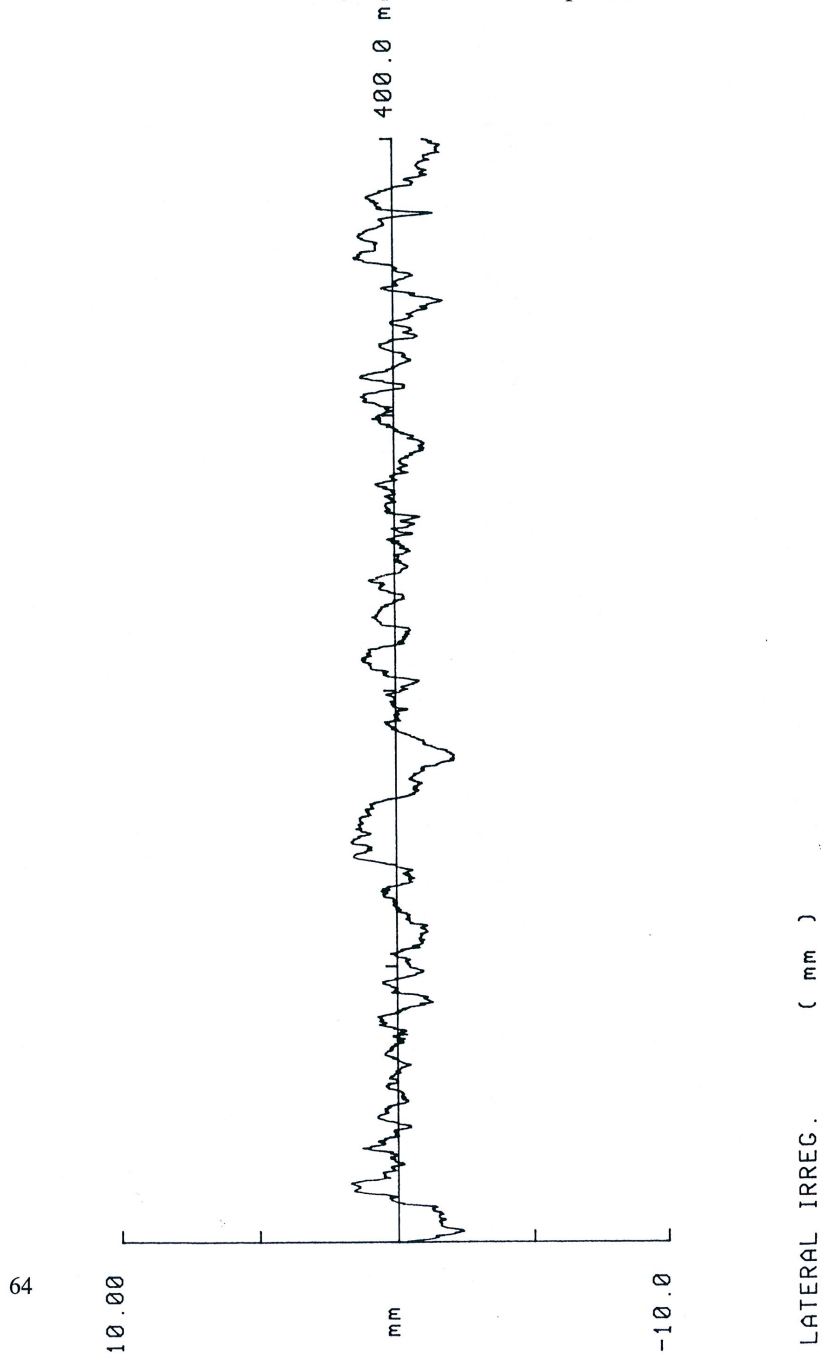


Figure A.15: Horizontal track irregularities for high speed passenger train. Extract from [5, Figure 2.1]

Appendix B

Speeds which do not require dynamic compatibility checks

Line category Locomotive class	Freight wagon	Locomotive	Passenger carriage	Multiple unit	Special vehicle
a10 ^a	-	-	-	-	-
a12 ^a	-	-	-	-	-
a14 ^a	-	-	-	-	-
A	120	120 ^b / 160	160 ^c	160 ^c	120
B1	120	120 ^b / 160	160 ^c	160 ^c	120
B2	120	120 ^b / 160	-	-	120
C2	120	120 ^b / 160	140 ^c	140 ^c	120
C3	120	120	-	-	120
C4	120	120	-	-	120
D2	120	120 ^b / 160	120 ^c	120 ^c	120
D3	120	120	-	-	120
D4	120	120	-	-	120
D4xL	120 ^d	120	-	-	120 ^d
D5	100	-	-	-	100
E4	100	-	-	-	100
E5	100	-	-	-	100
E6	80	-	-	-	80
L4	-	120 ^b / 160	-	-	-
L6	-	120	-	-	-

^a Light railways – normal operating speeds are generally significantly less than speed at which additional dynamic checks would need to be considered.
^b Three or more adjacent couples locomotives.
^c Additional values for max "p" (see Table F.2).
^d Option.

Figure B.1: Speed limit (in km/h) in relationship Line Category/Locomotive Class and vehicle type.
Extract from [11, Appendix F]

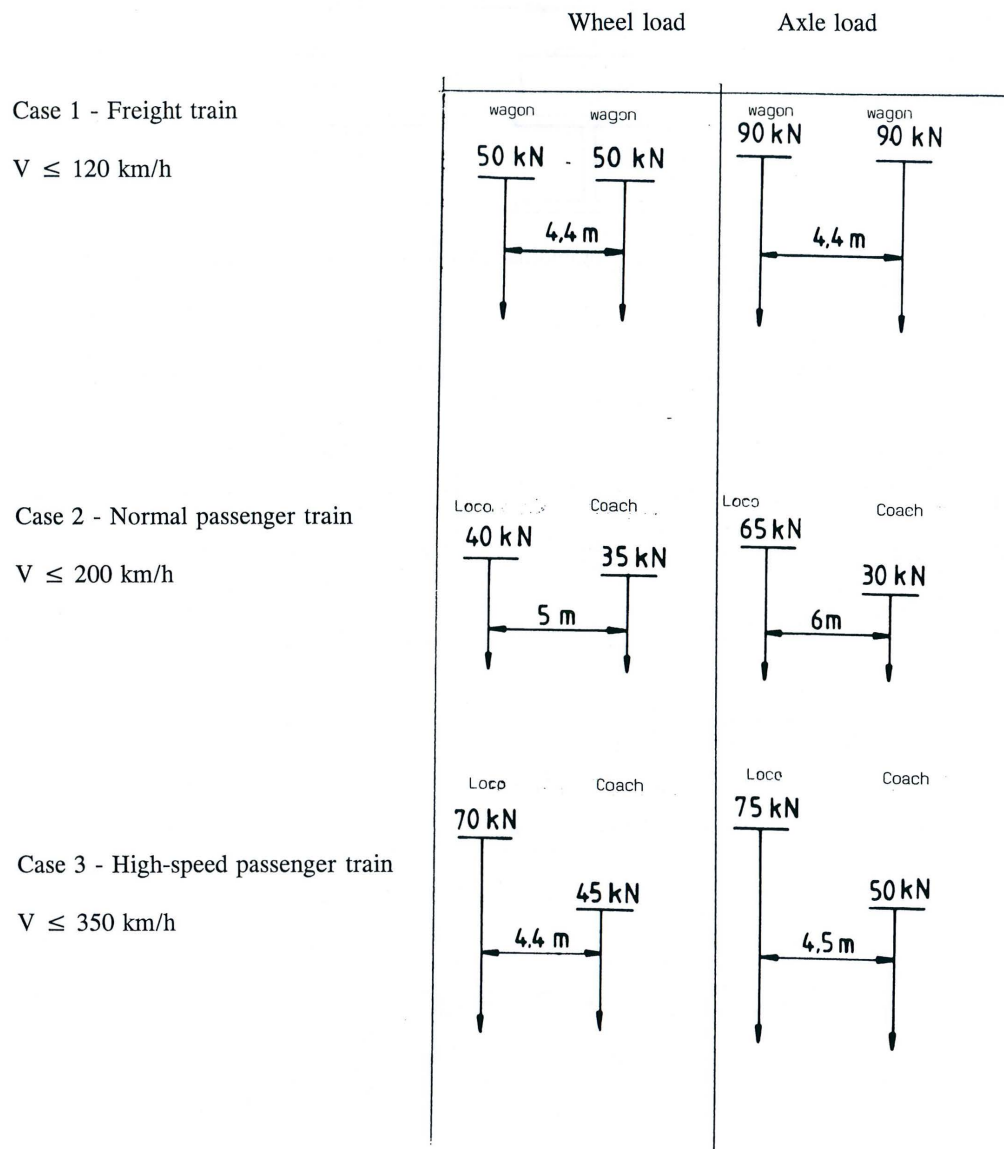


Figure B.2: LATERAL WHEEL AND AXLE FORCES FOR BRIDGES. Extract from [5, Fig 3.1]

EXAMPLE RUN FILE

```

Case 7: Passenger train/track, 160kph, 54m span, 1/10000 flex., 6 Mg/m
EUROLONG
*TRANSIENT
    470.  0.0010  0.01
        44.444

trackPN
*CREEP
    0.3000  0.3000  8.0000  0.0000  0.0000
NON-LINEAR
stdp1
*OUTPUT
Lat displacement of bridge @ mid span   mm
    1000*U01
Lat acceleration of bridge @ mid span  m/s2
    U02
LOCO body lat accel @ leading pivot   m/s2
    A01Y + 4.5*A01W
COACH 1 body lat accel @ leading pivot m/s2
    A08Y + 9.5*A08W
LOCO lat accel of leading bogie      m/s2
    A02Y
COACH 1 lat accel of leading bogie   m/s2
    A09Y
Total lat force on LOCO leading bogie kN
    FW01Y + FW02Y
Total lat force on COACH 1 leading bogie kN
    FW05Y + FW06Y
Lat force, COACH 1 wset 1, left wheel  kN
    FL05Y
Lat force, COACH 1 wset 1, right wheel kN
    FR05Y
Lat force, COACH 1 wset 2, left wheel  kN
    FL06Y
Lat force, COACH 1 wset 2, right wheel kN
    FR06Y
Lat force, LOCO wset 1, left wheel   kN
    FL01Y
Lat force, LOCO wset 1, right wheel  kN
    FR01Y
Lat force, LOCO wset 2, left wheel   kN
    FL02Y
Lat force, LOCO wset 2, right wheel  kN
    FR02Y
Lat force, LOCO wset 3, left wheel   kN
    FL03Y
Lat force, LOCO wset 3, right wheel  kN
    FR03Y
COACH 5 body lat accel @ leading pivot m/s2
    A36Y + 9.5*A36W
COACH 5 lat accel of leading bogie   m/s2
    A37Y
Total lat force on COACH 5 leading bogie kN
    FW21Y + FW22Y
Lat force, COACH 5 wset 1, left wheel  kN
    FL21Y
Lat force, COACH 5 wset 1, right wheel kN
    FR21Y
Lat force, COACH 5 wset 2, left wheel  kN
    FL22Y
Lat force, COACH 5 wset 2, right wheel kN
    FR22Y
*

```

968223/01

Figure B.3: Example run file. Extracted from [4].

Appendix C

MU-Groups and MU-Classes

C.1 Definition

Multiple units can be grouped according to type of traffic service (high speed - long distance, intercity - regional and commuter/suburban) or to the kind of running gear (conventional bogies, articulated bogies and single axles).

In some cases due to potential excessive dynamic load effects in bridge line category checks are not sufficient to demonstrate compatibility. To minimise the need for undertaking a dynamic check of individual trains, several typical and wide spread MU-designs have been grouped in MU-classes. For these groups of vehicles, load models covering the specified design parameter ranges have been developed to allow the efficient dynamic analysis of bridges. For practical reasons, the number of MU classes was limited and for trains outside the range of parameters covered, the process of checking an individual train existing at the time of publication of this standard as state of the art shall be used.

Each MU-class is defined by:

- ranges of train parameters covered and;
- a corresponding load model for carrying out dynamic checks on bridges.

Each MU-Group comprises of several MU-Classes. Table

MU-Group	MU-Class
conventional bogie(CB)	CB_1 CB_2
articulated bogie(AB)	AB_1 AB_2 AB_3 AB_4
single axle(SA)	SA_1 SA_2

Table C.1: Relationship MU-groups - MU-classes

C.1.1 Train parameters of MU-Class CB_1

C.1.2 Train parameters of MU-Class CB_2

C.1.3 Train parameters of MU-Class AB_1

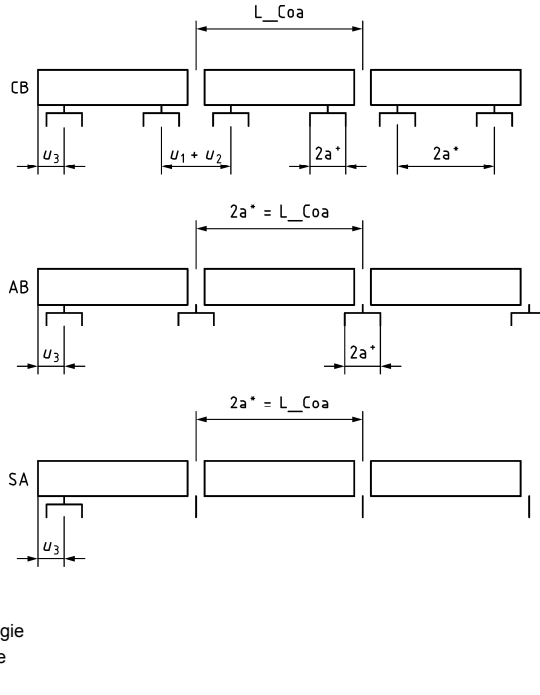


Figure C.1: Train parameters related to MU-Groups. Extracted from [11, Annex C]

Name	Parameter	Unit
$2a^*$	Bogie spacing between pivot centres within a vehicle	m
$2a^+$	Axle spacing in bogie	m
$u_1 + u_2$	Bogie spacing between pivot centres of adjacent vehicles	m
u_3	Overhang of end coaches	m
L_{Coa}	Coach length	m
No_Coa	Number of coaches within an unit	-
No_Units	Number of units within a train	-

Table C.2: Explanation of train parameters. Extracted from [11, Annex C]

C.1.4 Train parameters of MU-Class AB_2

C.1.5 Train parameters of MU-Class AB_3

C.1.6 Train parameters of MU-Class AB_4

C.1.7 Train parameters of MU-Class SA_1

C.1.8 Train parameters of MU-Class SA_2

max No_Units	2
max No_Coa	8
L_Coa	$23.8m \leq L_Coa \leq 25.3m$
$2a^*$	$16.8m \leq 2a^* \leq 18.0m$
$2a^+$	$2m \leq 2a^+ \leq 3m$
$(u1 + u2)$	$7.0m \leq (u1 + u2) \leq 7.6m$
$u3$	$4m \leq u3 \leq 6m$

Table C.3: Train parameters for conformity with MU-Class CB_1

max No_Units	2
max No_Coa	7
L_Coa	$25.3m \leq L_Coa \leq 27.5m$
$2a^*$	$18.0m \leq 2a^* \leq 19.5m$
$2a^+$	$2m \leq 2a^+ \leq 3m$
$(u1 + u2)$	$7.2m \leq (u1 + u2) \leq 8.0m$
$u3$	$4m \leq u3 \leq 6m$

Table C.4: Train parameters for conformity with MU-Class CB_2

max No_Units	4
max No_Coa	5
$2a^*$	$14.9m \leq 2a^* \leq 16.0m$
$2a^+$	$2m \leq 2a^+ \leq 3m$
$u3$	$3m \leq u3 \leq 5.5m$

Table C.5: Train parameters for conformity with MU-Class AB_1

max No_Units	4
max No_Coa	5
$2a^*$	$18.8m \leq 2a^* \leq 19.5m$
$2a^+$	$2m \leq 2a^+ \leq 3m$
$u3$	$3m \leq u3 \leq 5.5m$

Table C.6: Train parameters for conformity with MU-Class AB_2

max No_Units	2
max No_Coa	11
$2a^*$	$17.0m \leq 2a^* \leq 17.5m$
$2a^+$	$2m \leq 2a^+ \leq 3m$
$u3$	$4.5m \leq u3 \leq 5.7m$

Table C.7: Train parameters for conformity with MU-Class AB_3

max No_Units	2
max No_Coa	10
$2a^*$	$18.7m \leq 2a^* \leq 19.2m$
$2a^+$	$2m \leq 2a^+ \leq 3m$
$u3$	$4.3m \leq u3 \leq 5.3m$

Table C.8: Train parameters for conformity with MU-Class AB_4

max No_Units	3
max No_Coa	10
$2a^*$	$9.2m \leq 2a^* \leq 9.8m$
$u3$	$4.25m \leq u3 \leq 6.25m$

Table C.9: Train parameters for conformity with MU-Class SA_1

max No_Units	2
max No_Coa	14
$2a^*$	$12.8m \leq 2a^* \leq 13.5m$
$u3$	$4.25m \leq u3 \leq 6.25m$

Table C.10: Train parameters for conformity with MU-Class SA_1

Appendix D

Regression commands for R console

```
> F <- c(0,110,170,185)
> v <- c(0,60,100,120)
> f <- function(a,b,v) {a*v^b}
> dat <- data.frame(v,F)
> dat
   v     F
1 0     0
2 60   110
3 100  170
4 120  185

> fm <- nls(F ~ f(a,b,v), data = dat, start = c(a=1, b=1))
> fm
Nonlinear regression model
  model: F ~ f(a, b, v)
  data: dat
      a      b
 5.2064 0.7498
 residual sum of squares: 47.84

Number of iterations to convergence: 6
Achieved convergence tolerance: 2.868e-06
```

Appendix E

Matlab scripts

E.1 fog.m

```
function O=fog(EJ,l,mu,c,zeta)

if EJ<1
    EJ = 100000*l^2/(48*EJ);
end

omega1 = pi^2/l^2*sqrt(EJ/mu);
omega = pi*c/l;
omegab = zeta*sqrt(EJ/mu);
omegal1 = sqrt(abs(omega1^2 omegab^2));

r1 = omega1 + omega;
r2 = omega1 - omega;

if c >= (200/3.6)
    Q = 1000*3.10*(c*3.6)^0.7495;
end

if c >= (120/3.6) && c < (200/3.6)
    Q = 1000*3.58*(c*3.6)^0.7495;
end

if c < (120/3.6)
    Q = 1000*5.2064*(c*3.6)^0.7495;
end

v_0 = Q*l^3/(48*EJ);

v1 = @(t) l^3*Q*omega1/(pi^4*EJ) * cos(omega1*t)/(omega^2+omegab^2);
v2 = @(t) omega*(cos(omega*t) exp(-omegab*t) omegab*sin(omega*t));
v = @(t) v1(t) * v2(t);

% v11 = 1/((omega1^2 r2^2)^2+4*omegab^2*r2^2);
```

```

% v12 = @(t) (omega1^2 r2^2)*(cos(r2*t) exp(omegab*t)*cos(omega1a*t));
% v13 = @(t) 2*omegab*r2*sin(r2*t);
% v14 = @(t) omegab/omega1a*(omega1^2+r2^2)*exp(omegab*t)*sin(omega1a*t);
% v21 = 1/((omega1^2 r1^2)^2+4*omegab^2*r1^2);
% v22 = @(t) (omega1^2 r1^2)*(cos(r1*t) exp(omegab*t)*cos(omega1a*t));
% v23 = @(t) 2*omegab*r1*sin(r1*t);
% v24 = @(t) omegab/omega1a*(omega1^2+r1^2)*exp(omegab*t)*sin(omega1a*t);
% v = @(t) Q/(mu*l)*(v11*(v12(t)+v13(t)+v14(t))+v21*(v22(t)+v23(t)+v24(t)));

```



```

a11 = @(t) 1^3*Q*omega1^3*cos(omega1*t)/(pi^4*EJ*(omega^2+omegab^2));
a12 = @(t) omega*(cos(omega*t) exp(omegab*t)) omegab*sin(omega*t);
a21 = @(t) 1^3*Q*omega1*cos(omega1*t)/(pi^4*EJ*(omega^2+omegab^2));
a221 = @(t) omega*(cos(omega*t)*omega^2 exp(omegab*t)*omegab^2);
a222 = @(t) omegab*sin(omega*t)*omega^2;
a22 = @(t) a221(t)+a222(t);
a31 = @(t) 2*1^3*Q*omega1^2*sin(omega1*t)/(pi^4*EJ*(omega^2+omegab^2));
a32 = @(t) omega*(sin(omega*t)+exp(omegab*t)*omegab) omegab*cos(omega*t)*omega;
a = @(t) a11(t)*a12(t)+a21(t)*a22(t)+a31(t)*a32(t);

maxt = 1/c;
dt = maxt/1000;
tdomain = [0:dt:maxt]';

for i=1:length(tdomain)
    p(i,1) = v(tdomain(i,1));
    p(i,2) = a(tdomain(i,1));
    p(i,3) = p(i,1)/v_0;
end

O = [max(abs(p(:,1))),max(abs(p(:,2))),max(abs(p(:,3)))];
%
% namedef = strcat('defEJ',int2str(EJ),'L',int2str(l),'mu',int2str(mu),'c',int2str(c));
% nameacc = strcat('accEJ',int2str(EJ),'L',int2str(l),'mu',int2str(mu),'c',int2str(c));
% nameaco = strcat('dcEJ',int2str(EJ),'L',int2str(l),'mu',int2str(mu),'c',int2str(c));
% name = strcat('EJ',int2str(EJ),'L',int2str(l),'mu',int2str(mu),'c',int2str(c),'.tik');
%
% figure(1)
% plot(tdomain,p(:,1))
% title(strcat('Max Deflection:',mat2str(O(1,1))));
% matlab2tikz(namedef,'height','\figureheight','width','\figurewidth','showInfo');
%
% figure(2)
% plot(tdomain,p(:,2))
% title(strcat('Max Acceleration:',mat2str(O(1,2))));
% matlab2tikz(nameacc,'height','\figureheight','width','\figurewidth','showInfo');

```

```

%
% figure(3)
% plot(tdomain,p(:,3))
% title(strcat('Dynamic coefficient ',mat2str(O(1,3))));
% matlab2tikz(nameaco,'height','\figureheight','width','\figurewidth','showInfo');

function O=Speedenvelop(EJ,l,mu,min,max,zeta)

dv = 0.2;
v = [min:dv:max]';

for i=1:length(v)
    maxres(:,i) = fogtest(EJ,l,mu,v(i,1),zeta);
    speed = v(i,1);
end

% figure('name','speed_envelop');
% plot(v,maxres);

namedef = strcat('spedef','EJ',int2str(EJ),'L',int2str(1),'min',int2str(min),'max',int2str(max));
nameacc = strcat('speacc','EJ',int2str(EJ),'L',int2str(1),'min',int2str(min),'max',int2str(max));
nameaco = strcat('speaco','EJ',int2str(EJ),'L',int2str(1),'min',int2str(min),'max',int2str(max));

figure(1)
plot(v,maxres(1,:))
title(strcat('SpeedEnvelop def from',int2str(min),' to ',int2str(max)));
matlab2tikz(namedef,'height','\figureheight','width','\figurewidth','showInfo');

figure(2)
plot(v,maxres(2,:))
title(strcat('SpeedEnvelop acc from',int2str(min),' to ',int2str(max)));
%matlab2tikz(nameacc,'height','\figureheight','width','\figurewidth','showInfo');

figure(3)
plot(v,maxres(3,:))
title(strcat('SpeedEnvelop dc from',int2str(min),' to ',int2str(max)));
%matlab2tikz(nameaco,'height','\figureheight','width','\figurewidth','showInfo');

```

E.3 Spanenvelop.m

```

function O=Spanenvelop(EJ,min,max,mu,c,zeta)

dl = 2;
l = [min:dl:max]';

for i=1:length(l)

```

```

maxres(:, i) = fogtest(EJ, l(i, 1), mu, c, zeta);
stiff = l(i, 1);
end

figure(1)
plot(l, maxres(1,:))
title(strcat('SpanEnvelop def from ', int2str(min), ' to ', int2str(max)));
%matlab2tikz(namedef, 'height', '\figureheight', 'width', '\figurewidth', 'showInfo', 'tikz')

figure(2)
plot(l, maxres(2,:))
title(strcat('SpanEnvelop acc from ', int2str(min), ' to ', int2str(max)));
%matlab2tikz(nameacc, 'height', '\figureheight', 'width', '\figurewidth', 'showInfo', 'tikz')

figure(3)
plot(l, maxres(3,:))
title(strcat('SpanEnvelop dc from ', int2str(min), ' to ', int2str(max)));
%matlab2tikz(nameaco, 'height', '\figureheight', 'width', '\figurewidth', 'showInfo', 'tikz')

```

E.4 Stiffenvelop.m

```

function O=Stiffenvelop(min,max,l,mu,c,zeta)

ds = 1e9;
s = [min:ds:max]';

for i=1:length(s)
    maxres(:, i) = fogtest(s(i,1),l,mu,c,zeta);
end

namedef = strcat('stedef','min',int2str(min),'max',int2str(max),'L',int2str(1),'c',int2str(0));
nameacc = strcat('steacc','min',int2str(min),'max',int2str(max),'L',int2str(1),'c',int2str(0));
nameaco = strcat('steaco','min',int2str(min),'max',int2str(max),'L',int2str(1),'c',int2str(0));

% figure('name','stiff_envelop');
% plot(s,maxres);

figure(1)
plot(s,maxres(1,:))
title(strcat('StiffEnvelop def from ', int2str(min), ' to ', int2str(max)));
%matlab2tikz(namedef, 'height', '\figureheight', 'width', '\figurewidth', 'showInfo', 'tikz')

figure(2)

```

```

plot(s,maxres(2,:))
title(strcat('StiffEnvelop acc from ',int2str(min),' to ', int2str(max)));
% matlab2tikz(nameacc, 'height', '\figureheight', 'width', '\figurewidth', 'showInfo')

figure(3)
plot(s,maxres(3,:))
title(strcat('StiffEnvelop dc from ',int2str(min),' to ', int2str(max)));
% matlab2tikz(nameaco, 'height', '\figureheight', 'width', '\figurewidth', 'showInfo')

```

E.5 Massenvelop.m

```

function O=Massenvelop(EJ,l,min,max,c,zeta)

dm = 100;
m = [min:dm:max]';

if EJ<1
    EJ = 100000*l^2/(48*EJ);
end

for i=1:length(m)
    maxres(:,i) = fogtest(EJ,l,m(i,1),c,zeta);
end

namedef = strcat('medef','EJ',int2str(EJ),'L',int2str(l),'c',int2str(c),'min',int2str(min));
nameacc = strcat('meacc','EJ',int2str(EJ),'L',int2str(l),'c',int2str(c),'min',int2str(min));

figure(1)
plot(m,maxres(1,:))
title(strcat('MassEnvelop def from ',int2str(min),' to ', int2str(max)));
%matlab2tikz(namedef, 'height', '\figureheight', 'width', '\figurewidth', 'showInfo', 'showInfo')

figure(2)
plot(m,maxres(2,:))
title(strcat('MassEnvelop acc from ',int2str(min),' to ', int2str(max)));
%matlab2tikz(nameacc, 'height', '\figureheight', 'width', '\figurewidth', 'showInfo', 'showInfo')

```

Appendix F

Train vehicles

F.1 Locomotives

F.1.1 4-axle locomotives

Generally, the relevant parameters for categorisation of 4-axle locomotives are axle load P (18 t to 22,5 t) and the bogie axle spacing (2,2 m to 3,4 m).

Typically the mass per unit length is less than 6,4 t/m and the distance from the end axle to the end of the nearest coupling plane is greater than 1,9 m

F.1.2 6-axle locomotives

Generally, the relevant parameters for categorisation of 6-axle locomotives are:

- the maximum axle load P (18 t to 22 t) in combination with;
- the distance between axles within a bogie (1,80 m to 2,25 m).

Typically, the mass per unit length (p) is less than 6,4 t/m and the distance from end axle to the end of the nearest coupling plane (a) is greater than 2,1 m.

F.2 Trains in Netherlands

Passenger trains now in service include following models:

1. The DD-AR (Dubbeldeksaggloregiomaterieel)

EMUs were delivered as DDM-2/3 resembling the bilevel rail cars series DDM-1 from 1985 and operates in fixed formations of 3 or 4 coaches. 4 car trains use a class 1700 locomotive for traction, 3 car trains use an mDDM motorcar, which resembles a DD-AR driving trailer but has electric motors and a single passenger deck on top; the level of this deck is higher than that of a regular single deck rail car, but lower than the upper deck of the other coaches. Three types of coaches are available: Bv (second class), ABv (first and second class) and Bvk (second class driving trailer). The DDM-2/3 series are being modernised from 20102013 and after modernisation the series was renamed as NID (Nieuwe Intercity Dubbeldekker).

2. The VIRM (Verlengd Interregiomaterieel)

also called Regiorunner was partially rebuilt from trainsets DD-IRM (Dubbeldeks Interregiomaterieel). DD-IRM was delivered in 3- and 4-car trainsets. 3-car trainsets got one extra coach, 4-car trainsets got two extra coaches. Also, new 4- and 6-car trainsets were built. Thus, a train consists of one or more combinations of 4 or 6 double deck coaches; each combination (multiple unit) has electric motors. More than three hundred coaches are currently operative in the Netherlands.

3. The Koploper (ICM) (Intercitymaterieel)

is a 3- or 4-car multiple unit that when coupled with another one, allows passengers to walk through (the name Koploper being a play on words literally "head walker", but in actual use meaning "front runner"). The Dutch Railway Company decided to close the heads permanently on 31 October 2005 because the mechanism broke down too often. A scheduled modernisation of around 7 million euro will see the ICM fleet updated. The renovated ICM trains provide 13% more seats (reducing the leg room to uncomfortable small for the long haul journeys they serve in 2nd class, which is further aggravated by a waste bin that is placed on the backsides of the seats in front), have a new interior, a bathroom accessible by wheelchairs, airconditioning as well as upgrades to the engine and connection systems. The head doors are removed. Also, these (renovated) trains are the first trains in the NS fleet equipped with OBIS. OBIS provides a (free) WiFi-connection on board, along with in-train journey information provided through screens and (automated) vocal announcements through the trains speakers. This journey information provides the actual status, and thus is always up-to-date to the actual situation this trip, and the stations is passes.

4. The Sprinter (SGM, Stads Gewestelijk Materieel)

is a two or three car electric, used on small distances. They are named Sprinter because they're able to accelerate and brake quite fast, making them very suitable for 'stoptrein' services. They were also specifically designed for urban environments where they run commuter services. As a result, they are most commonly found in the Randstad area. The initial idea was that the Sprinter would provide somewhat of a subway/metro service but this plan failed as the cities of Amsterdam and Rotterdam continued to construct their own rapid transit systems. Nevertheless, in the densely populated Randstad, the Sprinters remain popular. Two car versions were revised and renamed to Citypendel. All Sprinters are now refurbished into the new white/yellow/dark blue livery.

Bibliography

- [1] M Abu-Hilal and M Mohsen. “Vibration of beams with general boundary conditions due to a moving harmonic load”. In: *Journal of Sound and Vibration* 232.4 (2000), pp. 703–717.
- [2] CEN. *EN 13848-5:2008+A1 Railway applications - Track - Track geometry quality - Part 5: Geometric quality levels - Plain line*.
- [3] UIC Code. “518: Testing and approval of railway vehicles from the point of view of their dynamic behaviour—Safety—Track fatigue—Ride quality”. In: *International Union of Railways, 3rd ed., Paris* (2005).
- [4] ERRI D181 Committee. *ERRI D 181/DT 329 E: LATERAL FORCES ON RAILWAY BRIDGES, PARAMETRIC STUDY PART1, PART 2*. UIC, 1995.
- [5] ERRI D181 Committee. *RP6: Final report, D181 LATERAL FORCES ON RAILWAY BRIDGES*. UIC, 1996.
- [6] Manuel Cuadrado Sanguino et al. “Analysis of Lateral Displacements in Large Railway Viaducts Under Traffic Loads. Impact on Ride Safety and Passenger Comfort.” In: (2008).
- [7] BS EN. “14363: 2005”. In: *Railway applications-Testing for the acceptance of running characteristics of railway vehicles-Testing of running behavior and stationary tests* (2007), pp. 6–36.
- [8] *EN 1990 AMD 2 : 2005(E) Annex A2 to EN 1990*.
- [9] Coenraad Esveld. “Modern railway track”. In: (2001).
- [10] CEN Eurocode. “1: Actions on structures, Part 2: Traffic loads on bridges”. In: *Brussels: European Standard EN 2* (1991), p. 2003.
- [11] CEN Eurocode. “prEN 15528:2013, Railway applications Line categories for managing the interface between load limits of vehicles and infrastructure”. In: *Brussels: European Standard EN* (2013).
- [12] L. Fryba and L. Frýba. *Dynamics of railway bridges*. T. Telford, 1996. ISBN: 9780727720443.
- [13] Ladislav Fryba and Ladislav Frýba. *Vibration of solids and structures under moving loads*. Thomas Telford, 1999.
- [14] British Standards Institution. *Eurocode: Basis of structural design*. BSI, 2002.
- [15] Simon Iwnicki. *Handbook of railway vehicle dynamics*. CRC Press, 2006.
- [16] Michal Majka and Michael Hartnett. “Effects of speed, load and damping on the dynamic response of railway bridges and vehicles”. In: *Computers & Structures* 86.6 (2008), pp. 556–572.
- [17] A.V. Metrikine. *Dynamics, Slender Structures and an Introduction to Continuum Mechanics: CT 4145*. Delft University of Technology.
- [18] Giuseppe Piccardo and Federica Tubino. “Dynamic response of Euler-Bernoulli beams to resonant harmonic moving loads”. In: (2012).

- [19] International Union of Railways(UIC). *Design requirements for rail-bridges based on interaction phenomena between train, track and bridge*.
- [20] Rui Filipe da Silva Dias. "Dynamic Behaviour of High Speed Railway Bridges. Vehicles Lateral Dynamic Behaviour". In: (2007).
- [21] Yan Quan Sun and Manicka Dhanasekar. "A dynamic model for the vertical interaction of the rail track and wagon system". In: *International Journal of Solids and Structures* 39.5 (2002), pp. 1337–1359.
- [22] UNE-ENV 12299: *Aplicaciones ferroviarias. Comodidad de viaje para los viajeros. Medición y evaluación*. 2000.
- [23] UNE-ENV 13803-1 EX: *Aplicaciones ferroviarias. Parámetros de proyecto de trazado de la vía. Ancho de vía de 1 435mm y mayores. Parte 1: Plena vía*. 2006.